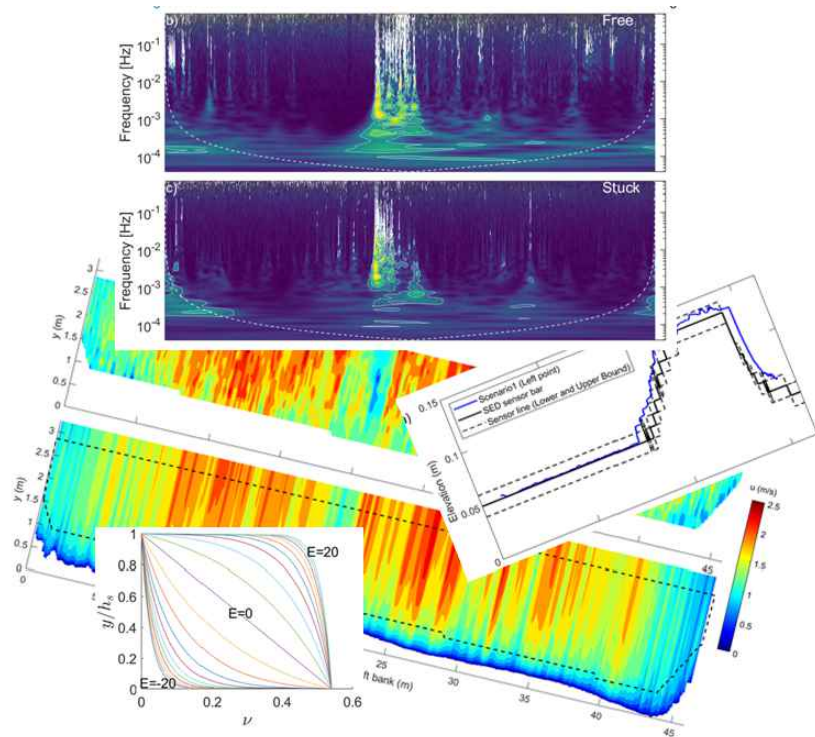


Ashkan Pilbala

Bio-sensors and Miniaturized Technology for Fine Sediments Monitoring in Laboratory and Field Sites, Associated with Entropic Interpretation of Ordinary and Intense Bed-load





UNIVERSITY OF TRENTO

DOCTORAL THESIS

**Bio-sensors and Miniaturized
Technology for Fine Sediments
Monitoring in Laboratory and
Field Sites, Associated with
Entropic Interpretation of Ordinary
and Intense Bed-load**

Author:

Ashkan Pilbala

Advisors:

Prof. Luigi Fraccarollo
Prof. Sebastiano Piccolroaz

XXXVI cycle 2020/2024

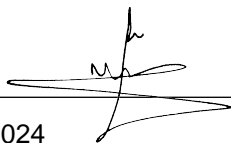
Department of Civil, Environmental, and Mechanical
Engineering (DICAM)

Declaration of Authorship

I, Ashkan Pilbala, declare that this thesis titled, “Bio-sensors and Miniaturized Technology for Fine Sediments Monitoring in Laboratory and Field Sites, Associated with Entropic Interpretation of Ordinary and Intense Bed-load” and the work presented in it are my own. I confirm that:

- This work was done wholly or mainly while in candidature for a research degree at this University.
- Where any part of this thesis has previously been submitted for a degree or any other qualification at this University or any other institution, this has been clearly stated.
- Where I have consulted the published work of others, this is always clearly attributed.
- Where I have quoted from the work of others, the source is always given. With the exception of such quotations, this thesis is entirely my own work.
- I have acknowledged all main sources of help.

Signed:

A handwritten signature in black ink, appearing to be 'A. Pilbala', written over a horizontal line.

Date: 05/07/2024

To my mother, who enabled me getting all the opportunities she was never given to...

To my father, who didn't live long enough to see my success today...

To my brother and sisters, for all their love and care...

Acknowledgements

First and foremost, I am grateful to my scientific advisors, Prof. Luigi Frac-carollo and Prof. Sebastiano Piccolroaz, whose continuous support and guidance allowed me to develop, enjoy and conclude this PhD experience.

I am grateful to all the technicians at the hydraulic laboratory of the University of Trento, for their support during the experiments in lab and field activities.

I am grateful to Stefan Ghetta and Roberto Dinale, from the Department of Hydrology and Dams, Province of Bolzano (Italy), for their help with acquiring and transmitting field data, with attendant explanation and support.

Special thanks to the project manager of PRIN "Enterprising" project, and all the other colleagues of this project, for sharing the effort and motivation to push forward our common and truly inspirational challenge.

I acknowledge the Italian PRIN 2017 project Enterprising for financial support (2017SEB7Z8).

Last but not least, my deepest gratitude belongs to my family and my friends for supporting me and believing in me.

*“You are a treasure, if the gems are your aim
No more than a grain, if a loaf is your claim*

*Recall this secret, when you play this game:
Whatever you pursued- is what you became”*

Rumi (1207 – 1273)

UNIVERSITY OF TRENTO

Abstract

Department of Civil, Environmental, and Mechanical Engineering (DICAM)

Doctor of Philosophy

Bio-sensors and Miniaturized Technology for Fine Sediments Monitoring in Laboratory and Field Sites, Associated with Entropic Interpretation of Ordinary and Intense Bed-load

by Ashkan Pilbala

This study has been carried out in the PRIN project “Enterprising”, aiming to monitor and model river flow processes during floods. In this context, in my work, I dealt with the impact of hydrodynamic processes on river biotic communities (exploited as biological sensors), miniaturized gauges, and theoretical methods. Therefore, the aims of the present PhD work followed different paths that share a fascinating common phenomenology, trying to form a robust and consistent understanding of some relevant aspects. The work can be described through the following list of separate activities: 1) evaluating the impact of external stressors on aquatic ecosystems directly by using biotic communities as real-time indicators; 2) developing low-cost systems for monitoring bedload and suspended sediment transport; and 3) developing sediment transport theories based on Entropic theory. In the following, I provide a summary of each of these three aspects.

Future climate scenarios predict an increase in the frequency and intensity of extreme events; thus, it is crucial to understand how flood conditions affect biotic communities in aquatic ecosystems. In this study, freshwater mussels (FM), as reliable bioindicators for detecting environmental disturbances in aquatic ecosystems, were utilized. We performed experiments in a laboratory flume to evaluate the suitability of using FM for developing a tailored real-time biological early warning system (BEWS) for disturbances in the aquatic ecosystem. Stressors inducing such disturbances may be external (i.e., anthropic) or internal (i.e., floods). In particular, we used the valvometric technique to measure the FMs’ behaviour when subjected to increasing discharges/sediment transport in laboratory experiments, mimicking the onset of floods. On 30 March 2022, after laboratory validation, the FM system was installed at the Paglia River in Orvieto, where a gauging station was available for monitoring water level and discharge. On March 31st a flood occurred, which was recorded by the gauging station at the project site. This event caused a visible change in the individual FM behaviour, which was clearly evident when the gaping signals were analysed using the Continuous Wavelet Transform (CWT), a technique that proved particularly suitable for characterising FM behaviour also in laboratory experiments.

Besides FM investigation, two low-cost systems for continuous monitoring of streambed scour/deposition and turbidity were introduced and tested in laboratory. We exploited a vertical string of photoresistors, partially buried in the sediments and used as streambed detector. Different river bed dynamics were considered for testing the streambed measurement device: propagation of sediment front and scour dynamics in different points around a pier of a bridge. The performance of the turbidimeter device was examined in the flume with the flow turbidity undergoing increasing and decreasing stepwise variations. Both measurement devices provided convincing results and showed the potential for being used in the field.

Finally, as far as the theoretical contribution to the Enterprising project was concerned, two different types of sediment transport theories, ordinary bedload, and intense bedload, were developed, based on Entropy theory. Estimation of the velocity distribution based on the Entropy probability density function was developed and applied in past works with the lack of information about the sediment discharge. In this study, by using surface velocity, we were able to link the sediment discharge to the statistics of particle resting time at low Shields stress (ordinary bedload). This approach was subsequently applied to data on one cross-section of Adige River (Bolzano, Northern Italy), and also on Estero Morales River (Chile). As far as the comparison of theory and field measurements was possible, it looked satisfactorily. For the case of intense sediment transport (high Shields values), the extended kinetic theory has been applied to unidirectional steady-uniform flow through a statistic-mechanical model endowed with entropic information on the concentration profile. This made the solution pseudo-analytical, which can be straightforwardly achieved (without numerical approximation tools), and with great advantage in the understanding of the role of any terms in the physical balances.

Overall, during my PhD project, because of its interdisciplinary nature, I encountered numerous challenges. At the same time, I experienced collaboration and multi-disciplinary joint efforts, which enabled me to gain a more comprehensive understanding of the problem from a variety of perspectives. Consequently, I and my supervisors gained a deeper understanding of the nature of hydrodynamic effects on ecosystem biotic communities, which was the main objective of the project "Enterprising", along with a novel awareness of how the entropic theory can be used in sediment transport and how the advancing technology can support the endless need of monitoring resources.

Publications

Some of the main results presented in this thesis are summarized in the following papers:

1. Pilbala, A., Riccardi, N., Benistati, N., Modesto, V., Termini, D., Manca, D., Benigni, A., Corradini, C., Lazzarin, T., Moramarco, T., Fraccarollo, L., and Piccolroaz, S., "*Real-Time Biological Early Warning System based on Freshwater Mussels' Valvometry Data*", *Hydrology and Earth System Sciences*, 28, 2297–2311, 2024;
DOI: [10.5194/hess-28-2297-2024](https://doi.org/10.5194/hess-28-2297-2024)
2. Modesto, V., Tosato, L., Pilbala, A., Benistati, N., Fraccarollo, L., Termini, D., Manca, D., Moramarco, T., Sousa, R., and Riccardi, N., "*Mussel behaviour as a tool to measure the impact of hydrodynamic stressors*", *Hydrobiologia*, 850, 807–820, ISSN 1573-5117, 2023;
DOI: [10.1007/s10750-022-05126-x](https://doi.org/10.1007/s10750-022-05126-x)
3. Fraccarollo, L., Pilbala, A., and Berzi, D., "*Extended kinetic theory applied to unidirectional collisional suspensions with entropic distributions of particle concentration*", *Under Review, Journal of Fluid Mechanics*, Jun 2024.
4. Pilbala, A., Piccolroaz, S., Mao, L., Bahmanpouri, Farhad., Moramarco, T., and Fraccarollo, L., "*An Entropic Approach to Ordinary Bedload Applied to Flume and Case Studies*", to be submitted 2024.

Contents

Declaration of Authorship	iii
Acknowledgements	vii
Abstract	ix
Publications	xiii
1 Introduction	1
2 Real-Time Biological Early Warning System based on Freshwater Mussels' Valvometry Data	5
2.1 Introduction	5
2.2 Laboratory Experiments	8
2.2.1 Experiments with Free-to-move FMs (Phase 1)	8
2.2.2 Experiments with Immobilized FMs (Phase 2)	9
2.3 Field Experiments (Phase 3)	11
2.4 Data collection and Signal Analysis (Phase 4)	13
2.4.1 Valvometry data collection	13
2.4.2 Signal processing	14
2.5 Results and Discussion	16
2.5.1 Laboratory results	16
2.5.2 Field results	19
2.6 Conclusion	22
3 Towards the Development of an Affordable and Practical Measurement Device for Turbidity and Stream-bed Monitoring	27
3.1 Introduction	27
3.2 Methodology	30
3.2.1 Design of monitoring systems	30
3.2.2 Laboratory Experiments	31
Deposition/Scour Tests	31
Turbidity Calibration and Tests	33
3.2.3 Analysis Approaches	34
Deposition/Scour Tests	34
Turbidity Tests	35
3.3 Results and Discussion	35
3.3.1 Scour/Deposition Experiments	35

3.3.2	Turbidity Experiments	38
3.4	Conclusion	39
4	An Entropic Approach to Ordinary Bedload applied to Flume and case studies	43
4.1	Introduction	43
4.2	Dataset	45
4.2.1	Flume experiments	45
4.2.2	Adige River (Italy)	46
4.2.3	Estero Morales (Chile)	46
4.3	Theoretical backgrounds	48
4.3.1	Ordinary bed-load regime	48
4.3.2	Determination of resting time pdf via the Shannon entropic approach	48
4.4	Results and Discussion	51
4.4.1	Experiments	51
4.4.2	Adige River	52
4.4.3	Estero Morales	56
4.5	Conclusion	59
5	Extended kinetic theory applied to unidirectional collisional suspensions with entropic distributions of particle concentration	61
5.1	Introduction	61
5.2	Theoretical backgrounds	64
5.3	Results and comparisons	74
5.4	Concluding remarks	76
6	Conclusions and future research	79
A	Appendix A	83
	Bibliography	91

List of Figures

2.1	a) Sampling of mussels at Lake Caldonazzo (TN), Italy; b) Samples of <i>Unio elongatulus</i> species; c) and d) Side and plan views of Mussels' aquarium; e) Natural algae.	8
2.2	a) Experimental setup of free-to-move mussels in the laboratory; b) and c) Flow direction and plan views of mussels' arrangement in the flume; d) an example of FM equipped with a Hall sensor and a magnet.	9
2.3	a) Experimental setup of immobilized mussels in the laboratory; b) and c) side and plan views of mussels' arrangement in the flume.	11
2.4	a) Map of the River Paglia and its catchment, showing the location of the field monitoring site and of Lake Montepulciano, where the FMs were collected; b) Joseph Mallord William Turner (1775–1851), <i>View of Orvieto, Painted in Rome</i> (1828, reworked 1830), © Photo: Tate, CC-BY-NC-ND 3.0.	12
2.5	Field Installation - Enterprising pilot site, Orvieto City, Italy: a) overview of the FM cage, location of the multiparametric probe and flow direction; b) top view of the FM cage; c) front view (schematic); d) side view (schematic).	13
2.6	Mean (\pm SD) valve gaping frequency (Hz) of 32 FMS behaviour experiments with constant discharges (Q1, Q2, Q3, and Q4) and variable discharges (Q2–Q4, Q3–Q4, Q2–Q5, Q3–Q5, Q2–Q6, and Q3–Q6). The different experimental periods C1, C2, C3, and C4 in constant discharges and V1, V2, V3, and V4 in variable discharges are represented by dark blue, light blue, light green, and dark green bars, respectively.	17
2.7	Laboratory experiment: a) left y-axis: median valve opening signals of free and immobilised mussels with 25th and 75th percentiles indicated by the shaded area; right y-axis: discharge (dashed, black line); b) scalogram showing the median normalised magnitude of the continuous wavelet transform over all the free FMs; c) scalogram showing the median normalised magnitude of the continuous wavelet transform over all the immobilised FMs; d) pseudo-frequency-averaged wavelet spectrum. White contours in b) and c) represent the 95th and 99th percentiles of the CWT coefficient.	18

2.8 Results from the thirteen FMs deployed at the River Paglia field monitoring site during the flood on March 31, 2022; a) valve opening signals for the individual FMs (dots indicate abrupt change points in the mean of the opening signals when the mean opening changes by more than 25%; the asterisk * depicts FMs that are excluded from the wavelet transform analysis); b) left y-axis: median valve opening signals with 25th and 75th percentiles indicated by the shaded area (all FMs except FM2); right y-axis: water level (dashed, black line); c) scalogram showing the median normalised magnitude of the continuous wavelet transform over the FMs; d) pseudo-frequency-averaged wavelet spectrum. White contours in c) represent the 95th and 99th percentiles of the CWT coefficient. 21

3.1 Final sensor designs: a) BED-sensors string design, b) installed BED-sensors string in the flume with showing 5 sensors upper that bed surface level, c) turbidimeter design, d) two turbidity sensors fixed in waterproof housing, e) one waterproofed turbidity sensor fixed in the shielded pipe. 31

3.2 a) Experimental flume setup; b) plan views of BED-sensors string setup in the flume; c) plan views of turbidimeters setup in the flume 32

3.3 Different designs of Piers with the BED-sensors string; from the left to the right: B-Test2,B-Test3,B-Test4 33

3.4 An extract of the bed surface line in one frame: a) Original frame, b) colour segments, c) Extracted line based on pixel index. 35

3.5 5 time-series frames showing an increase (frame1 to frame3) and decrease (frame and frame5) in streambed elevation in front of BED-sensors string 37

3.6 Extracted bed surface line based on the BED-sensors string and Frame analysis: a) BED-sensors string versus Scenario1; b) BED-sensors string versus Scenario2; c) BED-sensors string versus Scenario3; d) BED-sensors string versus Scenario4 . . . 37

3.7 3 time-series frames showing scour around the in front to the pier (B-Test2): a1, 2) frame 1 showing the bed elevation condition at the beginning of flume run from two different side views; b1) frame 2 showing the bed elevation condition at a random time step during flume run from a side view; c1, 2) frame 3 showing the bed elevation condition at the end of flume run from two different side views. 38

3.8 Extracted streambed line based on the BED-sensors string and Frame analysis (Scenario1) 39

3.9 Calibration results showing the correlation functions between NTU and Volt for two different Temperature 40

3.10 Result of T-Test1 with 5 low-cost turbidity sensors in the flume. 40

4.1	Left panel: map of the Adige River and its catchment, showing the location of the hydrometric station. Right panel: map of the stream Estero Morales and its catchment, showing the location of the hydrometric station.	47
4.2	Left: view of the stream. Center: size distribution of PIT tracers, bed surface, and subsurface. Right: intra and inter-day measurement of local depth.	48
4.3	Regime map for the sediment transport. Blue dots refer to the four experimental runs, red to Adige River, black to Estero Morales.	49
4.4	Probability density functions of the resting times from measurements (solid lines) and Entropy theory (dotted lines). . .	52
4.5	Colour maps of the Velocity field in the cross-section for the high flow condition: a) based on the ADCP data, b) based on the Entropy theory. Ponte Adige cross section, high flow condition. c to g) random velocity profiles from the left bank to the right bank. h) distribution of Shields stress.	54
4.6	P.d.f. of the resting time for the three monitored flow conditions in Adige.	56
4.7	Left: Normalized values of \tilde{E}_{iN} , \tilde{L}_{iN} , \tilde{q}_{siN} , where $b_{iN} = b_i / \max(b_i)$, with $b = \tilde{E}_i$, \tilde{L}_i or \tilde{q}_{si} , as d_i spans over the PIT grainsize range. Right: the normalized histogram of the measured resting times in Estero Morales (Chile) and the entropic outcome	59
5.1	Sketch of the flow configuration with the frame of reference and concentration reference values at specific positions	65
5.2	Entropic concentration profiles from equation (5.3) for different values of the entropic parameter.	66
5.3	Measured (circles, Capart and Fraccarollo [37]) and predicted (line, equation 9, with $k_0 = 0.35$, $\sigma = 1.51$ and $v_c = 0.61$, as appropriated for plastic cylinders) mass hold-up, $\bar{\nu}h$, against $\Theta / \cos \phi$	68
5.4	Measured (circles, Revil-Baudard et al. [168]) and predicted (line, equation 15, with $v_{rep} = 0.64$ and $h = 10$) mixing length as a function of the distance from the erodible bed.	71
5.5	Optimum entropic parameter as a function of the Shields number for three different angles of the inclination of the bed in the case of sediment transport of plastic cylinders in water.	75
5.6	Profiles of particle, liquid $ $ and total shear stress in the transport layer for $\phi = 1.9^\circ$ and $\Theta = 1.7$, with the corresponding optimum $E = 0.95$	75

5.7	Experimental measurements (symbols) and theoretical predictions (lines) of profiles of concentration (black lines and circles), particle (red lines and triangles) and liquid (blue lines) velocity, and granular temperature (green lines and squares) when: (a) $\phi = 1.9^\circ$ and $\Theta = 1.7$, with the corresponding optimum $E = 0.95$; (b) $\phi = 3.0^\circ$ and $\Theta = 2.9$, with the corresponding optimum $E = 1.35$	77
A.1	Valve opening signals for the individual free and immobilised FMs deployed in the laboratory experiment (dots indicate abrupt change points in the mean of the opening signals when the mean opening changes by more than 25%).	84
A.2	Valve opening signals for the individual free and immobilised FMs deployed in the laboratory experiment after detrending and removal of step changes in the mean valve opening.	85
A.3	Data from the multiparametric sensor installed at the field monitoring site; a) left y-axis: median valve opening signal with 25 th and 75 th percentiles indicated by the shaded area; right y-axis: water level; b) left y-axis: as in a); right y-axis: water temperature; c) left y-axis: as in a); right y-axis: water conductivity.	86
A.4	Valve opening signals for the individual immobilised FMs deployed at the field monitoring site after detrending and removal of step changes in the mean valve opening. The asterisk * depicts FMs that are excluded from the wavelet transform analysis presented in Figure 5 in the main text.	87
A.5	Colour maps of the Velocity field in the cross-section for the low flow condition: a) based on the ADCP data, b) based on the Entropy theory. Ponte Adige cross section, high flow condition. c to g) random velocity profiles from the left bank to the right bank. h) distribution of Shields stress.	88
A.6	Colour maps of the Velocity field in the cross-section for the moderate flow condition: a) based on the ADCP data, b) based on the Entropy theory. Ponte Adige cross section, high flow condition. c to g) random velocity profiles from the left bank to the right bank. h) distribution of Shields stress.	89

List of Tables

2.1	Exposure scenarios of the hydrodynamic conditions considering: water flow rate Q/B (being B the width of the channel and Q the discharge); water depth; the cross-section averaged flow velocity; the specific solid discharge, Q_s/B (i.e. per unit of width); the Shields parameter $[\theta = u^{*2}/(s-\rho)gd]$ - being u^* the shear velocity and d the median sediment diameter] indicating the incipient sediment motion conditions.	9
2.2	Description experiments in phase 1	10
3.1	BED-sensors string setup for the experiments	33
3.2	Calibration concentrations based on 4000 NTU Formazin standard solution with 200mL flask	34
4.1	Information about the three ADCP measurements in Adige River.	46
4.2	M for the chosen transects	53
A.1	Functions of extended kinetic theory in the dense limit.	90

Chapter 1

Introduction

Many countries worldwide have experienced flood damage, causing large amounts of loss to individuals and governments. Implementing flood monitoring and warning systems, along with approaches to understand morphodynamic changes during and after flood events are essential to reducing these losses. In recent decades, the development of smart, accurate, real-time flood monitoring and early warning systems has been a hot topic for research [10]. One of the key challenges in this field is the high cost and maintenance of the necessary infrastructure. Developing countries often lack the financial resources to implement comprehensive flood monitoring/warning systems [121]. Therefore, research is also focused on creating cost-effective and scalable solutions that can be deployed in resource-limited settings. Innovations such as low-cost sensors, community-based monitoring programs, and the use of open-source software for data analysis are being explored to make these systems more accessible. Furthermore, understanding the morphodynamic changes during and after flood events is crucial for effective river management and flood risk mitigation. Floodwaters can cause significant alterations to river channels, eroding banks, and depositing sediments [89, 199]. Monitoring these changes helps in predicting future flood risks and planning river restoration and management activities. Developing theories and techniques such as LiDAR (Light Detection and Ranging), bathymetric surveys, and GIS (Geographic Information Systems) mapping are invaluable tools in capturing these dynamic changes [84, 30]. In addition to physical monitoring and modelling, the use of biotic communities as bioindicators offers an insightful approach to understanding the ecological impacts of flood events. Aquatic organisms, such as mussels, respond sensitively to changes in water quality and toxicant concentrations [203, 177, 103, 208, 209, 18, 81]. These biotic indicators can provide valuable information about the health of river ecosystems and the long-term effects of flooding [144]. By integrating biotic monitoring with traditional flood monitoring/evaluating methods, a more comprehensive understanding of flood dynamics and their ecological consequences can be achieved.

This study has worked out within the PRIN project "Enterprising," which

is dedicated to monitoring and modelling the dynamics of river flow during flood events. As a part of this project, the overall objective is to develop technological capabilities and innovative methodologies, utilizing biological sensors, theoretical frameworks, and miniaturized technology to develop precise predictions of river flow dynamics, especially during high flood events, as well as assess its impacts on riverine biotic communities. Therefore, the present PhD work followed different paths that share a common phenomenology but contribute from different perspectives to form a robust and consistent understanding. The work can be described through the following list of separate activities:

- evaluating the impact of external stressors on aquatic ecosystems directly by using biotic communities as real-time indicators;
- developing low-cost systems for monitoring bedload and suspended sediment transport; and
- developing sediment transport theories based on Entropic theory.

Significantly, the interdisciplinary nature of these pursuits necessitated navigating various challenges inherent in collaborative efforts across diverse fields. In order to effectively address the challenges of working with live organisms and developing electronic instrumentation and sensors, we decided to collaborate with experts in biology and electronics. This thesis is organized in the following manner in order to fully exploit and establish the previously introduced concept.

Chapter 2 describes the impact of hydrodynamic processes on river biotic communities based on laboratory and field experiments with the aim of using freshwater mussels as a real-time biological early warning system. To determine whether FM can be used to develop a tailored real-time biological early warning system (BEWS) for detecting disturbances to the aquatic ecosystem due to external stressors, we performed experiments in a laboratory flume, in different flow and sediment discharge conditions. A valvometric technique was used to measure FMs' valve gapping behaviour, which was then analyzed using Continuous Wavelet Transform (CWT), a method that proved particularly suitable for analyzing FM behaviour. The field study case is also discussed in this chapter. The FM system was installed at the Paglia River in Orvieto after being validated in the laboratory. At the site of the project, the gauging station recorded a flood that occurred on March 31st. As a result of this event, individual FM characteristics changed dramatically, as demonstrated by the CWT analysis of the gapping signals.

Chapter 3 introduces two measurement devices for turbidity, scour and deposition monitoring of stream beds. The results of some experiments are also presented. The two measurement devices were developed as practical and affordable monitoring systems for experimental investigations with the potential for field application. As part of this chapter, we will also discuss the challenges we encountered during the development process.

Chapters 4 and 5 discuss how we have applied the entropic theory in a few different ways. First, as done in previous approaches, we have dealt

with velocity fields in fluvial cross-sections; second, we applied the entropy theory, in an original way, to the resting times of grains involved in ordinary bed-load processes; finally, in another part of this Thesis, by supplying an entropic input into a rather complex model predicting profiles of velocity and other quantities through the highly concentrated sheet layers, we obtained straightforward access to the analytical solution. Indeed, it appears that the entropy theory is ubiquitous in geophysical flows. On one side, therefore, we encourage to boost up interpretations based on it; on the other side, it urges building a theoretical framework addressing the potential applications and giving them substantial validation.

As a final point, we draw the conclusion of the thesis in chapter 6.

Chapter 2

Real-Time Biological Early Warning System based on Freshwater Mussels' Valvometry Data

2.1 Introduction

Sustainable water resource management requires the protection of water-dependent ecosystems, as they play a pivotal role in maintaining the ecological balance and overall health of our water resources [223, 123]. This is a challenging task, that is further compounded by the ongoing effects of climate change on water resources, which intensifies conflicts related to water resource allocation. Indeed, besides impacting water availability and quality, climate change influences water demand, thereby affecting the availability of water needed to sustain the ecological functioning of water bodies [17, 179]. There are several manifestations of climate change's impact on water resources, encompassing floods, droughts, rising temperatures, deterioration of water quality, and in general intensification of extreme events [114, 163, 198]. These phenomena, combined with anthropogenic alterations of flows and water quality resulting from various activities (e.g., irrigation, hydropower production, aquaculture), can exert profound influences on aquatic ecosystems, causing alterations in their structure, function, and overall ecological balance [216, 166, 7]. Consequently, the establishment of comprehensive monitoring systems and analytical tools is imperative for accurately quantifying these impacts on aquatic ecosystems.

In the field of river monitoring, technological advancements have significantly improved our ability to assess both water quantity and quality. Standard monitoring methods for key variables such as water level, temperature, and quality have been greatly enhanced through the utilisation of real-time sensors [85, 155], the establishment of cost-effective sensor networks [136], the development of more advanced monitoring instruments [47, 161], and

the access to remote sensing imagery [75, 36], ultimately leading to heightened precision and reliability. However, it is important to emphasise that none of these tools addresses a direct quantification of the impact of external stressors, whether they arise from natural or anthropogenic disturbances, on the aquatic ecosystem. Although early-warning indicators based on physical and biological state variables can be used to predict loss of system resilience and the occurrence of critical transitions, these indicators typically operate on long-term time scales (e.g., decades) and require knowing the underlying mechanisms that steer ecosystem transitions to identify the pertinent state variables [77]. If the aim is to assess the impact of external disturbances on the time scale of a flood event or management operation, a good level of assessment still requires labour-intensive *in situ* biological sampling with repeated sampling before and after the event [e.g., 137, 66].

A noteworthy source of inspiration can be found in the field of water pollution monitoring, where biotic communities have been used as direct ecosystem indicators for a long time [33, 49, 31, 74, 115, 88, 187]. Benthic communities, shrimps, and other animals have been targeted for this purpose. In particular, but quite relevant in this doctoral work, mussels have been used in bio-monitoring since the mid-1970s with the establishment of the "Mussel Watch" program [76] and since then they have been widely used worldwide as bioaccumulators for the assessment of aquatic pollution [180]. Going beyond their employment as bioaccumulators, dating from the 1980's, mussels started being explored as potential biological sensors (or biosensors) for biological early-warning systems (BEWS) [see e.g., 11] for real-time surface and drinking water pollution monitoring [78, 56, 215]. Over 40 years of studies show that the observation and analysis of mussels' behaviour is a reliable tool for water quality monitoring [194] because they change their valve opening and closing activity when they perceive a change in environmental conditions, such as toxicants concentrations [177, 103, 208, 209, 18, 81], food quantity and quality [86], tidal cycles, and salinity [51, 52, 2]. The immediacy of behavioural responses and the development of simple and cost-effective valve measurement (valvometry) methods have stimulated the production of commercial valvometric systems, such as the Mossel Monitor [103] or the Dreissena Monitor [28]. The interest in using valvometric responses as an alarm signal in real conditions has stimulated technological innovations, such as online data systems equipped with remote control capabilities [194] and, more recently, the integration of artificial intelligence for signal interpretation [201].

The extensive and successful use of mussels as reliable biosensors for real-time detection of water quality-related disturbances, suggests that mussels' valvometry can be a suitable technique also for the automated assessment of the effects of physical stresses, such as the occurrence of floods and droughts or the anthropogenic alteration of flow patterns, on the aquatic ecosystem. These and further hydrological perturbations are increasing in frequency and intensity due to climate change. The extension of mussels' valvometry beyond its initial use in ecotoxicological monitoring of water quality can indeed enhance the importance and highlight the unique insight

of this approach.

The present study, conducted within the framework of the Enterprising PRIN Project (2017), funded by the Ministry of Education, University and Research (MIUR) of Italy, aims to explore the use of mussels as an effective real-time BEWS in rivers, with a particular focus on assessing the response of aquatic communities to a change of flow intensity during natural floods. In this regard, in the first phase of this study, by the years 2020 and 2021, some experiments were conducted on freshwater mussels (FMs) in the laboratory with a simplified frequency analysis in order to verify how mussels are reliable as bio-indicators of hydrodynamic stresses. In the second phase of this study, from year 2022, laboratory and field experiments with advanced signal analysis approaches were conducted. The field studies addressed both the technical challenges related to the installation of live organisms in the field and the interpretation of the data obtained within the complexity of real-world conditions. The transition from laboratory-controlled conditions to the field represented a challenge in the development of monitoring methodologies and protocols. First, the installation of a monitoring system to assess the effects of discharge dynamics on FMs' behaviour necessitated securing the mussels using cages and/or anchoring systems to prevent them from being displaced by the flow. Secondly, to prevent the packing of FMs against the downstream wall of the cage during high discharge, we deemed it advisable to secure the FMs to steel rods that are anchored *in situ* rather than allowing them to move freely in the substrate as done in the laboratory tests. The use of steel rods to anchor the FMs was required also considering that the river bottom of the field monitoring site was characterised by bedrock, which is not an ideal substrate for FMs. The need to immobilise the mussels in an unnatural position, as is commonly practised to monitor the quality of aquatic environments [103, 154, 174], may alter the behavioural responses compared to those of mussels that can freely move within the substrate. This aspect should be carefully considered when analysing the results.

With the overall aim of proposing and assessing the operational use of FMs as a real-time BEWS for hydrological disturbances in rivers, in this study, we address four main challenges to: i) understand the response of free-to-move FMs to hydrodynamic changes (Phase 1), ii) compare the behaviour of free-to-move and immobilised FMs in the laboratory in presence of discharge perturbances (Phase 2), iii) transfer the experience acquired from laboratory-controlled experiments to applications in real river conditions (Phase 3), and iv) define a robust signal processing methodology to analyse the valvometric data and assess the FMs' behaviour (Phase 4),

This chapter is extracted from my recent two papers [164, 144], which were published during my PhD program. It is structured as follows. Section 2.2 describes the laboratory experiments. An overview of the field monitoring site location and field experiments is present in Section 2.3. Section 2.4 provides an overview of the signal recording and analysis approaches. The results of the laboratory experiments and field observations can be found in Section 2.5. Finally, in Section 2.6 we discuss the results of the work and draw the final conclusions.

2.2 Laboratory Experiments

2.2.1 Experiments with Free-to-move FMs (Phase 1)

In the first phase of the study, *Unio elongatulus* species were collected in the mesotrophic Lake Caldonazzo, Italy (figure 2.1 a and b). Mussels after the collection were sent to the Hydraulics Laboratory of the University of Trento (Italy) for the flume experiments. On arrival at the laboratory, the animals were acclimated for two weeks in a 500 L recirculating flow-through aquarium with aerated water and gravel-sand substrate and fed with a mixed culture of natural algae as recommended by the biologists of the Enterprising project (figure 2.1 c,d, and e).

Table 2.1 summarizes the experiments with free-to-move FMs conducted during the study's first phase. The experiments were conducted in a single flume, as shown in figure 2.2(a) where a bed made of fine sand and silt (is the $d_{50} \sim 0.06$ mm in this case) as bed material and mussels were free to move, but only within the limits of the Hall sensors' cable that was attached to them. Free-to-move mussels can be displaced on the bed surface, under the bed, and also drift on the water surface during high discharge. 32 Free-to-move mussels were divided into four subgroups (8 mussels in each group), and each experiment was performed on all the groups. First, mussels were sorted in the flume (figure 2.2 b and c) with the lowest discharge (Q1) for 1 hour (acclimation), then were exposed to constant flow discharges (Q2, Q3, Q4) during 4 h, followed by a rapid increase of discharge without (from Q2 and Q3 to Q4) and with (from Q2 and Q3 to Q5 and Q6) sediment transport during 1 h and 30 min (Table 2.2).

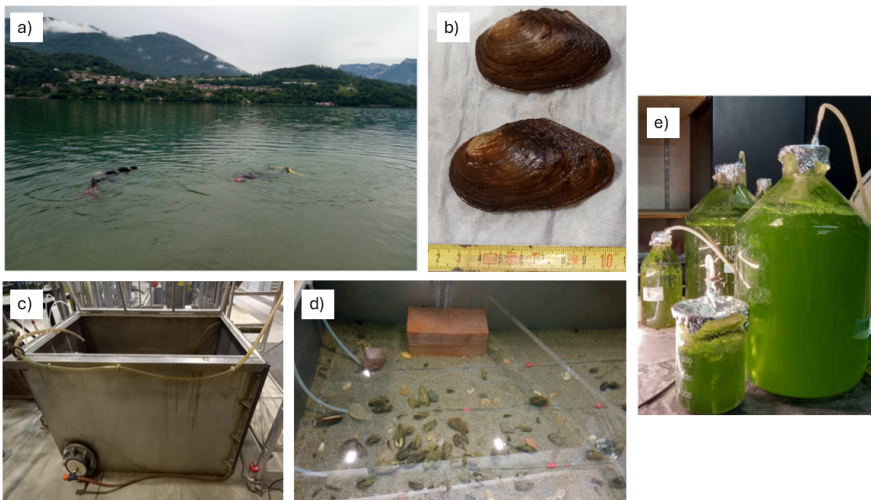


Figure 2.1: a) Sampling of mussels at Lake Caldonazzo (TN), Italy; b) Samples of *Unio elongatulus* species; c) and d) Side and plan views of Mussels' aquarium; e) Natural algae.

Table 2.1: Exposure scenarios of the hydrodynamic conditions considering: water flow rate Q/B (being B the width of the channel and Q the discharge); water depth; the cross-section averaged flow velocity; the specific solid discharge, Q_s/B (i.e. per unit of width); the Shields parameter [$\theta = u^*2/(s-\rho)d$ - being u^* the shear velocity and d the median sediment diameter] indicating the incipient sediment motion conditions.

Discharge	Q/B ($\text{m}^2 \text{s}^{-1}$)	Water depth (m)	Velocity (ms^{-1})	Q_s/B ($\text{kg}/(\text{ms})$)	θ
Q1	0.005	0.115	0.04	0	0.002
Q2	0.013	0.135	0.09	0	0.007
Q3	0.019	0.140	0.13	0	0.011
Q4	0.029	0.150	0.19	0	0.019
Q5	0.036	0.085	0.43	0.003	0.056
Q6	0.055	0.110	0.50	0.032	0.066

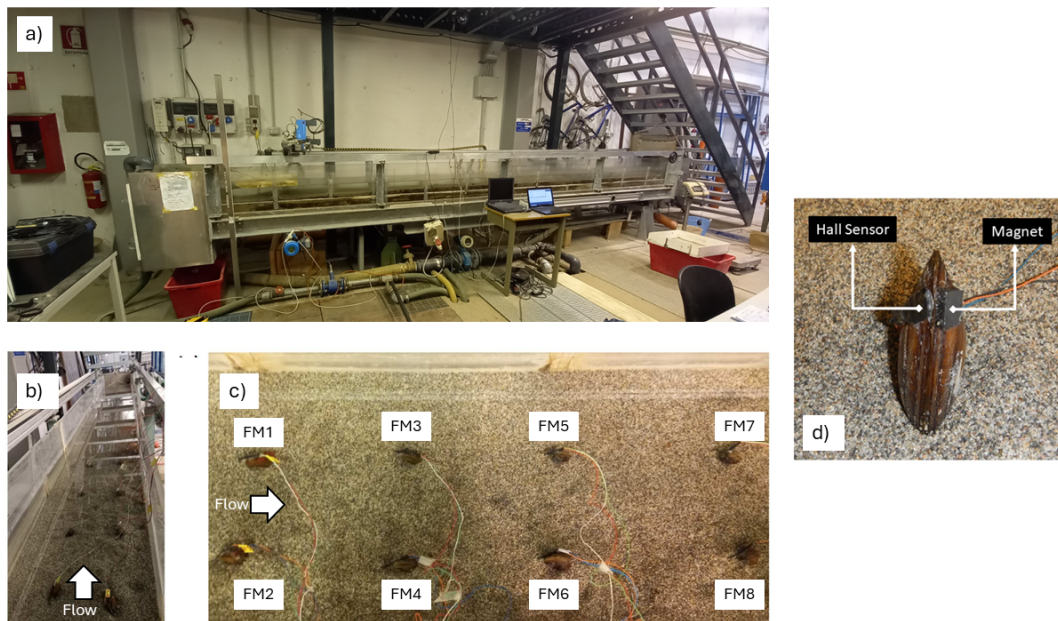


Figure 2.2: a) Experimental setup of free-to-move mussels in the laboratory; b) and c) Flow direction and plan views of mussels' arrangement in the flume; d) an example of FM equipped with a Hall sensor and a magnet.

2.2.2 Experiments with Immobilized FMs (Phase 2)

The second phase of the study was conducted in 2022. The *in situ* testing of FMs as a possible BEWS for flood events poses a number of challenges ranging from the selection of the field monitoring site to the choice of the most suitable system for FM installation. The exposure of the animals to the parameters to be monitored is one of the main operational challenges in

Table 2.2: Description experiments in phase 1

Variation type	Discharge	Sediment transport classes
Constant	Q1	-
	Q2	-
	Q3	-
	Q4	-
Small variation (SV)	Q2-Q4	-
	Q3-Q4	-
High variation (HV)	Q2-Q5	Low
	Q2-Q6	High
	Q3-Q5	Low
	Q3-Q6	High

natural environments. While for the monitoring of chemical contamination, it is possible to install the animals in lateral derivations of the watercourse or water pipes, for monitoring the responses of FMs to hydrological stresses (i.e., water velocity, turbulence, sediment transport) it is essential to expose the animals in the main channel of the watercourse. This requires installing the FMs in structures that are as transparent as possible to the flow, ensuring they do not substantially affect the natural flow pattern, and sufficiently stable to guarantee the integrity of both the FMs and the installation throughout the exposure [e.g., 102, 194]. For the sake of logistical convenience, the FMs are commonly fixed to solid structures such as steel rods, thus limiting their ability to move. Furthermore, it is important to note that FMs are frequently used in environmental conditions that may differ from their natural habitat, such as when using FMs accustomed to lentic waters in river environments [e.g., 128], as is the case in the present study. To assess the extent to which limiting FMs movement affects their behavioural response to environmental stress, a laboratory experimental comparison was carried out, analysing and comparing valve movements in both freely moving and immobilised animals on vertical rods.

In this phase, *Unio mancus* species were collected from Lake Montepulciano, Siena Province, Tuscany, Italy on March 29, 2022, and they were maintained in a tank filled with lake water. The mussels were divided into two groups, a group was installed at the field monitoring site in the afternoon of March 30, 2022 (Phase 3) (details of the field installation are given in Section 2.3), while the other group was sent to the Hydraulics Laboratory of the University of Trento (Italy) for the flume experiments (Phase 2). On arrival at the laboratory, the animals were acclimated for two weeks in a 500 L recirculating flow-through aquarium with aerated water and gravel-sand substrate and fed with a mixed culture of natural algae the same as Phase 1 experiments.

The FMs were exposed to the same external conditions for 24 hours. FMs from 1 to 4 were free to move, while the others i.e., from 5 to 8, were immobilised on vertical rods by glueing one valve to the rod, that was hung

vertically from the top of the flume (Figure 2.3 b and c). Free and immobilised mussels were positioned in the middle of the flume, sufficiently far from the upward and downward boundary conditions. After 10 hours of continuous discharge at a constant rate of Q_2 with 10 cm substratum (and without sediment transport), the discharge was instantaneously increased to Q_6 and maintained at this high value for 2 hours, before returning to the initial baseline value (Q_2). This baseline discharge has been kept constant during the rest of the experiment, i.e., for the following 12 hours. Additional information we sought during the experiments relates to sediment transport under different discharge configurations, as previous research has shown by the result of phase 1 of this study, which will explain in the following, that FMs are particularly affected by the presence of sediment transport. The baseline discharge of 5.3 L/s (Q_2) is characterised by negligible sediment transport, whereas the higher discharge of 22 L/s (Q_6) involves both bedload and suspended sediment transport. In the same previous study, the critical discharge, i.e. the value corresponding to the onset of sediment transport (also referred to as the incipient condition), was found to be around 14 L/s. Specifically, this is the discharge value capable of entraining the finest grains (~ 0.06 mm in this case) from the mobile bed mixture into the flow.

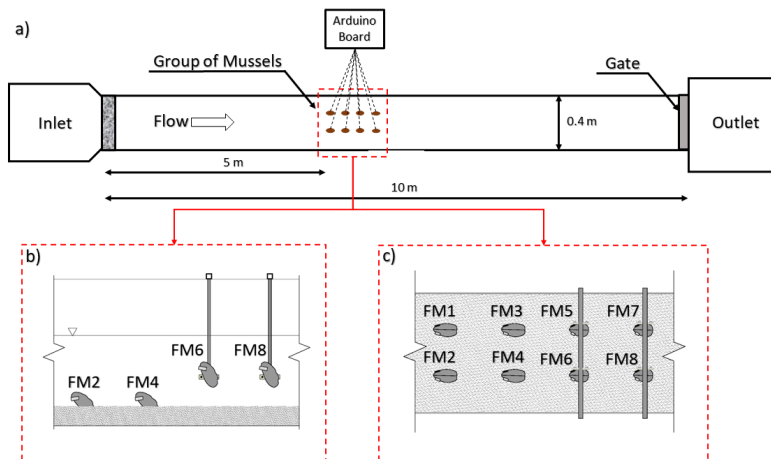


Figure 2.3: a) Experimental setup of immobilized mussels in the laboratory; b) and c) side and plan views of mussels' arrangement in the flume.

2.3 Field Experiments (Phase 3)

The field monitoring site is located along the River Paglia (Italy). The River Paglia (Figure 2.4a) originates in the southeastern region of Tuscany, specifically from Mt. Amiata (1738 meters above sea level). It is located in the central part of Italy and is one of the primary right-side tributaries of the

River Tiber. The River Paglia has a length of 86 km and its basin covers an area of approximately 1320 km². A painting of J.M.W. Turner (1775–1851), made during his journey to Rome in 1828, shows landmarks that remind us of snapshots of our fieldwork site: the towering city of Orvieto, the arches of a bridge, a flowing stream (presumably a tributary of River Paglia) and people at work with their hands in the water (Figure 2.4b). The monitoring system based on FMs was installed in the River Paglia at Orvieto city, under the Adunata Bridge, at the right bank of the river where the riverbed is rocky. A gauging station was available at this site for monitoring water level and discharge.

A preliminary survey of the river revealed that the native species of the area, *Unio mancus* [106], is locally extirpated. Therefore, specimens of the same species were collected from the neighbouring Lake Montepulciano, Siena Province, Tuscany, Italy (similar species used for the phase 2 experiments), and then installed at the field monitoring site in the afternoon of March 30, 2022.

At the River Paglia field monitoring site, thirteen FMs were fixed to vertical rods of the same type as those tested in the laboratory and installed in a cage secured at the riverbank. The use of steel rods was deemed necessary to mitigate the risk of FMs being displaced during flood events and due to the unsuitable bedrock substrate at the installation site. The cage was necessary to prevent damage to FMs and electronics. The cage has been designed to ensure robustness while minimising interaction with the flow. To achieve this, a thin steel frame covered by a coarse metal grid was used. The electronics for the valvometry recordings (see Section 2.4.1) were installed on the bridge above the riverbank where the cage was positioned. An overview of the installation is provided in Figure 2.5. A multi-parameter probe (OTT PLS-C) was installed at the FM cage site to measure water level, temperature and conductivity every 10 minutes. The FMs and multiparametric probe were in operation during a flood on 31 March 2022, which is the event analysed in this study.

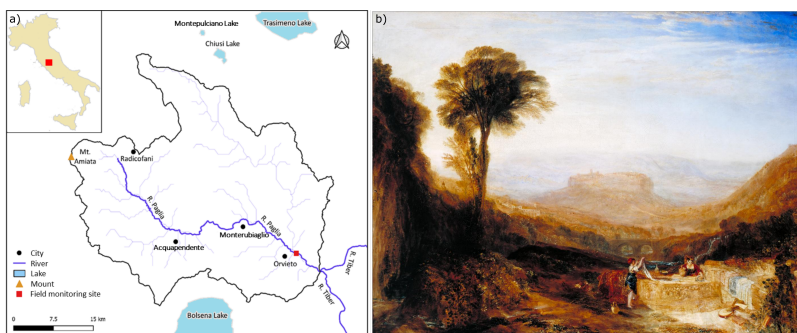


Figure 2.4: a) Map of the River Paglia and its catchment, showing the location of the field monitoring site and of Lake Montepulciano, where the FMs were collected; b) Joseph Mallord William Turner (1775–1851), *View of Orvieto*, Painted in Rome (1828, reworked 1830), © Photo: Tate, CC-BY-NC-ND 3.0.

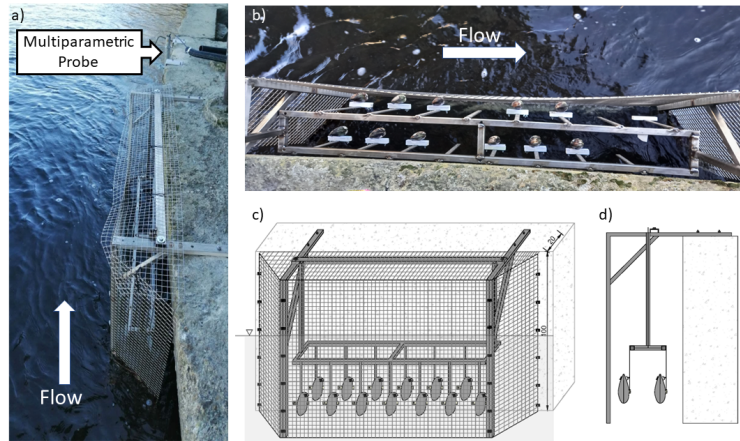


Figure 2.5: Field Installation - Enterprising pilot site, Orvieto City, Italy: a) overview of the FM cage, location of the multiparametric probe and flow direction; b) top view of the FM cage; c) front view (schematic); d) side view (schematic).

2.4 Data collection and Signal Analysis (Phase 4)

2.4.1 Valvometry data collection

In order to monitor the frequency and intensity of FMs gaping, different valvometry methods have been proposed for over one century [reviewed in 215]. In his pioneering work, Marceau [127] first used a kymograph (i.e., a rotating drum or moving paper strip onto which data is drawn as a function of time) to track the valve movement of mussels by attaching a balanced arm equipped with a scribe to one valve of the mussel. Electromagnetic induction to measure the valve displacement was first used by Schuring and Geense [181] and then further developed thanks to technological advancements. Wilson et al. [220] introduced the use of the Hall effect to record the valve movement of mussels. This approach requires installing a magnet on one valve and a Hall effect sensor on the other valve. The Hall effect sensor measures the magnetic field between the magnet and the sensor itself, which changes according to the distance between the two valves. In this way, both the frequency and intensity of valve gaping can be measured. When the mussel is closed, the magnetic field around the sensor is at its maximum, and when the mussel is fully opened the magnetic field strength around the sensor decreases due to the increased distance between the magnet and the sensor.

In this study, a Hall sensor (Honeywell SS495A1, 13×10.5 mm, 1.1 g weight) was glued on one side of the mussels' shell, a magnet (12×10 mm,

1.8 g weight) on the opposite side of the shell (see the right plot in Figure 2.2d). An Arduino board (Mega 2560) was used to record the response of the Hall effect sensor in mV, and then, by knowing the minimum and maximum values, the output was normalised and turned to percentage opening (see Section 2.4.2). An SD card connected to the Arduino was used to store the voltage values. In laboratory experiments, each mussel provided data at a frequency of 1 Hz, while in the field, due to a different set-up of the recording system, a frequency of 2 Hz was used.

2.4.2 Signal processing

Describing the behaviour of FMs in terms of the frequency and intensity of gaping using raw data expressed in mV may not be straightforward, because of inherent physiological variations among FMs, primarily influenced by their size and shape, as well as the nonuniform attachment of magnets and sensors to the individual FMs. For this reason, in order to have a common frame of response among all mussels, the opening signals were normalised between 0 to 100 %, employing linear scaling based on the minimum and maximum values recorded for each FM. Accordingly, 0% indicates that the mussel's valves are fully closed, and 100% that the mussel's valves are fully open.

In the first phase, a simple analysis was conducted, and after normalization, the valve gaping frequency of each FM behaviour was calculated using the statistical language Matlab (MATLAB software, 2010). For this analysis, we decided to turn the signals into smaller signals to have a better perspective of the changes. Thus, the signals before and after the discharge variation have been divided into 4 parts, which allowed us to divide the constant duration into 1-hour parts (C1, C2, C3, C4) and the variation duration into parts of 22.5 minutes (V1, V2, V3, V4).

For the second and third phases of the study, we were looking for a more robust and technical approach. The first step was to remove possible outliers due to occasional acquisition artefacts. In this context, outliers have been defined using the 0.1 and 99.9 percentiles as the lower and upper threshold bounds, respectively. The removed points were subsequently reconstructed through interpolation, and then the normalization was done as explained before. It should be noted that in order to effectively normalise a signal, the signal duration must be long enough to include both the fully closed and fully open periods of the FM. The resulting FM signals were analysed with the aim of identifying the occurrence of change points in the FMs' behaviour. As discussed in the Introduction, these changes may be linked to the normal behaviour of non-stressed FMs, but also to the response of these organisms to external perturbations. The monitoring of a sufficiently large number of FMs allowed us to discriminate between the specific behaviour of individual FMs driven by their own activity, and a systematic response of the FM community to external disturbances. Abrupt change points in the mean of the opening signals were identified using the Matlab function *findchangepts*, an iterative procedure that detects significant transitions in time-series data

through adaptive segmentation of the original time series. Parallel to abrupt changes in behaviour characterised by step-like discontinuities in the opening signal, it has been observed that when FMs are subject to stress they exhibit marked changes in both the frequency and intensity of their gaping. Here, the statistical analysis of the FM gaping frequencies was carried out using the Continuous Wavelet Transform (CWT), a mathematical technique that decomposes a signal into different frequency components. CWT is particularly useful when dealing with non-stationary signals. Indeed, unlike traditional Fourier analysis, CWT can capture both high and low-frequency variations in time-series data, making it especially effective for analysing signals that exhibit dynamic changes in frequency and amplitude over time [139, 169]. The CWT analysis is based on the convolution of a signal $f(t)$ with a set of functions $\psi_{ab}(t)$, known as wavelets, derived from translations and dilations of a so-called mother wavelet $\psi(t)$:

$$\psi_{ab}(t) = \frac{\psi}{\sqrt{a}} \left(\frac{t-b}{a} \right) \quad a, b \in \mathbb{R}, a > 0 \quad (2.1)$$

where a is known as the scale factor and b defines a shift in time. Different mother wavelets can be used to decompose a signal, all of which must meet specific conditions [see e.g., 139]. The convolution of the signal $f(t)$ with the set of wavelets is the wavelet transform:

$$T_{\psi}(a, b) = \frac{1}{\sqrt{a}} \int_{-\infty}^{+\infty} \psi^* \left(\frac{t-b}{a} \right) f(t) dt \quad (2.2)$$

where the superscript $*$ denotes the complex conjugate and $T_{\psi}(a, b)$ is the wavelet coefficient (which, for the sake of completeness, depends not only on a and b but also on the choice of the mother wavelet ψ). In this way, the signal $f(t)$ is analysed by comparing it to a set of wavelet functions ψ_{ab} characterised by continuously varying scale a and shift b . Unlike sinusoidal functions in Fourier analysis, these wavelet functions do not have a fixed frequency. Rather, they are versatile mathematical functions inherently flexible in both time and frequency domains, which adapt to the non-stationary characteristics of the signal being analysed. The scale factor a is inversely related to frequencies: smaller scales correspond to more "compressed" wavelets (thus higher pseudo-frequencies), and capture details in the signal at shorter time scales, while larger scales correspond to more "stretched" wavelets (thus lower pseudo-frequencies), capturing broader features at longer time scales. Note that the term pseudo-frequencies is often used to emphasise that these values should not be confused with the fixed frequencies associated with sinusoidal waves.

The results of the CWT analysis can be effectively visualised through the use of scalograms and pseudo-frequency (or scale)-averaged wavelet spectra. The scalogram is a graphical representation of signal power distribution across various pseudo-frequencies and through time. It is constructed by

considering the absolute value (or magnitude) of the complex wavelet coefficients introduced in Equation (2.2) and allows for a comprehensive examination of how different pseudo-frequencies and times contribute to the overall power of the signal. The pseudo-frequency-averaged wavelet spectrum provides a summary of the signal's energy distribution across multiple scales over time, offering insights into both localised and broad-frequency features present in the signal over time. The pseudo-frequency-averaged wavelet spectrum is obtained by scale-averaging the magnitude-squared scalogram over all scales. In this study, CWT was computed by applying the Matlab *cwt* function using the Morse wavelet as the mother wavelet to the time series signal of each FM, after the removal of abrupt changes in the mean of the opening signal. Identifying and removing step changes in the mean of the signal was necessary to avoid introducing spurious results. In fact, when a CWT decomposition is performed on a signal with an abrupt step change, the result is a mixture of high-frequency components that capture the abrupt transition and lower-frequency components that describe the smoother and more gradual changes in the signal, across the entire frequency spectrum. The presence of abrupt changes would generate an artefact in the resulting scalograms and pseudo-frequency-averaged wavelet spectra, possibly hindering the interpretation of the informative features of the signal. Step change removal was achieved by detrending the segments of the signal between two successive step changes (identified as discussed above), i.e. by subtracting the mean and removing the linear trend, hence without altering the informative, high-frequency content of the original signal.

Similar to the signal pre-processing described above, in order to get a consistent frame of reference, the scalogram of each FM was normalised between minimum and maximum values after the removal of outliers. This allows us to effectively appreciate the existence of coherent features across FMs and characterise them in terms of dominant pseudo-frequencies and position in time. In order to obtain a synthetic summary of the results, the normalized scalograms obtained from the wavelet analysis of all FMs were combined into one, corresponding to the median scalogram. The summary pseudo-frequency-averaged wavelet spectra was obtained from the median scalogram.

2.5 Results and Discussion

2.5.1 Laboratory results

Figure 2.6 illustrates the frequency analysis of Phase 1 experiments. Frequency analysis revealed no significant differences in gaping frequency at constant (0.0132 ± 0.00744 Hz) and small discharge variations without sediment transport (from Q2 and Q3 to Q4; 0.0177 ± 0.00473 Hz) (Table 2.1 and 2.2). Above this threshold (0.0256 ± 0.00660 Hz), the increase of discharge prompted the sediment transport (from Q2 and Q3 to Q5 and Q6), and the reaction of FMs passed from the normal behaviour with constant valve gaping

frequency to a variable behaviour. Indeed, significant increases in valve gaping frequency (0.0308 ± 0.00428 Hz) were observed immediately after the onset of high discharge rates with sediment transport, i.e. from the period C4 of constant discharges (Q2 and Q3) to the period V1 of high discharges (Q5 and Q6).

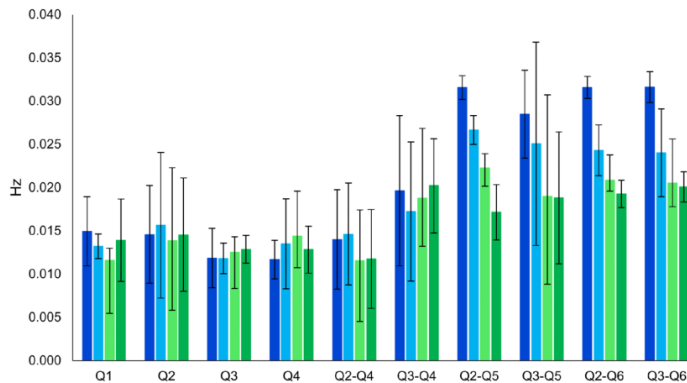


Figure 2.6: Mean (\pm SD) valve gaping frequency (Hz) of 32 FMS behaviour experiments with constant discharges (Q1, Q2, Q3, and Q4) and variable discharges (Q2–Q4, Q3–Q4, Q2–Q5, Q3–Q5, Q2–Q6, and Q3–Q6). The different experimental periods C1, C2, C3, and C4 in constant discharges and V1, V2, V3, and V4 in variable discharges are represented by dark blue, light blue, light green, and dark green bars, respectively.

based on the finding of the primary results, FMs respond to the hydrodynamic changes in the laboratory which means there is hope for evaluating the impact of external stressors on aquatic ecosystems directly by using biotic communities as real-time indicators. In this direction, the second phase of the study was based on new experiments with immobilised FMs. Figure 2.7a shows the median opening signal of free and immobilised mussels separately measured during the 24-hour laboratory experiment along with the 25th and 75th percentiles. The evolution of discharge in time is also shown in the second y-axis. The figure clearly shows that both groups of FMs responded to the discharge increase, 10 hours after the start of the experiment, with a sharp and localised change in the median opening (thick coloured lines). By examining the shaded area of this plot (representing the 25th and 75th percentiles), it becomes evident that, in general, the signals from free FMs exhibit a more complex and varied behaviour compared to that of immobilised FMs. Indeed, the shaded area for the free FMs is much thicker compared to that of immobilised FMs, if we analyse the periods away from the discharge perturbation. This is explained by the fact that the former group displayed a larger number of features, most of which did not appear to be directly related to hydrodynamic changes. By instance, the decrease in the median opening of free FMs after 6 h after the start of the experiment is only apparent and not related to a consistent response across the four free FMs,

but rather to independent and uncorrelated activities of the organisms. This is further evidenced in Figure A.1 in the Supplementary Material, which illustrates the distinctive behavioural patterns exhibited by each FM and the major discontinuities in the mean of the signal. However, during the perturbation (from 10 hours to 12 hours after the start of the experiment), the width of the shaded area (25th-75th percentiles) shrinks and matches that of the immobilised FMs, indicating a coherent response across the four free FMs.

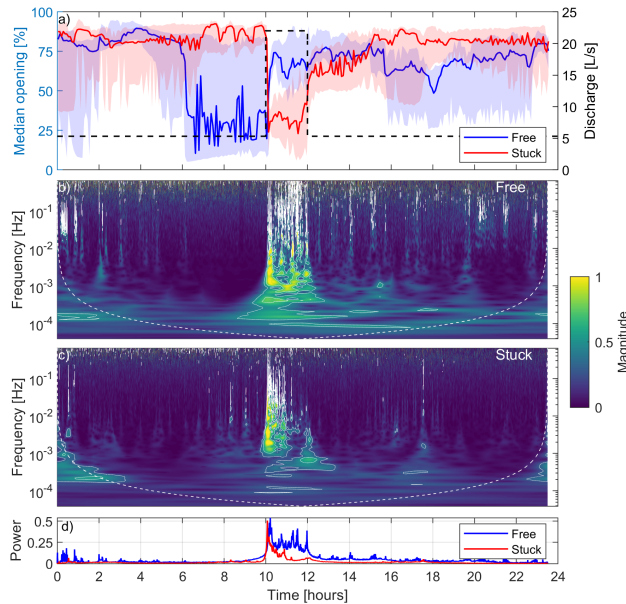


Figure 2.7: Laboratory experiment: a) left y-axis: median valve opening signals of free and immobilised mussels with 25th and 75th percentiles indicated by the shaded area; right y-axis: discharge (dashed, black line); b) scalogram showing the median normalised magnitude of the continuous wavelet transform over all the free FMs; c) scalogram showing the median normalised magnitude of the continuous wavelet transform over all the immobilised FMs; d) pseudo-frequency-averaged wavelet spectrum. White contours in b) and c) represent the 95th and 99th percentiles of the CWT coefficient.

The distinction between the two groups of mussels arises from the restricted mobility of immobilised FMs in contrast to free FMs, as behaviours such as walking and drifting are not possible, resulting in a more straightforward signal. Notably, all immobilised FMs responded by closing their valves when the discharge increased, while two out of the four free FMs responded with an increase of the opening (FM1 and FM2) and one with a decrease (FM4; see Figure A.1). Apart from exhibiting some noise, likely arising from electrical issues, which, however, did not significantly impact the results, the free FM3 displayed behaviour similar to that of FM4. While both free and

immobilised FMs responded clearly and promptly to the rapid increase in discharge, as evidenced by the change in the mean valve opening discussed above, only immobilised mussels displayed a similar response upon the re-establishment of the base flow (12 hours after the start of the experiment), albeit to a lesser extent compared to the signal variation the mussels exhibited when the flow increased (Figure 2.7a and Figure A.1).

Moving beyond the analysis of mean valve opening, however, a distinct signature of the discharge perturbation is discernible in both free and immobilised FMs through the occurrence of broad-frequency features localised over time around the perturbation period (see the period between 10 and 12 hours in Figures A.1 and A.2, the latter showing the signals after detrending and removal of changes in the mean valve opening). Such features are more clearly appreciable when looking at the scalograms of free (Figure 2.7b) and immobilised (Figure 2.7c) FMs. Prior to the increase in discharge (from the beginning of the experiment to 10 hours), the FMs' gaping was characterised by low pseudo-frequencies (below 10^{-3} Hz) with less energy. However, following the increase in discharge, they promptly began responding across the whole range of pseudo-frequencies (up to 1 Hz), displaying higher energy levels (as indicated by the more yellowish regions). The white contours on the scalogram plot represent the 95th and 99th percentiles of the CWT coefficient and were used to emphasise the energy-rich areas. The response is similar between free and immobilised FMs, although immobilised FMs adapted quicker to the new discharge conditions compared to free FMs. This is evident also looking at Figure 2.7d, which shows the pseudo-frequency-averaged wavelet spectrum for both FM classes: immobilised mussels' power returned to normal an hour after the discharge increase, followed by free mussels who responded with high power until the end of the event (two hours after the discharge increase). In both cases, the dominant pseudo-frequencies, after the discharge variations, reset to values consistent with those characterising the first part of the experiment.

2.5.2 Field results

Because laboratory experiments showed overall consistent responsiveness between free and immobilised FMs in the presence of hydrodynamic stresses, this supported the suitability of installing immobilised FMs in the field. Figure 2.8a illustrates the signals of the thirteen immobilised FMs at the field monitoring site along the River Paglia (see Figures 2.4 and 2.5) from 10 PM on March 30, 2022 until midnight on April 1, 2022. It should be mentioned that there is a gap of an hour and a half in the data for all FMs, with missing signals from mussels between 10.5 and 12 hours since the start of the signal (i.e., between 8:30 AM and 10:00 AM on March 31) due to unspecified technical issues. According to this plot, all FMs except for mussels numbered 2, 3, and 12 experienced a marked shift in the mean valve opening with a generalised closing of the valves approximately 5.5 hours after the start of the time series, specifically around 3:30 AM on March 31, coinciding with a flood event in the river. As can be observed in the data, the sensor installed

on FM2 experienced technical issues, preventing its use in the analysis. On the other side, the sensors installed on FM3 and FM12 were operating normally but the FMs were already closed before the flood event (likely because they were in the state of resting, see Introduction), hence not displaying any additional closure but a minor and progressive opening and gaping. All the other ten FMs were characterised by normal behaviour before the flood event, with their valves open and characterised by regular valve movements as expected during respiration and filtration.

In general, in terms of change in the mean valve opening, the mussels responded similarly to changes in hydrodynamic conditions as observed in the flume experiment and illustrated in Figure 2.8b, which depicts the median valve opening signal of the FMs (all individuals except FM2) in relation to the changes in water level measured by the multiparametric sensor every 10 minutes (see also Figure A.3). The median valve opening shows two main discontinuities, which coincide with marked changes in the water level line. The first discontinuity is evident at 5.5 hours from the start of the time series (i.e., at 3:30 AM), when the water level, as measured by the multiparametric sensor, rapidly increased from 0.3 m (corresponding to about 4 m³/s) to 2 m (corresponding to about 140 m³/s, based on the data from the official gauging station, available every 30 minutes). This rise in water level marked the onset of the flood event, which was characterised by a sharply rising front. The associated discontinuity in the valve opening signal is clearly visible when examining both the individual FM signals (Figure 2.8a) and the median signal (Figure 2.8b). The second discontinuity clearly emerges only by looking at the median signal (Figure 2.8b), while it is hindered in the individual time series. It occurred at about 23 hours after the start of the time series (i.e., at 9 PM), when the water level rose from 0.6 m (approximately 18 m³/s) to 1 m (approximately 45 m³/s), thus interrupting the previously gradual decrease in water level following the initial peak.

The FMs response to the hydrodynamic disturbance, as reflected in changes in the frequency of gaping, is shown in the scalogram of Figure 2.8c. This plot is obtained excluding FM2, which was affected by the technical issues discussed above, and for the sake of clarity also FM7 and FM13, respectively characterised by intense activity before the flood and a significantly damped response after the flood, to an extent that was not in alignment with the behaviour of the other FMs. These mussels are labelled with * in Figure 2.8a (and in the corresponding Figure S4 showing the signals after detrending and removal of changes in the mean valve opening). As indicated by the scalogram, the mussels exhibited responses at a low frequency (below 10⁻⁴ – 10⁻³ Hz) before the peak of the flood, displaying signals of lower energy. As soon as the level raised, parallel to the sudden closure of the valves seen in Figures 2.8a and b, the FMs showed a generalised response shifted towards higher frequencies (up to 0.1 Hz) and characterised by higher energy levels (yellowish regions). This response gradually diminished as the discharge decreased, resulting in lower frequencies and reduced energy levels. Between 15 to 23 hours from the beginning of the time series, the water level, and consequently the discharge, transitioned into the latter phase of

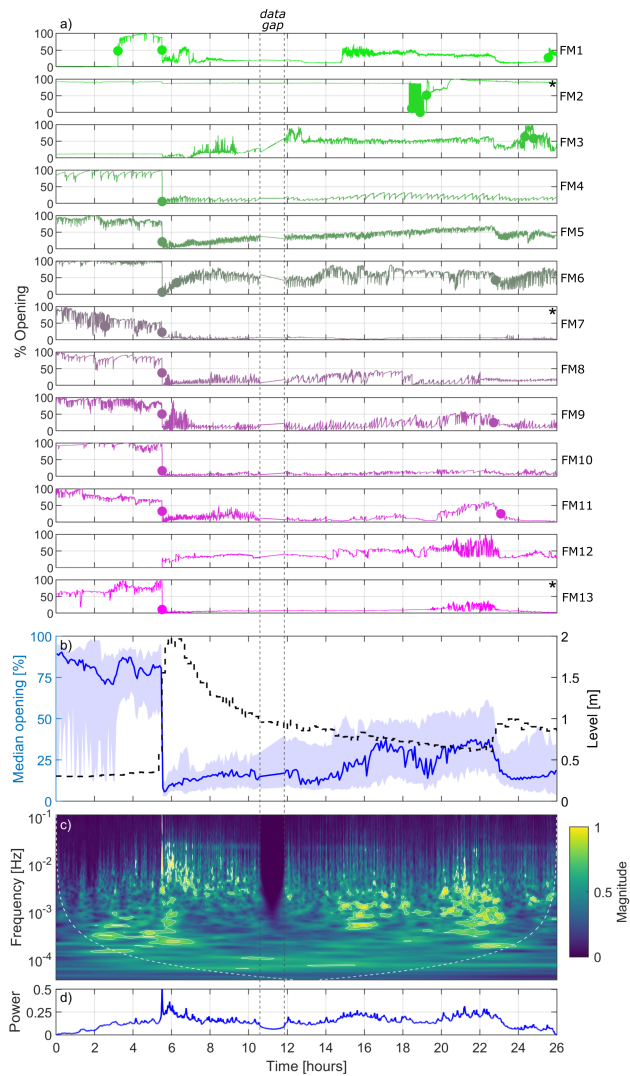


Figure 2.8: Results from the thirteen FMs deployed at the River Paglia field monitoring site during the flood on March 31, 2022; a) valve opening signals for the individual FMs (dots indicate abrupt change points in the mean of the opening signals when the mean opening changes by more than 25%; the asterisk * depicts FMs that are excluded from the wavelet transform analysis); b) left y-axis: median valve opening signals with 25th and 75th percentiles indicated by the shaded area (all FMs except FM2); right y-axis: water level (dashed, black line); c) scalogram showing the median normalised magnitude of the continuous wavelet transform over the FMs; d) pseudo-frequency-averaged wavelet spectrum. White contours in c) represent the 95th and 99th percentiles of the CWT coefficient.

the flood event, characterised by minor fluctuations over time. Additionally, water temperature and conductivity steadily returned to higher values and stabilised (see Figure A.3). During this time window, the FMs underwent a slight opening of the valves (Figure 2.8b) and intensified their gaping around frequencies of 10^{-3} Hz (Figure 2.8c). Following the occurrence of the second, smaller peak in water level (approximately 23 hours after the start of the time series), all FMs closed their valve once more (Figure 2.8b) and the majority of them exhibited a significant decrease in the frequency of gaping (Figure 2.8a and c). The overall picture is summarised also in the pseudo-frequency-averaged wavelet spectrum shown in Figure 2.8d, which clearly indicates the instantaneous evident response of the FMs to the main perturbation, similar to what was observed in the laboratory experiments.

2.6 Conclusion

Based on the results of primary laboratory experiments which show that FMs respond to the hydrodynamic perturbation, we proposed FMs as effective BEWS for assessing the impact of hydrodynamic stresses on the aquatic ecosystem. In this study, for the first time, FMs were deployed and evaluated in real river conditions, in the River Paglia at Orvieto, Italy. The initial challenge we faced was securing the mussels in place and preventing them from being carried away by the river's current. In consideration of other *in situ* exposure methods [e.g., 102, 194], we opted to glue the mussels to vertical rods anchored at the riverbank. To ensure that the use of immobilised mussels did not significantly alter their behavioural responsiveness, we conducted controlled laboratory experiments to confirm that immobilised and free mussels exhibit consistent reactions under the same hydrodynamic stressors.

The results demonstrated that immobilised and free mussels behave in a consistent way during a hydrodynamic perturbation, but the signals of the immobilised mussels exhibit less complexity, primarily due to the reduced number of features resulting from movement constraints (Figure 2.7). Consequently, these signals can be more easily interpreted and associated with perturbations in external conditions. In fact, immobilised mussels have limited means of response, primarily relying on gaping, as they are unable to engage in actions such as escaping or burying themselves more deeply. It is worth noting that concerning mussel behaviour classification, both free and immobilised mussels showed avoidance behaviour by immediately closing their valves and changing their gaping frequency at the onset of the higher flow levels. However, immobilised mussels showed a faster adaptation in response to a prolonged stimulus, facilitating the faster restoration of pre-event gaping frequencies. This could be explained by the positive correlation between the intensity of the stimulus and the degree of adaptation [38, 87]. In fact, immobilised mussels experience a stronger stimulus than free mussels due to the impossibility of actively searching for shelter at the time of the event, and as a result, they have a shorter adaptation period most likely because they get tired sooner. Overall, based on the laboratory comparison, we

could confidently assert that the installation of immobilised mussels in real river conditions ensures both site stability during floods and the representativeness of the results. This is particularly true in the context of using FMs as real-time BEWS, which requires timely detection of significant changes, while other information such as response type and duration may be of interest for deeper biological interpretation, but is not the primary concern.

Field data acquired at the field monitoring site in the River Paglia provided a solid validation of the effectiveness and reliability of using immobilised mussels as part of a real-time BEWS. All the FMs exhibited a synchronised and highly distinct response to the flood event that occurred during the monitoring campaign, promptly transitioning their behaviour in terms of both mean valve opening and gaping frequency. Of paramount importance for practical applications is the observation that these mussels responded immediately as the discharge increased, effectively detecting the flood at its very onset. These results confirm and validate what has been observed in the laboratory. The sharp and rapid mussel reactions can be explained by the almost abrupt rise in water levels and discharges of the flood, and also by the fact that, as in the flume experiments (see Section 2.5.1), the discharge values around the peak triggered sediment transport and turbidity. To establish for the River Paglia an incipient (alias critical) discharge value, we exploited the shear-stress distribution relative to the flood on May 31, 2022, determined by a 3D Reynolds-Averaged Navier-Stokes (3D-RANS) model described in Bahmanpouri et al. [14], and some bed material samples we collected from the bed surface just upstream and downstream of the Adunata Bridge site. With a constant flow discharge corresponding to that observed at the flood peak, the numeric shear stress distribution reached a maximum of about 100 Pa under the bridge, and smaller values away from the bridge. Looking at the numerical results, a reference value of 30 Pa is exerted over a large part of the flow domain. From the bed material sample, we found that the d_{90} (i.e., diameter corresponding to the 90th percentile of the granulometric distribution) of the sediments forming the substrate of the bed is about 0.01 m. With these values, the well-known dimensionless Shields stress number $\theta = \tau / [(\rho_s - \rho_w)gd]$ (where τ is the bottom shear stress, ρ_s (ρ_w) is the sediment (water) density, g the gravitational constant, and d the characteristic particle diameter), reached a value of about 0.6 at the discharge peak, well above the critical one, which can be assumed equal to about 0.06, as in many references [see e.g., 157]. According to the 3D-RANS model, a critical discharge for the initiation of bedload in this reach of River Paglia (Adunata Bridge) corresponds to about 4 m³/s. The ratio, in terms of peak flood-discharge over the critical value, is therefore about 35 (i.e., 140/4), whereas in the flume experiments, the mussels experienced a discharge about 1.6 times larger than the critical one (i.e., 22/14), as from the data reported in Section 2.5.1. Our laboratory and field results show that the responsiveness of the mussels is efficient in a wide range of peak/critical discharge ratios.

To improve the interpretation of behavioural signals, we proposed a statistical analysis based on the combined identification of abrupt change points in the mean of the opening signals and application of continuous wavelet

transform to the detrended time series after removal of these discontinuities (refer to Figures A.2 and A.4 to view the cleaned signals). This approach has proven to be a robust and reliable tool for FMs' signal processing, able to effectively identify the animals' response to external stressors. This identification can be achieved both visually, through the examination of scalogram plots, and quantitatively, through the generation of associated pseudo-frequency-averaged wavelet spectrum plots. For the sake of comparability, the scalogram of each FM was normalised between minimum and maximum values after the removal of outliers. Then, the median scalogram was calculated and used to identify dominant pseudo-frequencies and their temporal positions. This approach enables comparisons within the same frame of reference between different FMs and between median scalograms obtained under various conditions (e.g., in the laboratory and in the river). Similarly, the pseudo-frequency-averaged wavelet spectra derived from the median scalograms can be fairly compared to discern shared patterns and distinctions across the various setups. Notably, results from both the laboratory and the field indicate that during external stress events (i.e., an increase in discharge), the power of the spectrum reached and exceeded a value of approximately 0.25. While further data collection from additional sites is needed before proposing a threshold value as a simple indicator of aquatic ecosystem stress, these findings underscore the effectiveness of combining FM valvometry and CWT processing towards the establishment of real-time operational BEWS.

The utilisation of FMs in real riverine conditions did present logistical challenges. While the monitoring station at the River Paglia was operational for several months, the data acquired only covered the occurrence of a flood. The lack of significant events during the monitoring period and the mortality of some FMs prevented the acquisition of additional data that would have been valuable for the analysis. Additionally, during the monitoring activity after the flood event occurred on March 30, 2022, it happened that metal particles occasionally suspended in the water, likely originating from an upstream mine, accumulated on the magnets installed to the FMs, thus altering the valvometric signal. In addition, the extrapolation of laboratory results to natural conditions should take into account the greater variability of boundary conditions concerning the parameter being monitored. The response of the mussels is an expression of their reaction to changes in multiple conditions that can only be controlled and restored to previous conditions in the laboratory (and even then not completely). In this respect, the increased activity in terms of energy content at the highest frequencies observed at the end of the descending phase of the flood observed in the River Paglia (see Figure 2.6c and d, between 20-23 hours) cannot be explained based on the available measurements. For example, the water temperature (see Figure A.3) should not be influential, since it was always below the tolerance threshold of the eurythermal generalist species we used and showed minor changes during the period analysed (about 1.5 °C). It is likely that other environmental variables, such as turbidity or specific FM behaviour after a long disturbance, were involved. For these reasons, efforts to expand the dataset for a more comprehensive analysis are planned and underway, and further

studies should be conducted to deepen the behavioural characteristics of the FMs in the field, investigate the limitations of the method, and develop protocols addressing them appropriately.

The results obtained pave the way for the utilisation of the valvometry technique and of the signal processing framework presented here in operational BEWS in different contexts. Freshwater mussels can serve as indicators to quantify the impact of both natural stressors (e.g. heat waves, droughts) and anthropogenic stressors (e.g. hydropeaking, reservoir flushing, chemical contamination) on the aquatic ecosystem. As such, they can be instrumental in reporting the impacts of climate change on water resources and in the management and permitting processes implemented by local authorities. Future research should focus on extending the investigation of the responsiveness of freshwater mussels to other stressors (e.g. turbidity, temperature, chemicals) and on verifying the effectiveness of the signal processing technique presented here in identifying possible synthetic indicators related to different stressors.

In summary, based on the above insights the following conclusions can be drawn:

- both free and immobilised freshwater mussels can serve as effective ecosystem warning indicators in aquatic environments, with the choice between them depending on the riverbed and flow rate conditions;
- immobilising the mussels to support constrains their behaviour, but this results in sharper event detection compared to free mussels and easier interpretation of the signals;
- continuous wavelet transform proves to be a valuable tool for interpreting the FMs signals. It is effective in identifying pseudo-frequency features present in the signal over time and describing the response of FMs to external perturbations, providing more informative results than only looking at discontinuities in the opening time series;
- laboratory and field experiments with immobilised mussels demonstrate their response to hydrodynamic stresses within a frequency of valve gaping ranging from 10^{-3} Hz to 1 Hz. This frequency range is larger than the background frequency range during normal behaviour (around 10^{-4} – 10^{-3} Hz when taking the median across multiple individuals). These frequency values correspond to conditions that indicate the presence of stressful conditions for the FMs, thus underscoring the potential use of FMs as real-time BEWS for identifying potential threats to the aquatic ecosystem;
- the comparison between pseudo-frequency-averaged wavelet spectra obtained in the laboratory and in the field suggests the potential introduction (subject to further data acquisition) of a simple indicator based on power values to detect disturbances in the aquatic environment.

Chapter 3

Towards the Development of an Affordable and Practical Measurement Device for Turbidity and Stream-bed Monitoring

3.1 Introduction

Sediment is a set of naturally occurring particles that are broken down from rocks by weathering and erosion or formed by natural chemical processes or biological processes [108]. Typically, sediment transport refers to the movement of organic and inorganic particles in a moving medium, such as water [213]. Sediment, as well as larger particles, can be transported at greater rates when the flow rate is higher. During sediment transport in waterways, particles can be suspended in the water column or simply pushed along the bottom [63]. Generally, sediment transport can be divided into three types based on the characteristics of the streamflow and carried material, as well as the watershed: bed loads, suspended loads, and wash loads [79]. In a bedload, the force of the water flow is sufficient to overcome the weight and cohesion of the sediment, causing the sediment to move like roll, slide, or bounce along a waterway's bottom [138]. In the stream, some of the smaller and lighter particles can be pushed up into the water column and become suspended. Moreover, suspended sediment in equilibrium in the bed can change its concentration as a function of flow intensity. On the contrary, there is a fine fraction of the suspension which is not in equilibrium with the bed and is called washed-load. May not necessarily remain suspended if the flow rate decreases [172]. Wash load is a subset of suspended loads. A wash load differs from a suspended load in that it will not settle to the bottom of a waterway during periods of low or no flow [132]. Quantifying sediment

transport and deposition in the aquatic environment is essential for a better understanding of geomorphology and ecosystem health. Due to the high variability and complexity of sedimentary processes, the correlation between modelling results and field measurements may not always be satisfactory.

Several studies demonstrate the multiple benefits of monitoring, from determining turbidity levels and understanding scour/deposition patterns to identifying sediment-related hazards. Topczewski et al. [206] and Klingeman [100] both emphasize the importance of understanding the nature of scour around bridge piers, with Topczewski specifically discussing the use of mobile and fixed devices for monitoring. Fisher [64] provides a comprehensive review of scour monitoring techniques, highlighting the potential of a novel device that uses turbulence in open channels. Mueller and Landers [150] focuses on the development of instrumentation for measuring scour during high-flow conditions, with a particular emphasis on the use of fathometers. These studies collectively underscore the significance of effective monitoring in assessing the potential for scouring and maintaining water quality. Clare et al. [48] emphasizes the importance of monitoring platforms for understanding turbidity currents, suggesting design modifications to improve their resilience. Sutherland, Brampton, and Whitehouse [200] discusses the monitoring and prediction of toe scour at seawalls, highlighting the need for suitable timescales and the use of remote sensing. Howes, Lemckert, and Moss [90] underscores the significance of long-term monitoring in assessing water quality and understanding estuary processes, particularly in the context of turbidity in the Brisbane River. Skarbøvik and Roseth [193] explores the use of sensor data for water quality monitoring, demonstrating its effectiveness in detecting high values of suspended sediments and other parameters. Various engineering projects utilize these monitoring efforts, such as designing check dams to mitigate erosion and evaluating sediment impact on bridge pier stability and also water quality based on turbidity measurement. Adapting monitoring approaches based on sediment transport types and objectives allows researchers and practitioners to manage sediment-related risks effectively and support sustainable development in aquatic environments. To monitor sediments, different methods are utilized, with a particular focus on assessing streambed elevation changes to understand scour and deposition, as well as measuring turbidity to understand suspension load. In terms of monitoring streambed changes, some different discontinuous methods and technologies have been introduced include using erosion pins [70, 197], Surface Elevation Table (SET, [32]), Sedimentation Erosion Bar (SEB, [214]) and levelling (e.g. total station theodolite and differential GPS, Silva et al. [188]). The elevation can also be determined with great spatial coverage through the use of airborne laser altimetry (LiDAR), photogrammetric and Structure from Motion (SfM) techniques [141, 67, 124]. There have been numerous automated instruments developed over the years for continuously measuring sediment surface dynamics and turbidity, such as the PhotoElectronic Erosion Pin (PEEP) sensor developed by Lawler [111], resistive rods developed by Ridd [171], acoustic bed-level sensors [4], and fiber Bragg grating [119]. In addition to these methods, the

use of acoustic sensors, such as ALTUS [71], ADV (Acoustic Doppler Velocimeter) and PCADP (Pulse-Coherent Acoustic Doppler Profiler) [222, 99], solid electromagnetic properties [140] and Surface Elevation Dynamics (SED, [92]). As the newly low-cost developed methods, we can mention the methods based on temperature and light intensity. The thermal scour-deposition chain (TSDC) method uses temperature as a tracer to monitor streambed erosion and deposition [120, 183, 205]. TSDC is similar to a technique used for measuring seepage flux associated with surface water-groundwater exchange and hyporheic flows [83, 110, 134, 195], and it is based on the analytical solution of the one-dimensional heat transport equation in a semi-infinite domain [54]. Another cost-effective method is using infrared LED and three photodetectors as Matos et al. [133, 132] used. They used an infrared LED and three photodetectors with three different positions related to the light source—135°, 90° and 0°—resulting in three different types of light detection: backscattering, nephelometry and transmitted light, respectively. Using this design, it is possible to monitor in almost any type of environment, offering a wide dynamic range and high accuracy for low and high turbidity or suspended particulate matter (SPM) levels. An in-lab calibration of the sensor was made to establish a relation between SPM or the NTU to the photodetectors' electrical output value in Volts. In light of the fact that low-cost monitoring instruments present promising results and are cost-effective and widely accessible, they have attracted the attention of many researchers. Drawing inspiration from seminal works such as the Arduino-based water analysis [107, 135, 55], researchers have showcased the viability of employing Arduino-based platforms for turbidity measurement. Trevathan, Read, and Schmidtke [210] recalibrated an appliance sensor (DF Robot SEN0189 Gravity - also attenuation style) and designed a waterproof housing for deployment in the field. Although their test measurements were between 0-20 Nephelometric Turbidity Units (NTU). Further, they were unable to overcome the influence of ambient stray light on their sensor's data. In following of using the DF Robot turbidity sensor, Mokua, Ciira, and Kiragu [145] connected to a wireless network system which easily helped them access the data in a cloud drive. In this field study, the reported data was lower than 150 (NTU) which compares the turbidity during the flood event is significantly low. In 2022, Droujko and Molnar [55], created a sensor which detects scattered light from an LED source using two detectors in a control volume, which can be placed in a river. Two sediment types were used in a mixing tank experiment in which our sensor was compared to multiple commercial turbidity probes over a wide range of typical river concentrations. As a result, they were able to measure turbidity between 0 and 4000 NTU or 0 and 16g/L with precision and reproducibility. Their sensor can also be used directly as a suspended sediment sensor without the need to calibrate to Formazin. In addition to being much cheaper than existing options of comparable quality, the developed sensor was designed in particular for distributed sensing across a network of rivers.

This chapter conducted within the framework of the Enterprising PRIN Project (2017), aimed at the development of two affordable and practical

systems for continuous real-time monitoring of streambed scour/deposition and turbidity. In this regard, this work marks the next phase following the aforementioned laboratory tests. It addresses the technical challenges related to assembling and designing the system and sensors' waterproofing. The main monitoring system is designed using an Arduino board used as a data logger with two different innovative low-cost, low-power types sensors, one is a vertical BED-sensors (Bed Elevation Dynamics) string based on Light Dependent Resistor (LDR) to obtain the data about the Scour/Deposition in any fluvial environments, the second one is the new design of DFRobot turbidity sensor for the turbidity measurement. In this study, we address two main challenges: i) build a cost-effective and practical waterproof housing for the sensors, and ii) define a robust approach to analyse the signals. This chapter is structured as follows. Section 3.2 provides an overview of the sensor's design and also describes the laboratory installation and experiments, and then analyses approaches. In section 3.3, we show the results of the work and draw the final conclusions in section 3.4.

3.2 Methodology

3.2.1 Design of monitoring systems

An Arduino Uno Rev3 board was used as a data logger in each monitoring device, which is commonly used for sensor measurements. To enable the system to record data over a prolonged period of time, a clock and a data storage device must be implemented. Micro SD and a Real-Time Clock (RTC-DS1302) module were connected to the Arduino for real-time data storage. The light-dependent resistor (LDR) used to build the BED-sensors string was NSL-19M51, and the turbidity sensor was the DFRobot Gravity analogue turbidity sensor. The Arduino board is capable of supporting six sensors, but more sensors can be added by improving the board. For the BED-sensor string, two Arduino boards were synchronized and used to collect the data from 12 LDR sensors, whereas one Arduino was used for the turbidity device. As the first challenge of this study was to create waterproof housing for both types of sensors, several different waterproof housings for both sensor types were tested in the lab. Figure 3.1 shows the sensor housing that was selected for both monitoring systems during the experiments. In terms of cost, ease of assembly, and material availability, these designs were the best among other designs. Based on the fact that the analogue input of Arduino is converted to digital values in such a way that the maximum 5 Volts are equal to 1024. Therefore, the output of an Arduino board with any connected sensor may range from 0 to 1024[-] or 0 to 5 Volts. Depending on the sensor and application, outputs can be converted into any measurement unit. In this study, the raw output of Arduino, ranging from 0 to 1024 [-], was used for the BED-sensors string gauge. For the turbidity gauge, the raw outputs, ranging from 0 to 5 Volts, were turned into the Nephelometric Turbidity Unit

(NTU). This required a calibration procedure, which is described within the laboratory experiments section 3.2.2.

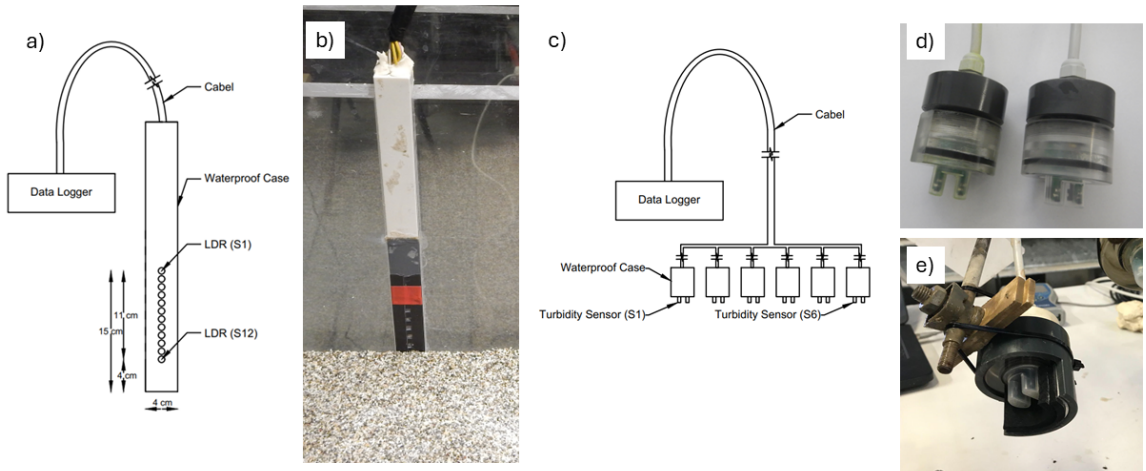


Figure 3.1: Final sensor designs: a) BED-sensors string design, b) installed BED-sensors string in the flume with showing 5 sensors upper than bed surface level, c) turbidimeter design, d) two turbidity sensors fixed in waterproof housing, e) one waterproofed turbidity sensor fixed in the shielded pipe.

3.2.2 Laboratory Experiments

The experimental investigation was conducted in two groups, with continuous real-time monitoring of streambed scour/deposition using BED-sensors string (B-series tests) and turbidity monitoring with low-cost turbidimeters (T-series tests), at the Hydraulics Laboratory of Trento University (Italy) in a flume with 10 (m) length and 0.4 (m) width (figure 3.2a). The experimental details will be explained in the following:

Deposition/Scour Tests

As a part of this study, we introduced and evaluated a new type of BED-sensors string based on LDR for different applications such as Check dams and bridge piers while considering the position of the sensors string to the flow directions (opposite to the flow direction and perpendicular to it) (figures 3.2 and 3.3). The LDR sensor's response to bed surface changes was validated by analyzing pictures taken with one camera (30 frames per second) placed perpendicular to the flume in the monitoring area (30 frames per second). By using MATLAB (MATLAB software, 2023R), we were able to extract the bed surface line frame by frame, which allowed us to calculate the elevation of the bed in front of the BED-sensors string over time.

Following this, the bed elevation over time was compared with the bed elevation obtained by the string of BED-sensors. According to table 3.1, four experiments were carried out with fine sand and silt ($d_{50} \sim 0.06$ mm) as bed material in a laboratory flume to test the performance of the BED-sensors string. For the first experiment, Check dam (B-Test1), the BED bar was embedded in the flume wall without protrusion (Figure 3.2). The operator of the channel maintained the bed elevation between S10 and S11 (the last two sensors under the bed) (see figure 3.1a) as normal bed elevation and kept the gate at the end of the flume closed, then the water discharge was increased to turn the fixed bed into mobile, leading to the formation of dunes with the height ranging between S2 and S3 (by keeping the first two sensors, S1 and S2, out of the bed). Once the bed surface was stabilized between S2 and S3, when the dune passed the front of the BED-sensors string, the gate at the end of the flume was suddenly opened (like a dam break) to decrease the bed elevation. In order to test the performance of the BED-sensors string for the second application, bridge piers, the string was fixed on two different shapes and three different positions (Figure 3.3). In the experiments with piers, the flow pattern around the piers was assumed to be symmetric, therefore, half the longitudinal of the piers was made as shown by figure 3.3. The vertical string was embedded in the piers' body and then fixed to the flume's wall (with protrusion) (figure 3.2). During these experiments (B-Test2,3, and 4) only scour (decrease in streambed elevation) was addressed. Hence, the operator began with a bed elevation between S2 and S3 (the first two sensors out of the bed) and then increased the discharge for the bed elevation to reach between S10 and S11 (the last two sensors under the bed).

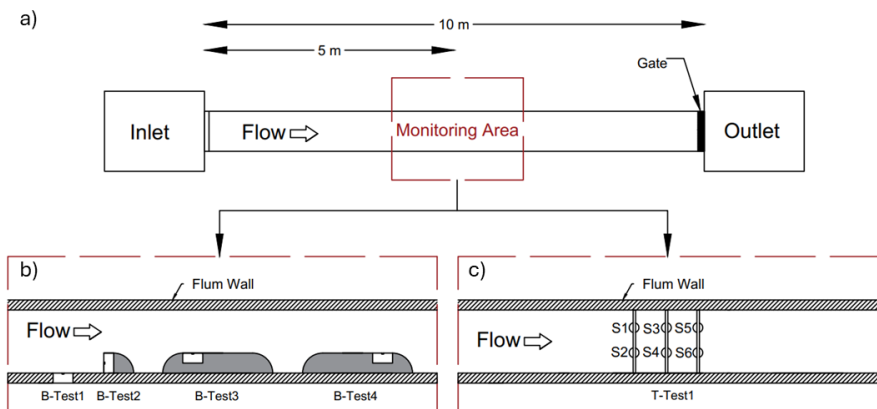


Figure 3.2: a) Experimental flume setup; b) plan views of BED-sensors string setup in the flume; c) plan views of turbidimeters setup in the flume

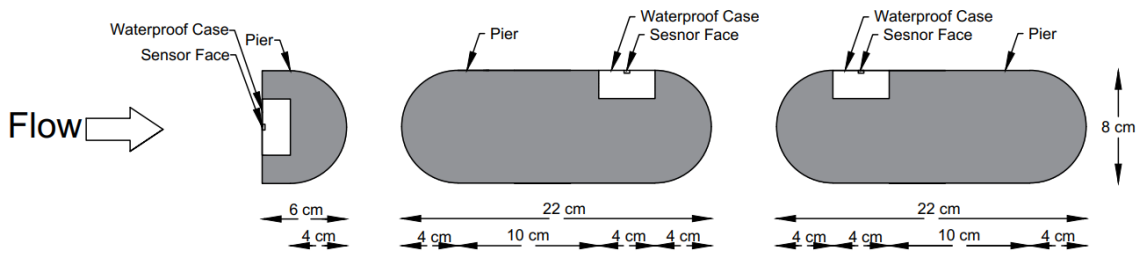


Figure 3.3: Different designs of Piers with the BED-sensors string; from the left to the right: B-Test2,B-Test3,B-Test4

Table 3.1: BED-sensors string setup for the experiments

Experiment type	Name	Sensor face position to flow direction
Check dam	B-Test1	Perpendicular
Pier1	B-Test2	Opposite
Pier2	B-Test3	Perpendicular
Pier2	B-Test4	Perpendicular

Turbidity Calibration and Tests

Turbidity monitoring systems do not directly display NTU as a standard measurement unit. The standard solution Formazin was used to extract the correlation function between Volt and NTU for each turbidity sensor. According to Table 3.2, a 5-point calibration was conducted using Formazin 4000 NTU. For the preparation of solutions, a 200 (ml) flask was filled with the necessary volume of Formazin (Table 3.2) and the remaining volume was filled up with distilled water. For one minute, each sensor was immersed in the solution with data recorded every 2 seconds (0.5 Hz). In order to determine how temperature environments affect sensor response in the laboratory and field (for future work), calibration was performed at 2 different temperatures (4°C and 16°C), the first with a cold liquid (4°C), and the second at a normal laboratory temperature (16°C). During calibration, one well-calibrated industrial turbidimeter was used to verify that the solution liquids had the correct value. Following the calibration experiment, we determined the Volt value corresponding to the NTU value and found the correlation functions for each sensor. After calibration, for the main turbidity experiment (T-series1), sensors were sorted in the flume as shown in figure 3.2. Once the turbidity sensors (figure 3.1c, d, e) were submerged in the water, random amounts of green clay were added to the water from the beginning of the flume to increase its turbidity. Following the 9 steps of increasing

turbidity, the channel operator increases the flow discharge to increase the quantity of clean water in the flume water circulation to reduce turbidity. A well-calibrated industrial turbidimeter was also installed in the flume to validate the data obtained by the sensors during this experiment.

Table 3.2: Calibration concentrations based on 4000 NTU Formazin standard solution with 200mL flask

Concentration (NTU)	Volume of Fomazin (mL)
0	0
25	1.25
100	5
500	25
2000	100

3.2.3 Analysis Approaches

Deposition/Scour Tests

The analogue input ranging from 0 to 1024 was used in these experiments. A lower value indicates that the sensor was placed in the dark, while a higher value indicates that the sensor detected more light. The crucial part of the experiment was determining the threshold value, the boundary between darkness and light in the laboratory. Before starting this experiment with BED-sensors in the flume, all the sensors were buried in the bed material to find this threshold. Once the bed material was removed from the monitoring area, the maximum values for each sensor were determined. Based on the minimum and maximum values for each sensor, we were able to normalize the sensor responses from 0 to 1. In this sense, a value of 0 indicates that the sensor is completely buried, which means that the elevation of the bed is higher than the elevation of the sensor, while a value of 1 indicates that the sensor is out of the bed, meaning that the elevation of the bed is lower than the sensor. It is also reasonable to assume that when the sensor value is close to zero the bed surface is located near the sensor or the sensor is placed in an active bed layer.

The images captured by the camera installed along the side of the flume in the monitoring area were analyzed using Matlab's image analysis toolbox (2023R). By using this approach, each frame is divided into two colour segments (one for the bed and one for the water) and by using an edge detection algorithm, the line between the two segments is determined to be the bed surface line (see figure 3.4b, c). Due to the fact that the camera captured the frames from the side or back of the BED-sensors string (the waterproof housing was not transparent), there is a discontinuity in the extracted line (figure 3.4c). It was necessary to connect the last left point and the first right point in the missing data area using four different scenarios as shown in figure 3.4c in order to obtain the bed elevation in front of the LDR sensors. For the first scenario, the last left point and for the second scenario, the first

right point were taken as reference points, and the bed elevation in front of the LDR was assumed to be at the same level as the left or right point. It should be noted that these two scenarios did not work for all experiments, but for B-Tests 2 and 4, the left value was the benchmark, and for B-Test 3, the right value was the benchmark. In the third scenario, the left and right points are interpolated linearly. Although this works, when the crest of the dune is behind the BED-sensors strings or when the distance between the left and right points is significant, this approach is not precise. In the last scenario, the right and left lines followed their own slopes until they crossed at the intersection point. This approach based on intersection points mostly works for experiment B-Test1. We tested all possible scenarios for each experiment and selected the best one based on the application. Consequently, seven different bed surface lines were identified for each deposition/scour test, four lines based on four image analysis scenarios and three lines based on BED-sensors string indicating the line based on the response of LDR sensors and lower and upper bound lines based on the resolution of the sensor string (with a vertical distance of one cm between the sensors).

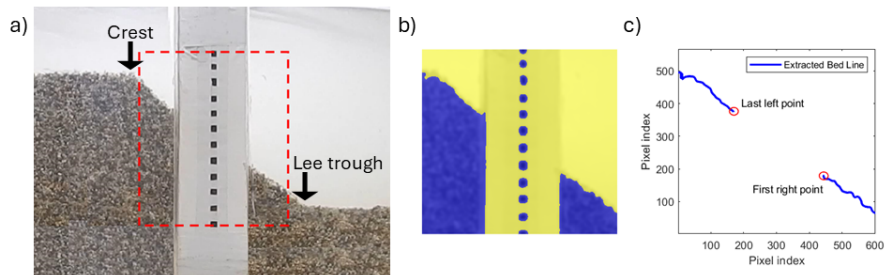


Figure 3.4: An extract of the bed surface line in one frame: a) Original frame, b) colour segments, c) Extracted line based on pixel index.

Turbidity Tests

In order to determine the correlation function (NTU-Volt), MATLAB's Curve Fitter Toolbox (2023R) was utilized. As recommended by the sensor manufacturer, a polynomial fit type (degree 2) was used in this study.

3.3 Results and Discussion

3.3.1 Scour/Deposition Experiments

Herein, to be concise, we will analyse the check dam (B-Test1) experiment and only one experiment of the bridge's pier (B-Test2), among the three piers. In Figure 3.5, 5 different frames at different time steps of the B-Test1 experiment show dune movement (frames 1 to 3) and dam break (frames 4 and

5). As explained in section 3.2.2, the experiment started with a stable bed elevation ranging between S10 and S11. By rapidly increasing the flow discharge, the operator formed an approximate 9 cm high dune, which means that the streambed elevation reaches between S2 and S3. In this case, the sensors were buried one by one from S10 to S3 (figure 3.5, frames 1 to 3).

After completing the first part of the experiment (e.g., increasing the bed elevation), the operator of the channel suddenly removed the gate installed at the end of the flume, such as the dam break, in order to reduce the elevation of the bed surface (figure 3.5, frame 4 to 4). In Figure 3.6, a set of four subplots is presented, each corresponding to one image analysis scenario, illustrating the detected streambed elevation by BED-sensors string, as well as the upper and lower bounds. Upper and lower bounds are basically lines 1 cm above and below the line extracted by sensors. In the check dam experiment (B-Test1) with step-by-step elevation increase, figure 3.6 clearly illustrates that the lines extracted from the frames and by the BED-sensors string are closely related. In the second part of the experiment, when the bed surface rapidly descends (dam break), there is a time gap between the lines obtained by frame analysis and the string obtained by sensors. The sensor string shows the decrease in the streambed elevation before frame analysis (by seconds), which indicates the frame analysis method based on the colour detection counts the sediment active layer as the bed. When the sensors are placed in the sediment active layer, a value greater than zero indicates the sensor is out of the bed in the analysis based on LDR sensors. We cannot expect the lines to overlap when there is an active layer, since the LDRs do not consider the active layer as a fixed bed due to the presence of light, and on the other hand, frame analysis detects similar colour between a fixed bed and a mobile bed. In considering which frame analysis scenario is most accurate and reliable for this experiment (B-Test1), it is important to note that it is highly dependent on the position of the crest and lee trough of the dune (figure 3.4), as outlined below:

- all the scenarios, when the crest and lee trough points both are on the left side of the sensor housing;
- only scenario 4, when the crest point is on the left side of the sensor housing and and lee trough point is behind it;
- scenarios 3 and 4, when the crest point is on the left side of the sensor housing and and lee trough point on the right side of it;
- only scenario 4, when the crest point is behind of sensor housing and lee trough point on the right side of it;
- all the scenarios, when the crest and lee trough points both are on the right side of the sensor housing;

In view of the above items, it is evident that the correct elevation of the bed surface for the check dam experiment can always be determined by scenario number 4.

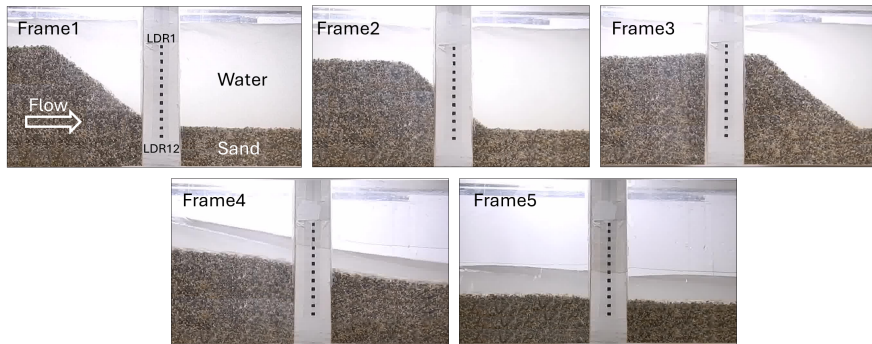


Figure 3.5: 5 time-series frames showing an increase (frame1 to frame3) and decrease (frame and frame5) in streambed elevation in front of BED-sensors string

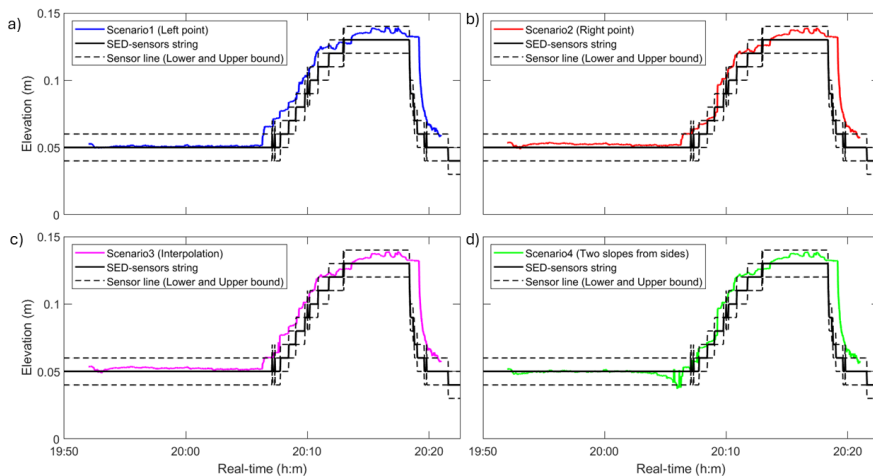


Figure 3.6: Extracted bed surface line based on the BED-sensors string and Frame analysis: a) BED-sensors string versus Scenario1; b) BED-sensors string versus Scenario2; c) BED-sensors string versus Scenario3; d) BED-sensors string versus Scenario4

Following the check dam experiment, the B-test2 experiment was conducted. Fig. 3.5 shows three time-series frames of this experiment. Frames 1 and 3 show the start and end of this experiment, whereas frame 2 shows a random frame during the flume run. The operator started this experiment with bed elevation ranging between S2 and S3 (the first two LDRs were out of the bed), then by increasing the flow discharge gradually, the scour around the pier was started. then by continuing to open the value of water till the streambed elevation stays between S2 and S3. In the B-test2 experiment, as shown in Figure 3.3, the face of LDRs was opposite to the flow direction. Therefore, scenario 1 represents the best solution because it represents the

exact elevation of the bed surface in front of the sensors. Figure 3.8 demonstrates the results of BED-sensors string and frame analysis of the scour experiment (B-Test2) based on only scenario number 2. Based on the results of this experiment, it appears that the BED-sensors strings can be successfully used in piers. From the beginning of the experiment, the line extracted by frames is between the upper and lower bounds and overlaps with the line obtained by BED-sensors string. However, after the scours began, sensors showed a lower bed elevation than the frame analysis, so by that time two lines stayed in the same domain until the experiment ended. After reviewing the recorded video footage of the experiment, this hypothesis confirmed that sediment stuck to the flume wall during scour formation and the real bed surface (in front of the LDRs) was lower than the streambed at the flume sides, and by increasing the discharge in time in order to increase erosion around the pier, the horseshoe vortex and down flow became stronger, washing the side flume walls, which is the main reason that after a while the bed line extracted by the frames back to domain between upper and lower bounds.

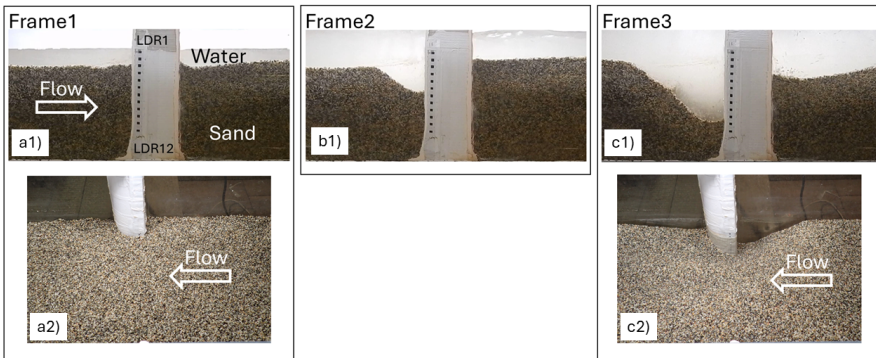


Figure 3.7: 3 time-series frames showing scour around the pier (B-Test2): a1, 2) frame 1 showing the bed elevation condition at the beginning of flume run from two different side views; b1) frame 2 showing the bed elevation condition at a random time step during flume run from a side view; c1, 2) frame 3 showing the bed elevation condition at the end of flume run from two different side views.

3.3.2 Turbidity Experiments

Figure 3.9 shows the fitting curve and correlation functions according to the 5-point calibration experiment for two different temperatures. During the calibration, sensor number 2 was not in service due to a technical problem, so we continued with the remaining five sensors. Each turbidity sensor responded differently to each turbidity concentration, highlighting the importance of collaboration sensors separately. As well, these graphs demonstrate that these low-cost sensors respond differently to different temperatures at

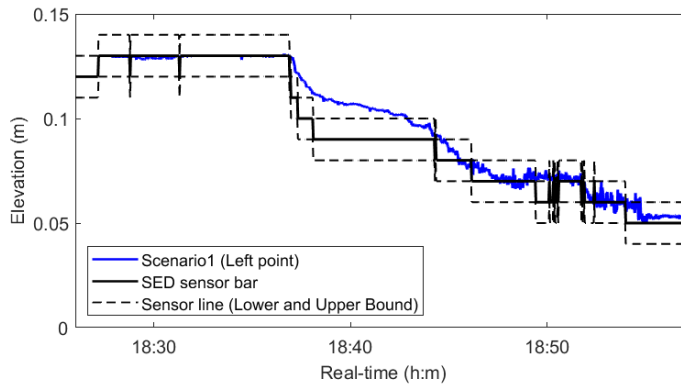


Figure 3.8: Extracted streambed line based on the BED-sensors string and Frame analysis (Scenario1)

the same concentrations of turbidity. Regarding starting the main experiment, We performed it as explained in Section 3.2.2 with a water temperature of around 16°C ($\pm 2^{\circ}\text{C}$), so we could consider the correlation function obtained with calibration at this temperature. Figure 3.10 shows the T-Test1 experiment's result with some steps in the increase and decrease of turbidity. This figure clearly illustrates that the low-cost sensors demonstrated step-wise behaviour both in increasing and decreasing turbidity during the experiments in the same manner as the expensive turbidimeters. The low-cost sensors did not have a good match and convincing overlap with expensive turbidimeters from the beginning. By the time, in the higher turbidity values, sensors show more acceptable responses than in the beginning. As it is clear, these sensors are not precise in low turbidity and more reliable at high turbidity which one of the reasons can be the calibration approach. By having more points and turbidity concentration at low turbidity, probably this part will be correct. Only sensor number 6 responded differently than other sensors by showing lower values, which can be related to the way that water was turbidized (random amounts of green clay were added to the water at the beginning of the flume, which was not thoroughly mixed in the flow), or the position of sensors in the flume. According to these results, the affordable device for the measurement and monitoring of turbidity shows the potential of the device, but it needs to be improved more for laboratory work as well as in the field.

3.4 Conclusion

The purpose of this chapter was to introduce and evaluate two practical and cost-effective measurement devices for turbidity and streambed scour/ deposition. It was an original idea to develop a streambed scour/deposition

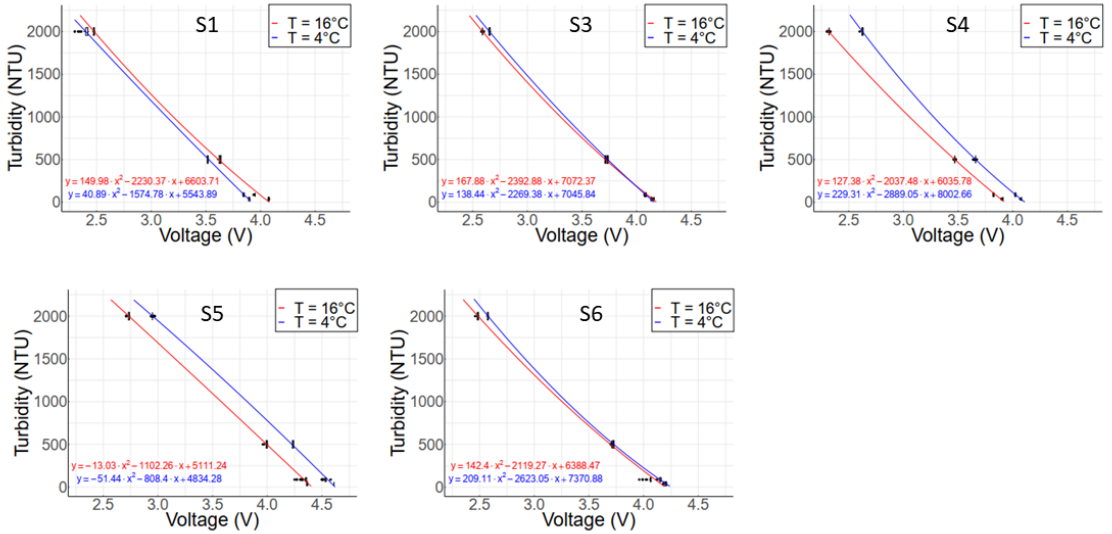


Figure 3.9: Calibration results showing the correlation functions between NTU and Volt for two different Temperature

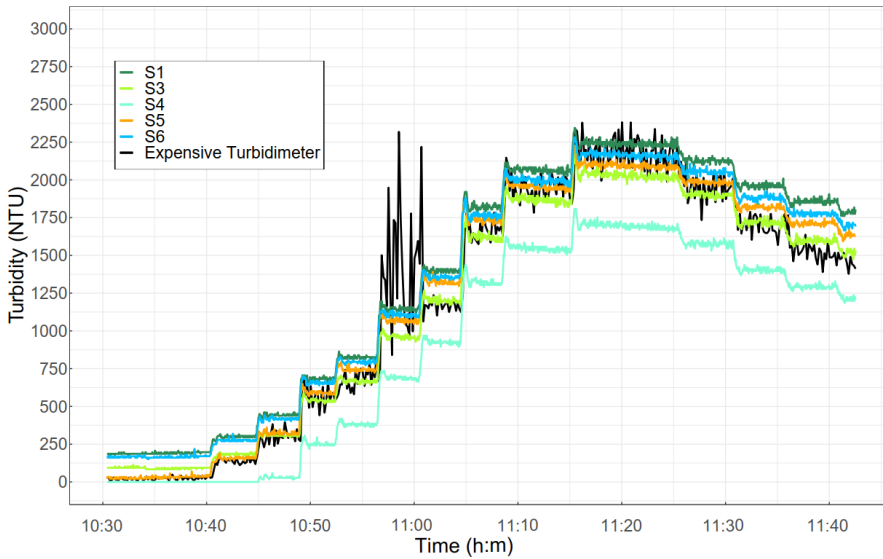


Figure 3.10: Result of T-Test1 with 5 low-cost turbidity sensors in the flume.

monitoring system using LDRs, which was developed, and tested in the laboratory, but the turbidity sensors used in this study were introduced in previous works, however, in this study, the design and assembly of the system have been improved with the potential of use in the field. The following

items can be mentioned as key research results and some suggestions for future works:

- a new BED-sensors string based on LDRs has been introduced and successfully tested in the laboratory for different applications such as check dam and pier of bridge dealing with streambed scour and deposition. A promising result indicates that this device can also be used in the field;
- a new turbidimeter based on low-cost turbidity sensors has been introduced with a new design and waterproof housing. this device was successfully calibrated and then tested in the flume with different turbidity stages (increase and decrease in flow turbidity). A promising result at high turbidity indicates that this device can be used in the laboratory and field and with an improvement in the calibration method, the device also can be reliable in low turbidity;
- the new BED-sensors string based on LDRs proved based on the present study that can be used in the field studies, but the designs of waterproof housing must be improved and equipped to the light source to remove the effect of day / night light on the sensor results;
- based on the present study, a new turbidimeter based on low-cost turbidity has been proven to be used in field studies. However, the sensors are not equipped with a wiper (expensive turbidimeters are equipped with a wiper), so the sensor cover will become dusty after some time, and the results will not be reliable unless the cover is cleaned regularly. Since we are still working on this device and trying to use it in field settings, I am pleased to inform you that we have found a temporary, yet cheap and environmentally friendly solution to keep the sensor's cover clean for approximately one to two weeks, depending on the turbidity of the flow stream.

Chapter 4

An Entropic Approach to Ordinary Bedload applied to Flume and case studies

4.1 Introduction

In far and recent years, theoretical and experimental studies have continuously been conducted on sediment transport in rivers and torrents. Sediment transport is a fundamental process in nature, governed by complex momentum and energy exchanges between water and solid phases, also involving particle collisions. Turbulent eddies in the liquid phase are strongly modulated by the suspended grains, or by their rolling and jumping over the bed, in a way that is still not fully understood. Several research works have been conducted to investigate the characteristics of sediment transport under different flow conditions [1, 44, 204, 224, 175, 221, 104, 112, 13, 93]. Ordinary and intense bed-load represent the two transport regimes that are focused on in this work and are characterized by the random movements of isolated particles, or by the formation of a sheet layer of moving particles (over the mobile or rocky bed), respectively. Monitoring bed-load transport in the field can be logistically onerous, costly, time-consuming, and affected by several uncertainties, especially during high flow conditions [53, 122, 125]. It has been the focus of scientists for the past several decades to develop reliable approaches for monitoring and evaluating morpho-dynamic changes with minimization of the effort in terms of cost, time, and physical activity in the field. Sime, Ferguson, and Church [189] discussed the calculation of bed shear stress based on the ADCP data. The authors tested various alternatives for estimating local bed shear stress in the lower Fraser River in Canada by using the logarithmic law of the wall and ADCP transects. By contrasting estimations from the outbound and return boat tracks, repeatability and accuracy were evaluated. According to the results, the most reliable method utilized a zero-velocity height according to the characteristics of the bed grain size, and a vertically averaged mean speed. In Mao et al. [125], it was analyzed

the effective slope, which is a fraction of the topographical slope to be associated to the bed load. They considered sediment transport data collected over 2014 and 2015 at Estero Morales, central Chilean Andes based on inter-day surveys of tracer displacement. They utilize passive-integrated-transponder tracers (PIT tags are transmitters without batteries) that emit an identification code by radio which are embedded in the sediment. They developed probabilistic distributions of resting times and flight distances of particles by exploiting the measurements and a generalization of the Einstein theory [59]. Guterres et al. [78], also used acoustic methods to quantify bedload transport in rivers, including the Acoustic Doppler Current Profiler (ADCP), the Dune Tracking Method (DTM), and Hydrophones. Based on the results of this study, it can be concluded that hydrophones represent an efficient and accurate tool for the evaluation, through the analyses of the signals, of the bedload fluxes in rivers. An Acoustic Mapping Velocimetry (AMV) method was proposed by Muste et al. [151] for determining the characteristics of bed load transport in the field. By using a dune-tracking method (DTM), AMV may be employed for characterizing the shape and dynamics of the bedform and estimating bed load transport rates. Because the AMV protocol is unique and relies heavily on numerous site-specific assumptions and user-defined parameters, an assessing comparison is presented in Muste et al. [152] between this new methodology and three existing non-intrusive DTM-based methods and analytical predictors. Among the outcomes of the Enterprising PRIN Project (2019), funded by the Ministry of Education, University and Research of Italy (MIUR), Modesto et al. [144], Termini et al. [203] and Pilbala et al. [164] developed biosensors for evaluating the inception of sediment transport processes (or their ceasing), testing them in controlled laboratory flows and applying afterward the system in real conditions. Based on frequency analysis of mussel valve gaping (opening and closing sequence), these studies demonstrated that freshwater mussels can be used as a reliable bioindicator to provide information on rapid changes in the discharge. However, it is still unclear how multiple external sources, such as flow velocity and bedload rate (but more ones could be considered, such as polluted suspensions), with or without sediment transport, can affect biotic communities in aquatic ecosystems. Developing hybrid theories by combining existing ones, can also yield a significant contribution to the interpretation of sediment transport. They typically require some specific field data to eventually evaluate the bedload transport. Following this line, we introduced the entropy theory in the context of ordinary bedload. The entropy theory is commonly used to get the velocity distribution of transects in clear water river flows [43, 45, 196, 46, 148, 202, 192, 57, 15, 14]. It was also applied to predict the location of the velocity dip [142], always in clear water river flows, or to get the concentration profiles of turbulent suspension of fine particles in plain rivers [131, 130], or the concentration profiles of collisionally suspended coarse fractions in steep torrent, e.g., in sheet and debris flows [118, 191].

Together with entropy theory, we adopted the Einstein statistical approach to the description of ordinary bedload. In particular, we utilized the fundamental Einstein's conjecture, stating that, for a specific sediment type, grain

displacements, in ordinary bed-load regime, have a mean value independent of bedload rate. This milestone concept opens a way to use the entropy theory to shed light on the resting-time statistics, as we have described in the paper. We applied this approach to three flow conditions, namely to experimental and field data, that offered us chances for various theoretical interpretations. The first flow condition is the laboratory experience described in Fraccarollo and Hassan [68]. They developed an analytical interpretation of the data by considering the effects of grain entrainment and deposition on the images. Their results showed that for a specific sediment type (they used almost identical particle analogues) and bed slope, grain displacements had a mean value independent of bedload rate, as suggested by Einstein [59]. We moved on from their results and inferred how the entropy theory can be applied to produce statistical information on resting times. The probability distributions derived from the experimental data and the entropic ones match satisfactorily.

Two real flow domains have been further considered. In the former, a major river in Italy, we had the chance to use ADCP flow data and applied extensively the entropy theory, to both the liquid velocity field and the particle resting times. We show how from topographic data and some unintrusive measurements (the flow velocity at the surface, for instance), it is possible to obtain information about sediment discharge and particle movement statistics. In the latter case, a small catchment, endowed with glaciers, feeds a steep stream presenting a complex bathymetry with macro-roughness, very different from the previous case. The challenge here was to include the grain-size distributions in the approach, which ended up with a deep revision of the Einstein conjecture when the moving grains have a poorly sorted distribution.

This chapter is organized as follows: Section 4.2 is devoted to the presentation of the case studies and relevant datasets. Section 4.3 is devoted to the approaches of both ordinary bed load, according to Einstein [59], and the inherent application of entropy laws. Section 4.4 will show all the obtained results, in the various applications, along with their discussion. Section 4.5 will deploy our conclusions.

4.2 Dataset

This paper presents data from three sources as explained in the following.

4.2.1 Flume experiments

The first dataset was obtained from nine experimental runs, conducted in a 10 cm wide and 6 m long recirculating flume at the Hydraulic Laboratory of University of Trento, Italy, by Fraccarollo and Hassan [68]. In each run, sediment and water discharges were constant, and the flow was uniform. All runs had low bed-slopes (approximately $0.3^\circ \div 0.5^\circ$) and mobile bed, consisting of well-sorted (in size and shape) PVC pseudo-cylindrical grains of

equivalent spherical diameter $d = 3.3 \pm 0.08$ mm (mean \pm standard deviation). The specific submerged density of the particles was $s = \rho_s / \rho_w = 1.51$, where ρ_s and ρ_w are the mass densities of grains and water, respectively. The fall velocity of the particles was approximately $w = 0.18$ m/s and their critical angle of internal friction was about 31° , measured at very slow shear rates. The runs present flow depths h between 2 ± 3 cm and flow discharges per unit width between 5 and 15 $\text{m}^3 / (\text{ms})$.

4.2.2 Adige River (Italy)

The Adige River is the second largest river in Italy (after Po River), is located in North-East Italy with 409 – km long and has a basin of around 12, 100 km^2 (Figure 4.1). Its stream crosses, from the source, several important urban centres such as Bolzano, Trento, and Verona. For the present study, field measurements at three different flow conditions (high, moderate, and low discharges) have been carried out at the Hydrometric station of Ponte Adige (UTM WGS84 676827 m / 5150310 m) by the Department of Hydrology and Dam, Autonomous Province of Bolzano (Table 4.1). During the field campaigns, since 2020, an Acoustic Doppler Velocity Profiler (ADCP) was used to collect the flow velocity field in about the same cross-section. Adige River in this section has a slope of about 0.067% with a width from 36 to 46 meters and a water depth between 2.1 to 3.3 meters, considering the three flow events. Beyond some perusal of in situ photos, additional information on morpho-dynamics and bed texture of Adige River, in the reach of interest, has been sieved from Welber et al. [217], and Scorpio et al. [182]. As mentioned by Welber et al. [217], d_{50} at the Adige section is equal to 0.0105 m. From in situ observation of the bed surface, through visual surveys and sample collection, we inferred that the texture of the sediment forming the bed surface and sub-surface can be adequately depicted as well sorted. A single value of the grain size is therefore representative of the particles in the bed and in the transport. From velocity fittings with logarithmic profiles, we found $e_s \approx 2d_{50}$.

Table 4.1: Information about the three ADCP measurements in Adige River.

Data	Flow Condition	Discharge (m^3 / s)	Maximum Depth (m)	Chanel width
1.6.2021	Low	74.64	2.1	35.3
2.8.2021	Moderate	116.13	2.4	37.6
31.8.2020	High	173.83	3.2	45.7

4.2.3 Estero Morales (Chile)

The study was conducted in a reach of the Estero Morales, a steep stream in the central Chilean Andes (Figure 4.2). The basin extends for 27 km^2 , with an elevation between 1780 and 4497 m a.s.l. Several relatively small glaciers above 2700 m a.s.l. [126]. Mean annual rainfall, as measured in the

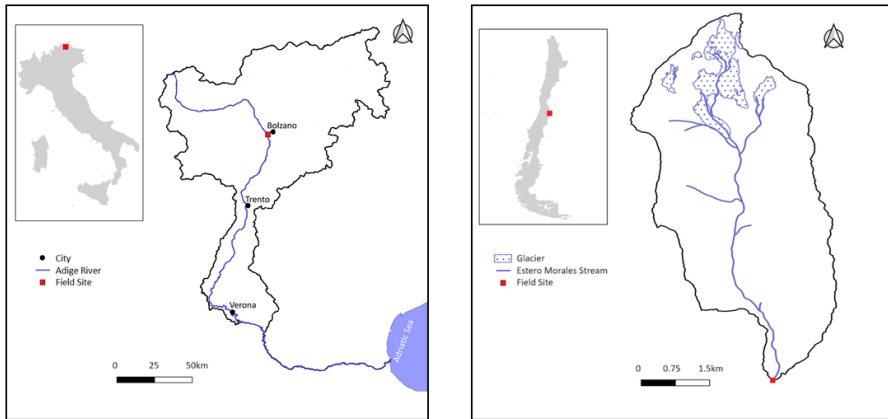


Figure 4.1: Left panel: map of the Adige River and its catchment, showing the location of the hydrometric station. Right panel: map of the stream Estero Morales and its catchment, showing the location of the hydrometric station.

lower part of the basin, is around 550 mm. The climate is Mediterranean, with snowfall from April to September, with occasional convective summer storms and late summer rain. The catchment is covered by snow for approximately 5 months a year; discharge mainly results from snowmelt in late spring (from late September to November) and glacier melt from December to March. Due to the hydrologic input, the fluent discharge is characterized by almost regular, repeatable, daily fluctuations. The stream in the study reach is steep (0.14 m/m), and the channel width is approximately 7 m. The study reach is 760 m long and is located just upstream from the confluence with the El Volcan River. Figure 4.2 shows a typical channel unit, with rapid flow, small cascades, and sparse boulders. Coarse sediment mobility in Estero Morales was investigated using natural clasts equipped with 23 mm - long radio frequency identification (RFID), and passive integrated transponder tags (PIT), [82, 116]. PIT tags are transmitters without batteries that emit a code by radio frequencies, which are detected, and their position is determined by a short-range antenna. In all, in 2014 - 2015, about 850 grains were equipped with PITs and poured in Estero Morales, with sizes in the range from 27 to 420 mm (Figure 4.2). After several surveys, hundreds of resting times or flight distances were measured.

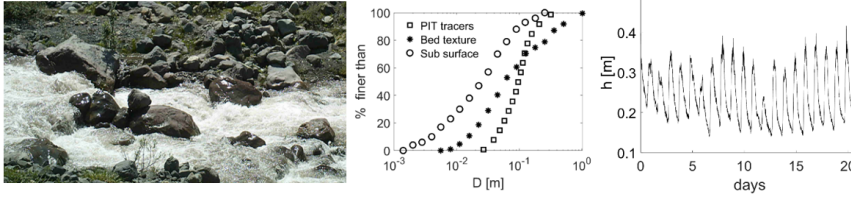


Figure 4.2: Left: view of the stream. Center: size distribution of PIT tracers, bed surface, and subsurface. Right: intra and inter-day measurement of local depth.

4.3 Theoretical backgrounds

4.3.1 Ordinary bed-load regime

The Shields parameter (θ), the longitudinal slope (i_f), the density ratio ($s = \rho_s / \rho$) (between solid and liquid densities), and particle Reynolds number (Re_p), are the four parameters that dictate the transport regime in turbulent flows. Shields and particle Reynolds numbers are:

$$\theta = \frac{hi_f}{\Delta d}; \quad Re_p = \frac{d\sqrt{g\Delta d}}{\nu} \quad (4.1)$$

being d the reference grain size, h the uniform flow depth, g the gravity acceleration, $\Delta = s - 1$ the submerged density ratio, and ν the liquid kinematic viscosity. They represent, respectively, the dimensionless shear stress at the bed, and the ratio of submerged particle gravity and viscosity forces. Berzi and Fraccarollo [21, 22] used two of them to build a regime map to illustrate the different transport regimes. Figure 4.3 reports a two-dimensional representation of the regime map, where the density ratio is assumed order of thousand and the slope mild ($< 1^\circ$). This map distinguishes the boundaries between ordinary bedload, collisional, mixed, or fully turbulent suspensions. It also reports the Shields line, which represents the incipient condition for the grain motion. When θ is larger than θ_c , some sparse grains start moving. As reported by Berzi and Fraccarollo [21, 22], sediment transport ceases to be free from the lifting effects of turbulence for the large magnitudes of the Shields number. We populated the map with data referring to the three situations focused on in this paper. We see from the graph that they all dwell in the ordinary bedload regime.

4.3.2 Determination of resting time pdf via the Shannon entropic approach

The dimensionless volume of sediment per unit width (\bar{q}_s) can be estimated by using a capacity formula (i.e., the bed is mobile and on its surface, the rate of grains entrained and dis-entrained is in equilibrium), among the several available ones deemed appropriate to quantify ordinary bed-load sediment

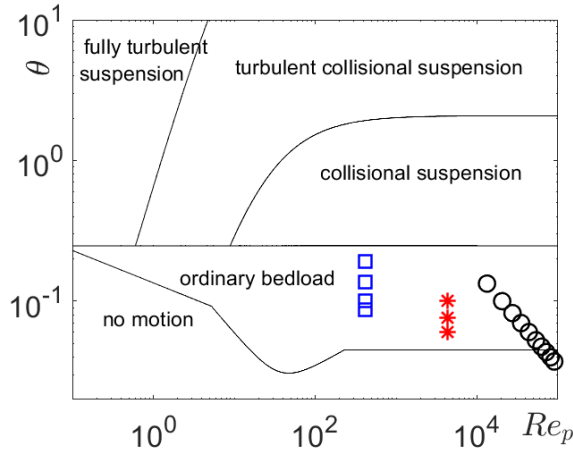


Figure 4.3: Regime map for the sediment transport. Blue dots refer to the four experimental runs, red to Adige River, black to Estero Morales.

discharge and based on a pseudo-mechanical rationale. It was not the purpose of the present analysis to deepen this topic by deploying weaknesses and merits of the various formulas. Instead, we choose one of these capacity formulas, and accept the sediment discharge values it gives, beyond any comparison with the other ones and without calibration against data. We opted for the well-known Meyer-Peter and Müller [138] equation:

$$\tilde{q}_s = \frac{q_s}{\sqrt{(s-1)gd^3}} = 8(\theta - \theta_c)^{1.5} \quad (4.2)$$

where θ is reported in equation 4.1, θ_c is the critical Shields magnitude, below which the sediment discharge is null or negligible (see Figure 4.3), a concept which has been thoroughly discussed in the last two centuries and more (e.g., Brahm [29]). θ_c in a well-sorted bed can be simply assumed constant and can be assigned a value, as reported in many papers, dating back to Shields diagram [186], though old and recent contributions deeply address doubts [59] and/or inconsistencies, which must be must be addressed and resolved [157]. Though we acknowledge the importance of the work behind it, we deem this is not among the foci of our analysis and put $\theta_c = 0.047$, as suggested by Meyer-Peter and Müller [138]. Regarding the ordinary bedload, Einstein [59] introduced a breakthrough in the calculation of sediment discharge, consisting of a probabilistic approach to describe and evaluate the sediment discharge per unit width, which ends up with:

$$q_s = ELV_p \quad (4.3)$$

in dimensional and non-dimensional ways, a simple product of three multipliers, or statistical predictors. The E is the mean number of particles entrained per unit of bed surface and per unit of time; L is the mean travel

distance run by particles between two subsequent rests (or flight distance); V_p is the representative particle volume. Einstein's basic conjecture is that L is proportional to the grain size, independent of the transport stage, in the bed-load regime. Following Einstein [59], several models based on a probabilistic description of the bed-load process have been proposed [158, 156, 3, 105, 61]. Be T_r the resting time, which elapses from any dis-entrainment of grain and its subsequent entrainment. Since we can neglect the times associated to the movement compared to the resting times, we can assume $E = \langle T_r^{-1} \rangle = d^{-2}$. The particle volume is about $V_p \approx \frac{\pi d^3}{6}$, while L is associated to the grain size (d), according to some algebraic law, and, quite important, is independent of the sediment-discharge intensity. Einstein [59] seminal proposal was $L \approx 100 d$. We use d, g, s to get the predictors in dimensionless form. Hence, the dimensionless resting time is $\tilde{T}_r = T_r \sqrt{g(s-1)d}/d$. With this and the previous definitions, we get this dimensionless form of equation 4.3:

$$\tilde{q}_s = \tilde{E} \tilde{L} \tilde{V}_p \quad (4.4)$$

where:

$$\tilde{q}_s = \frac{q_s}{\sqrt{g(s-1)dd}}; \quad \tilde{E} = \langle T_r^{-1} \rangle = E \sqrt{g(s-1)}/d^{5/2}; \quad \tilde{L} = \frac{L}{d} \quad \text{and} \quad \tilde{V}_p = \frac{\pi}{6} \approx \frac{1}{2} \quad (4.5)$$

In equations 4.4 and 4.5, \tilde{L} is the dimensionless form of L , for which Einstein [59] proposed

$$\tilde{L} \approx 100(-) \quad (4.6)$$

Some research studies considered the range of $\tilde{L}(-)$ between 1 and 100 [184, 113, 105, 129, 35, 68]. By substituting the dimensionless predictors (equation 4.5) into equation 4.6, and accepting the Einstein assumption (equation 4.7), we find:

$$\tilde{E} = \langle \tilde{T}_r^{-1} \rangle \approx 0.02 \tilde{q}_s \quad (4.7)$$

which shows a linear relation between the dimensionless sediment discharge, \tilde{q}_s , and $\langle \tilde{T}_r^{-1} \rangle$. We will see afterwards, in the Estero Morales situ, how a change in the relation between L and d would affect the proportionality reported in equation 4.7.

To connect the above-described finding based on Einstein's statistical approach to the probability density function (pdf) of \tilde{T}_r , we address our attention to the entropic procedures presented in several studies [42, 43, 147, 149, 69], among others. Let us annotate with $\tilde{p}(\tilde{y})$ the probability distribution density function of the random dimensionless variable \tilde{y} . The fundamental premise consists of the definition of the Entropy equation [185], which, among a set of probability distributions, draws the $\tilde{p}(\tilde{y})$ satisfying the maximum Entropy principle, as follows:

$$\max H(\tilde{p}), \text{ with } H(\tilde{p}) = \int \tilde{p}(\tilde{y}) \log\{\tilde{p}(\tilde{y})d\tilde{y}\} \quad (4.8)$$

For the optimum distribution, the Shannon Entropy is reduced to

$$\tilde{p} \left(\tilde{T}_r^{-1} \right) = e^{\lambda_1 - 1} e^{\lambda_2 (\tilde{T}_r^{-1})} \quad (4.9)$$

where we substituted $\tilde{y} = \tilde{T}_r^{-1}$; λ_1 and λ_2 are Lagrange multipliers associated the following constraint equations:

$$\int_0^\infty \tilde{p} \left(\tilde{T}_r^{-1} \right) d \left(\tilde{T}_r^{-1} \right) = 1 \quad (4.10)$$

$$\int_0^\infty \tilde{T}_r^{-1} \tilde{p} \left(\tilde{T}_r^{-1} \right) d \left(\tilde{T}_r^{-1} \right) = \langle \tilde{T}_r^{-1} \rangle \quad (4.11)$$

By substituting equation 4.9 into equations 4.10 and 4.11, and solving the integrals in equation 4.12 and 4.13, we get:

$$e^{\lambda_1 - 1} \frac{1}{|\lambda_2|} = 1 \quad (4.12)$$

$$e^{\lambda_1 - 1} \frac{1}{|\lambda_2|^2} = 0.02\tilde{q}_s \quad (4.13)$$

Finally, λ_1 and λ_2 can be made explicit: $\lambda_1 = 1 + \ln \left(\frac{1}{0.02\tilde{q}_s} \right)$ and $\lambda_2 = -\frac{1}{0.02\tilde{q}_s}$. With them, finally, $\tilde{p} \left(\tilde{T}_r^{-1} \right)$, given in equation 4.9, is achieved.

The final step is to move from $\tilde{p} \left(\tilde{T}_r^{-1} \right)$ to $\tilde{p} \left(\tilde{T}_r \right)$, as it was pursued in Fraccarollo and Hassan [68] and Mao et al. [125], as well. In statistics, this requires:

$$\tilde{p} \left(\tilde{T}_r \right) = \tilde{p} \left(\tilde{T}_r^{-1} \right) \left(\tilde{T}_r^{-1} \right)^2 \quad (4.14)$$

The theoretical procedure above outlined eventually was able to merge the Einstein theory to describe and evaluate a physical process like bed-load and the general Shannon Entropy theory borrowed from the Information or Thermodynamics worlds. In the present study, these theories are linked to each other straightforwardly.

4.4 Results and Discussion

4.4.1 Experiments

The developed theory is compared to the experimental data set described by Fraccarollo and Hassan [68] to see how they compare. The experimental conditions and measurements are fully described in Fraccarollo and Hassan [68]. From their study, the size of the mono-dispersed grains is $d = 0.0031(m)$, the dimensionless sediment flux is measured ($\tilde{q}_s = 0.0180, 0.035, 0.089, 0.2$), and $\tilde{p} \left(\tilde{T}_r \right)$ are obtained. Figure 3 compares the distributions $\tilde{p} \left(\tilde{T}_r \right)$ provided in Fraccarollo and Hassan [68] and corresponding ones given by equation 4.14.

The results confirm a good matching between the experimental and Entropy theoretical outputs.

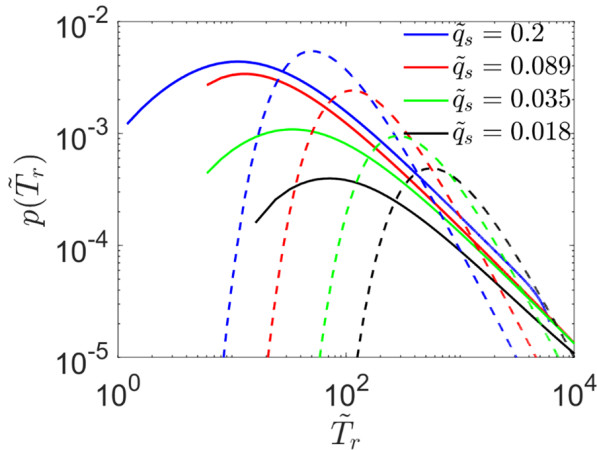


Figure 4.4: Probability density functions of the resting times from measurements (solid lines) and Entropy theory (dotted lines).

The distribution peaks have decreasing values as the intensity of discharge increases, and vice versa, the corresponding modes are getting higher. The measured modes span from a few seconds ($\tilde{q}_s = 0.2$), up to a couple of minutes ($\tilde{q}_s = 0.018$), the mode values decrease as the discharges decrease. They vary from a few minutes for the high flow condition, up to hours for the less intense case.

4.4.2 Adige River

In Adige River, we had the opportunity, and the need, of a double employment of the Entropy theory. In the first, the velocity distribution is targeted and then, we examine sediment transport.

We will deal with the velocity field in a cross-section (Ponte Adige, Bolzano), where the ADCP data have been collected by Ufficio Idrologia e Dighe, Provincia Autonoma di Bolzano. An important branch of the entropic approach developed and reported in several works [43, 146, 148, 147, 190, 14], deals with the velocity field; hence, we decided first to assess it against the measured data and then to extract the Shield dimensionless stress all over the boundary of the cross-section. After that, we will evaluate the sediment discharge through a capacity formula for a monodispersed bed; finally, we will get the p.d.f. of the resting time, following what was previously described in the experimental case (Section 4.1), which shares with the present river reach a monodisperse grain size of the bed.

The cross-section is split with vertical bins of constant width. According to Chiu [43] and Moramarco, Saltalippi, and Singh [146], the following function defines vertical velocity distribution along a vertical axis in a generic i -th bin:

$$u(x_i, y) = \frac{u_{\max}(x_i)}{M} \ln \left[1 + \left(e^M - 1 \right) \frac{y - h_B}{h(x_i) - D(x_i)} \exp \left(1 - \frac{y - h_B}{h(x_i) - D(x_i)} \right) \right] \quad (4.15)$$

where the coordinate x is the transect line placed at the free surface, running in the spanwise direction, with the origin at the left bank; x_i is the center position of the i -th vertical bin, y is the local vertical coordinate, with origin at the bed where velocity is null, and h_B is the local vertical coordinate of bed surface from the thalweg position, u is the local time-averaged magnitude of velocity, $u_{\max}(x_i)$ is the maximum value of u along the i -th vertical, $h(x_i)$ the local flow depth, $D(x_i)$ is the dip, i.e., the difference between h and the position of y corresponding to $u_{\max}(x_i)$; it can be placed at ($D = 0$), or below ($D > 0$), the water surface. In equation (15), four inputs are supposed to be available. They are: M, h, D and $u_{\max}(x_i)$. The knowledge of the cross-section topography, and of the position of the free surface, gives $h(x_i)$. We own this datum from the surveys associated to the ADCP measurements. M could be considered a unique value for the entire cross-section [146], but we allow it to change with the discharge. There, Table 4.2 reports the values of M we got based on Moramarco, Saltalippi, and Singh [146].

Table 4.2: M for the chosen transects

Flow Condition	Mean u (m/s)ADCP	Maximum u (m/s)ADCP	M
LF	1.26	1.8	2.73
MF	1.57	2.2	2.97
HF	1.83	2.5	3.27

Figures 4.5 (a,b) illustrate the cross-sectional velocity maps obtained by the Entropy with the ADCP measurements for high flow conditions (for the low and moderate flow conditions please see figures A.5 and A.6). Dplot (Hydesoft Computing, LLC) interpolated the velocity data across the whole cross-section. To ensure consistency between the ADCP data in the transverse and vertical directions, the data had to be interpolated, since the two sets of data had different mesh sizes and were unorganized. The interpolation allowed the ADCP data to have the same mesh size as the output velocity distribution produced by the Entropy model. In this direction, Dplot (Hydesoft Computing, LLC) interpolated the velocity data across the cross-section. Dplot offers two different interpolation options: planar and quadratic. We applied both and presented, the smoother colour maps, obtained with the latter one. The calculated velocity map (Figure 4.5b) is interpolated with the same cell size of 0.1 m of the ADCP measurements. The information on links between the maximum, mean and surface velocities, the Entropy parameter (M), dip (D), and depth (h), provided by Moramarco, Saltalippi, and Singh

[146]. Figure 4.5(a) presents blank areas near the surface and the bed in the ADCP output; the Entropy theory is also useful to make up this missing information, getting the full velocity field. However, the lack of data in these zones has a minor effect on predicting the mean velocity, and consequently, on the total flow discharge and sediment discharge [15, 16]. In Figure 4.5(b), we appreciate that the Entropy model simulates well the measured velocity field, with better accuracy in zones with large velocity values.

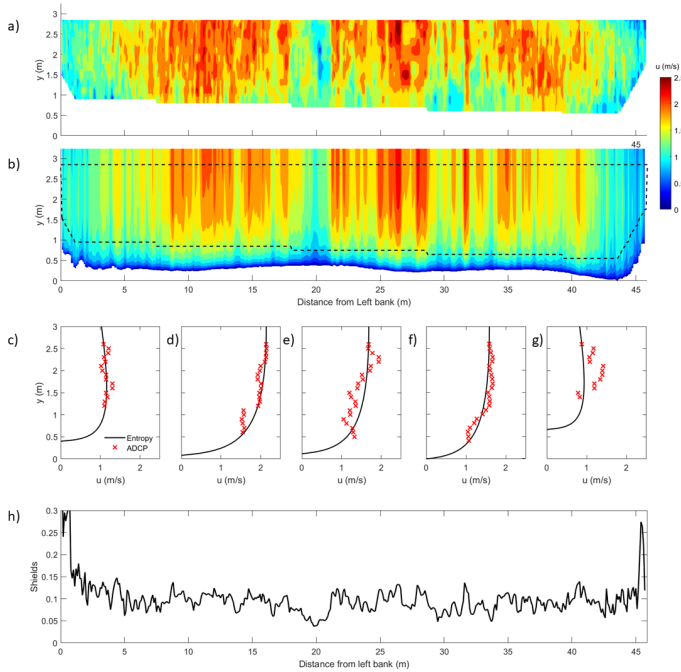


Figure 4.5: Colour maps of the Velocity field in the cross-section for the high flow condition: a) based on the ADCP data, b) based on the Entropy theory. Ponte Adige cross section, high flow condition. c to g) random velocity profiles from the left bank to the right bank. h) distribution of Shields stress.

In Figure 4.5(c, d, e, f, and g) the velocity profiles for five verticals at random positions ($x_i = 0.2m, 0.32B, 0.5B, 0.68B, 0.8B$, where $B(m)$ is the channel width of the free surface in the transect). These figures point out that the velocity profiles obtained by Entropy are in good agreement with the velocity profiles measured by ADCP. Some factors are responsible for the deviations between the measured velocities near the bed and the dip values and their corresponding computed ones, as it appears in the c and g panels of Figure 4.5: a) secondary currents; b) postprocessing and smoothing the raw data of ADCP [153]. In addition, let us shortly recall that entropic velocity profiles in rivers apply in clear water conditions. There is no literature contribution considering the flow of a mixture (water and solids) with significant stress generation in both phases. By accepting the entropic distribution of equation

4.15, we are therefore going to assume that the presence of a thin bedload layer over the bed does not significantly alter the velocity field.

Our aim, in this section, is to obtain the shear velocity at the bed, u_* at each vertical, which may be then associated with grain entrainment and sediment transport. We locally chose an approach based on the classic turbulent logarithmic velocity profile over a rough wall [219, 213], which leads to:

$$u_* = ke_s \frac{du}{dy} (y = e_s) \quad (4.16)$$

where k is the Von-Karman constant and e_s is the roughness, the distance from the bed where the velocity becomes null, according to the previous approach [219, 213]. The velocity strain rate is calculated by exploiting the entropic profile (equation 4.15). Then, the mobility Shields parameter, θ (equation 4.1), can be calculated.

Finally, the dimensionless and dimensional (\tilde{q}_s, q_s) sediment volumetric discharge, per unit width, can be estimated by using both the Einstein equation 4.4 and the Meyer-Peter and Müller equation 4.2.

To face the bedload process in the Adige River site, we left from the shear stress value above determined along the cross-section. Figure 4.5(h) illustrates the Shields distribution along the cross-section. The mean values of the Shields are 0.06, 0.08, and 0.1 for the low, medium, and high flow rates, respectively. The Shields values, in all flow conditions, were close to the critical Shields, $\Theta_c = 0.05$, which means that the bed load is not intense, but ordinary (Figure 4.3). Equation 4.5, or any other capacity sediment discharge can be used to evaluate the dimensionless sediment discharge.

Once the Shields distribution and the sediment discharge are known, the statistics of particle resting times can be represented by applying the Entropy approach above outlined (see Section 4.3), exactly as before was done with the experimental data. The bed material is well-sorted and represented by a single value. Figure 4.6 shows the obtained probability distribution functions ($\tilde{p}(\tilde{T}_r)$) for the three flow conditions at the Adige cross-section. This figure indicates that the higher the flow discharge, the higher the peak values of $\tilde{p}(\tilde{T}_r)$, and a similar trend holds for the mean resting time. Associated with the peaks, the mode values decrease as the discharges decrease. They vary from a few minutes for the high flow condition up to hours for the less intense case. Incidentally, these real situations exhibit much higher resting times than the value measured in the above-presented experimental runs.

According to this outcome, it is possible to figure out a physical definition of what the boundary between ordinary and collisional suspended bed-load is. Let us imagine starting from an ordinary bed-load condition and then gradually increasing the flow intensity, namely the Shields stress. As described in Berzi and Fraccarollo [21] and the regime map of Figure 4.3, the boundary with collisional suspension is approached; along with Shields increment, a layer of moving grains that undergo mutual collisions and have little, nearly no rest time [68, 23] is progressively taking place. Under these

conditions, resting times become unimportant and the Einstein theory does not apply anymore; what matters is the frequency and type of collisions.

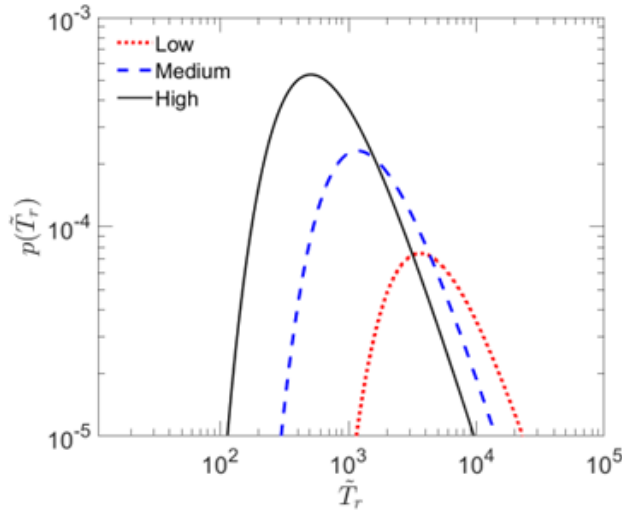


Figure 4.6: P.d.f. of the resting time for the three monitored flow conditions in Adige.

4.4.3 Estero Morales

Mao et al. [125] presented a work on Estero Morales (Chile) in which the presented resting times are either directly measured or inferred. These data refer to a sequence of daily floods and the direct measurements took place during the low stage between two or more subsequent floods, when it was possible to wade the stream and recover the PIT tracers. To interpret our dataset, Mao et al. [125] relaxed the Einstein constraint and adopted the following linear relationship [34, 126], still independent of the bed load intensity:

$$\tilde{L} = \tilde{L}_0 + \tilde{\omega} \quad (4.17)$$

Being $\tilde{L}_0 = L_0/d$; in it, the L_0 is expected to be a constant greater than 0, given that \tilde{L} must be positive for any value of the grain size d . Hence, it is possible, at least theoretically, to assign a negative value to the constant coefficient $\tilde{\omega}$, though it was always positive in experimental studies [34]. The presence of \tilde{L}_0 alters the original formulation of Einstein ($\tilde{L}_0 = 0, \tilde{\omega} = 100$); it implies that there are parts of the bed surface occupied by stable bedform structures over which particles do not stop during ordinary events (i.e., floods are not able to destroy the bedforms). Our results further show that the relation between L_i and d_i does not confirm Einstein's assumption that $\omega = 100$ and $c = 0$ m. Indeed, the flight distance of single grains decreases with particle size, and we obtained values of ω and c of 200 [-] and 50 m,

respectively (Figure 4.7). Interestingly, ω is negative, revealing that in a naturally structured step-pool channel experiment. Sediment mobility is completely different from flume runs with well-sorted sediments and no bedforms [34, 68, 105, 113]. Deviations from Einstein's conjecture were reported by Habersack [80] in one of the first reports on step lengths and rest periods using tracers in the field.

The resting times in Mao et al. [125] were obtained by direct measurements or, indirectly, through equation 4.14, which permitted to extraction of one or more resting times from any inter-survey displacement. These data showed no clear dependence on the grain size. Nonetheless, it is quite obvious that the grain size should matter when processes relevant to sediment discharge in well-sorted beds are considered. However, in poorly sorted beds the discharges of different grain size fractions are mutually influenced. A simple and robust way to consider this aspect is, as reported by Mao et al. [125], through the use of the hiding function [58, 159]. In the following expression, we use the hiding function ζ_i to evaluate the sediment discharge q_{si} , for the i -th grain size fraction, being ζ_i the hiding factor calculated as $\zeta_i = (d_i/d_{50})^n$ [6, 160]. Based on Meyer-Peter and Müller [138], a fractional value q_{si} , relevant to d_i , which is the sediment discharge involving the i -th volumetric percentage F_i of grains being in the size range $(d_{i-1} + d_i) / 2 \div (d_i + d_{i+1}) / 2$, reads:

$$\tilde{q}_{si} = \left[\left(\frac{u_*^2}{g(s-1)d_i} - \theta_c \frac{d_{50}}{d_i} \right) \zeta_i \right]^{3/2} \quad (4.18)$$

The functions ζ_i work to enhance the discharge of sediment coarser than d_{50} , and to dwindle that of the finer ones. In poorly sorted beds, in fact, grain clusters made by grains of different sizes form and pave the bed. Their typical configurations, whatever the scale of the cluster (they may be small aggregates or bigger, as ripples or dunes, for instance), are more stable when the coarser grains protrude into the flow and protect, in their wakes, the smaller ones. In the hiding function, the exponent n is close but smaller than one. With $n = 1$, the role of the size is completely masked, and a condition of equi-mobility is attained. The literature often offers values of n slightly smaller than one, as by instance $n = 0.905$. In equation 4.18, we applied the hiding factor to the entire difference between the dimensionless i -th shear stress and the i -th critical value. In previous works, when the bedload transport rates for uniform sediment do not consider any threshold [9, 60, 62], the hiding function applies to the critical Shields. Here, like in approaches without thresholds [59, 159], the hiding function affects also the stress applied to any grain size fraction. Applied to Estero Morales, this approach allowed us to satisfy two constraints, i.e.: first, the PITs are mobilized in all the size range, in agreement with the measured data [125]; second, the dimensionless sediment discharge q_{si} is decreasing with size, as expected from the physical description on the role of coarse over small grains, above given.

The knowledge of \tilde{q}_{si} , through equation 4.18, makes it possible to link

the mean resting time, $\langle T_r \rangle$, relevant to d_i , through the equation 4.7, here re-written and gradually expanded, with the help of previous equations 4.4,4.5 and 4.17, to make it specific to the i – th grain size:

$$\tilde{q}_{si} = \tilde{E}_i \left(\frac{L_0}{d_i} + \tilde{\omega} \right) \frac{\pi}{6}; \quad (4.19)$$

The l.h.s of equation 4.19 is calculated through Meyer-Peter and Müller [138], while in the r.h.s. the only unknown is \tilde{E}_i , which can then be determined.

To accomplish the implementation of the entropic treatment of resting times, as done in Section 4.3.1, but for a poorly sorted bed, as in Estero Morales, we still need to get the global predictor \tilde{E} and the comprehensive solid discharge, \tilde{q}_s . \tilde{E} comes from the weighting operation expressed in equation 4.19, in which the summation is made for $i = 1 \div N$, with N the number of grain size fractions.

$$\tilde{E} = \sum_{i=1}^N F_i E_i \quad (4.20)$$

This value of \tilde{E} is, therefore, the mean of the inverse of the resting times that took place during a specific flood and regards all the PIT grains. It is not, therefore, a direct function of the discharge, as it was for the previous two steady-state cases, examined in this paper. To calculate \tilde{q}_s we first make a mean of each \tilde{q}_{si} over the considered time interval, that is one day ($\tilde{T}_{1 \text{ day}}$), and then applied the weight criterium already exploited to get \tilde{E} , in equation 4.20:

$$\tilde{q}_s = \sum_{i=1}^N F_i \frac{1}{\tilde{T}_{1 \text{ day}}} \int_{\tilde{T}_{1 \text{ day}}} \tilde{q}_{si} d\zeta \quad (4.21)$$

being ζ a dummy dimensionless variable. In the left panel of Figure 4.7, we display the behaviour of the dimensionless flight distances, discharge, and entrainment frequency as a function of the grain size. \tilde{q}_{si} and \tilde{L}_i are both decreasing with d_i , as expected, but at a different rate. \tilde{E}_i , instead, is increasing, meaning that the dimensionless mean resting time is decreasing with d_i . In well-sorted beds, this trend would be the opposite. This latter result is a principal result of the mutual influence of the size classes forming the clusters and macro-roughnesses (Figure 4.2). Figure 4.7, in the right panel, plots the probability density function we get from the Shannon Entropy, applying the equation 4.14 with the value of \tilde{q}_s given by 4.21, and the normalized histograms of the dimensionless resting times we got in the Estero Morales, as reported in Mao et al. [125]. It can be appreciated that the entropic pdf is quite well representing the histogram distribution.

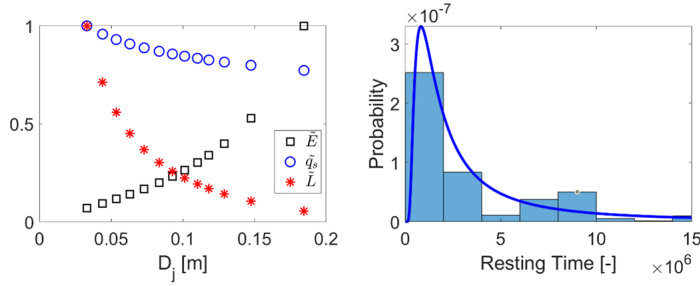


Figure 4.7: Left: Normalized values of \tilde{E}_{iN} , \tilde{L}_{iN} , \tilde{q}_{siN} , where $b_{iN} = b_i / \max(b_i)$, with $b = \tilde{E}_i, \tilde{L}_i$ or \tilde{q}_{si} , as d_i spans over the PIT grainsize range. Right: the normalized histogram of the measured resting times in Estero Morales (Chile) and the entropic outcome

4.5 Conclusion

In the present research, statistical information for ordinary bed-load transport is inferred through an innovative methodology based on surface velocity measurements. Experimental data, and field data collected in a river and a torrent, offer different flow conditions and chances for various theoretical interpretations. The study mainly focuses on resting-time statistics, specifically its probability distribution $\tilde{p}(\tilde{T}_r)$, which is achieved within the frame of the general Shannon Entropy principle and by adopting the Einstein approach to ordinary bed-load processes. Experimental data provide the basic dataset to assess the entropic approach. Adige River, Italy, presents as a bed almost monodispersed and flat, as, to some extent, the experimental one, but offers the chance to work on the entropic representation of the velocity field. This latter finding was then exploited to get the Shields stress over the bed. This methodology paved the way to get information on volumetric and solid discharges also in cases where limited data are available, such as the surface velocities and the flow depth. Finally, the case of a torrent offers the chance to gain an insight into the complexity of sediment processes over a bed endowed with macro-roughness and a poor grain size distribution.

Chapter 5

Extended kinetic theory applied to unidirectional collisional suspensions with entropic distributions of particle concentration

5.1 Introduction

The topic of sediment transport has a long history of research and a variety of nomenclatures has been introduced to describe, at least partially, its vast phenomenology, with special emphasis on the characteristics of the motion of the solid particles carried by, at least on Earth, either air or water. Bedload [138, 173], saltation [12], sheet flow [96, 72], and suspension load [176] have been and are still used to define various types of sediment transport, often with partial super-positions and ambiguity. Part of the issue is that sediment transport involves a distribution of sizes of the solid particles, and sizes matter when, e.g., comparing the forces acting on the grains. Hence, different regimes of sediment transport usually coexist, complicating the physical understanding and the mathematical modelling of the phenomenon.

To clean up the field, let us focus on an assembly of mono-sized particles transported by a shearing, turbulent fluid over a basal boundary that does not move. The latter can be a rigid bottom or comprise a packing of not moving or barely moving [101] particles identical to those flowing above it. We refer to these two scenarios as sediment transport over rigid or erodible beds, respectively. Then, bedload, in its original spirit [138], is the regime of sediment transport in which only a few particles are moving, and these particles leave the bed at a certain instant, fly over the bed under the effect of gravity and fluid forces, and eventually re-touch the bed at the end of their solitary flights. Occasionally, there might be a few mid-fluid collisions above the bed, but their effect on the transport rate is negligible. We might also call

bedload as the ballistic regime: the particles are like projectiles moving under the influence of gravity. In the field of windblown sand, this ballistic regime is called saltation [178, 5, 211] and represents the main mode of sediment transport.

On the other side of the spectrum, we term suspension the regime of sediment transport in which particles can fly over the bed without directly interacting with the bed itself. For this to happen, we must look for physical mechanisms able to provide one or more forces that balance the buoyant weight of the particles. This physical mechanism can be either the momentum exchange in interparticle collisions or the turbulent lift generated by the interstitial fluid. We can thus distinguish between collisional and turbulent suspensions.

Next, quantitative criteria must be provided to identify the regimes mentioned above. The length of the particle trajectories comprised between two successive interactions with the bed or other particles can be suitably employed to distinguish between the ballistic and the collisional regimes. Indeed, there is a maximum length, called the mean free path in the literature of kinetic theory [39], for which the influence of the external forces acting on the particles, such as gravity, buoyancy and drag, can be safely ignored when calculating the stresses originated from the collisional exchange of momentum in the particle phase of the mixture (treated as a continuum). There is a transition from ballistic to collisional regime of sediment transport when the averaged trajectory length equals the mean free path [162]. Given that the mean free path is a decreasing function of the particle concentration [39], there is a minimum concentration above which the regime is collisional. In the collisional regime, constitutive relations of the kinetic theory of granular gases can be employed [97, 73].

If the intensity of the turbulence is large enough to overcome the particle buoyant weight, the sediment transport enters the turbulent suspension regime. Given that, in a fluid at rest, the competition between gravity, buoyancy and drag determines the particle settling velocity, and that a good measure of the turbulence intensity is given by the fluid shear velocity (the square root of the fluid shear stress over the fluid mass density), the ratio of the fluid shear velocity over the particle settling velocity, which is inversely proportional to the Rouse number [176], has been proposed as a criterion for the onset of turbulent suspensions. There is a minimum value of this ratio above which the turbulent suspension regime takes over [165].

Even in the idealized case of sediment transport of mono-sized particles, the concentration and the fluid shear velocity are local fields, non-uniform in the flow domain. As such, the ballistic, collisional and turbulent suspension regimes can be simultaneously present in different regions of the spatial domain, perhaps in a stratified fashion. More troublesome, there might be regions of the flow where two or more of the above-mentioned regimes coexist and are equally important. Models of sediment transport stratified into a purely collisional and a turbulent-collisional layer have been proposed [22]. On the other hand, the existence of a region in which both ballistic and collisional regimes conspire to determine the particle stresses has recently been

assessed [40], and we deem it will be crucial to understand the transition from ordinary bedload to collisional suspensions [167].

In this work, we focus on modelling the sediment transport over erodible beds in the collisional regime, particularly on the transport of solid particles in water in inclined channels, for which detailed measurements of the distributions of particle volumetric concentration, particle mean velocity and velocity fluctuations are available [37], allowing for a severe test of continuum models. Some of the authors of the mentioned paper have used the kinetic theory of granular gases in the past, in an attempt to solve this regime of sediment transport [19, 21, 22]. In so doing, they formulated a system of differential equations governing the motion of the two phases, solid particles and liquid, but were unable to find full numerical solutions of the system. They only provided approximate analytical solutions obtained by stratifying the flow domain into a few layers characterized by different physical mechanisms and integrating the differential equations through crude trapezoidal rules.

Complications of solving balance equations with closures from the kinetic theory of granular gases come from the fact that the particle phase must be treated as compressible, and the equation of state, the granular viscosity and pseudo-thermal conductivity, and the dissipation rate of fluctuation energy are all strongly nonlinear functions of the particle concentration. Chassagne, Bonamy, and Chauchat [40] proposed a two-phase continuum model for collisional suspensions based on the kinetic theory of granular gases that includes the presence of both saltating particles and a Coulomb-like frictional behaviour of the solid phase near the bed. They were able to numerically integrate the differential equations and make comparisons against coupled fluid-discrete element simulations of spheres. When compared against physical experiments, however, it seems to strongly underpredict the intensity of particle agitation.

Here, we introduce a strong simplification by decoupling the determination of the particle concentration from the other hydrodynamic variables. First, we assume that the concentration distribution in the flow is such that it maximizes some definition of the Shannon Entropy. This permits, then, to solve analytically the momentum and energy balances, with the constitutive relations of the kinetic theory of granular gases, extended to include the role of particle friction [98, 27], velocity correlation [94, 95], particle softness [24], cylindrical shape [20]. We also include the role of the particle in modulating the fluid turbulence [23] and the mutual influence of the turbulent fluctuations and the particle agitation [91, 23]. We limit the analysis to the region of the flow dominated by collisions, but, through comparisons with experiments of plastic cylinders in water [37], we confirm, as suggested in Chassagne, Bonamy, and Chauchat [40], that the ballistic regime, and/or a combination of the ballistic and collisional regime, are important in the case of sediment transport in water, and they should be accounted for.

The chapter is organized as follows: we introduce the governing equations and show how to solve them in Section 5.2; in Section 5.3, we make

comparisons between the predictions of the theory and the experimental results on the sediment transport of plastic cylinders and gravel in water; the chapter ends with some concluding remarks in Section 5.4.

5.2 Theoretical backgrounds

The sketch of the flow configuration is depicted in Figure 5.1. We focus on the steady, fully-developed, free-surface flow of a mixture of a liquid, of mass density ρ and molecular dynamic viscosity η , and identical, inelastic spheres, of diameter d , and mass density ρ_p , over an erodible bed composed of the same particles, assumed at rest. Particles are driven into collisions by the combined effect of gravity and the drag exerted by the turbulent liquid. We characterize the collisions through the coefficients of normal, e_n , and tangential restitution, e_t , i.e., the negative ratio of pre- to post-collisional relative velocities normal and tangential to the plane of contact; the coefficient of sliding friction, μ ; and the effective coefficient of restitution, e , which is a function of e_n , e_t and μ , and accounts for the role of friction in the rate at which energy is dissipated in collisions [98, 109].

We limit the analysis to situations in which the thickness of the transport layer, h is, at least, a few particle diameters. We assume that the momentum exchange in collisions is at the origin of the dominant stresses in the particles. We provide a criterion to distinguish between this collisional-dominated region and the region where the particles follow ballistic trajectories above it. On top of the transport layer there is a turbulent liquid layer, The total thickness of the transport and liquid layer over the erodible bed is H . The range of validity of the aforementioned assumption of a collisional-dominated regime is given in Berzi and Fraccarollo [21, 22] as a region in the phase diagram with the Shields number, the dimensionless strength of the shearing flows, on one axis and the angle of inclination of the bed, ϕ , on the other. We limit the analysis to flows for which the turbulent lift on the particles is weaker than the particle weight.

We take x and y to be the direction parallel and perpendicular to the erodible bed, respectively, and neglect variations in the spanwise direction. The surface of the bed is located at $y = 0$. The local particle velocity and concentration are u and v , respectively. In what follows, all quantities are made dimensionless using the particle density and diameter, and the reduced gravitational acceleration, $g(\sigma - 1)/\sigma$, where g is the gravitational acceleration and $\sigma = \rho_p/\rho$ is the density ratio. With this, the inverse of the dimensionless molecular viscosity of the liquid is σR , with $R = \frac{\rho d \sqrt{g \frac{\sigma-1}{\sigma}}}{\eta}$ the fall particle Reynolds number

Following Lien and Tsai [117], we found that the Shannon maximum Entropy principle leads to the following Probability Density Function (PDF) of

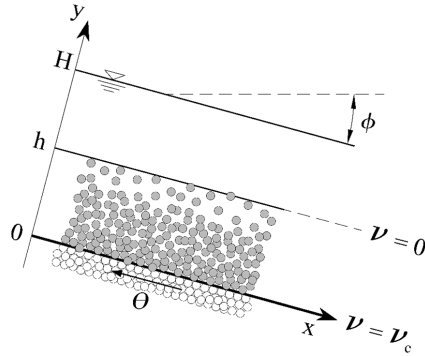


Figure 5.1: Sketch of the flow configuration with the frame of reference and concentration reference values at specific positions

the particle concentration v :

$$P(v) = \frac{E}{v_{\max}} \frac{\exp(Ev/v_{\max})}{\exp E - \exp(Ev_{\min}/v_{\max})} \quad (5.1)$$

where E is the entropic parameter. The PDF in equation (5.1) has been normalized so that its integral over the admissible range of concentration (say from a minimum v_{\min} to a maximum v_{\max}) is equal to one. $P(v)$ is a monotonic exponential distribution. To infer the spatial distribution of the concentration in the transport layer, we define the conditional probability, $P(y | v)$, where y must be thought as a random variable in the range $\{0, h\}$. Given the monotonicity of $P(v)$, the probability of finding a concentration value in the infinitesimal interval dv around v must correspond to the probability of this concentration interval to occupy the physical space dy around y . Hence, it must be that $P(v)dv = P(y | v)dy$. Lien and Tsai [117] assumed that y and v are uncorrelated and that y has a uniform distribution, i.e., $P(y | v) = P(y) = 1/h$, so that

$$\frac{E}{v_{\max}} \frac{\exp(Ev/v_{\max})}{\exp E - \exp(Ev_{\min}/v_{\max})} dv = \frac{1}{h} dy \quad (5.2)$$

We will discuss later the unphysical consequences of the strong assumptions of Lien and Tsai [117] on $P(y | v)$.

Integrating equation (5.2), we obtain the following concentration profile, already reported in Lien and Tsai [117]

$$v = \frac{v_{\max}}{E} \ln \left\{ [\exp E - \exp(Ev_{\min}/v_{\max})] \frac{y}{h} + \exp E \right\} \quad (5.3)$$

Figure 5.2 exhibits how the concentration profile changes as a function of E , in the range between -20 and 20. Negative or positive values of E give concave or convex concentration profiles respectively. With E close to zero (but different from zero, as $E = 0$ would make equation 5.3 singular), the

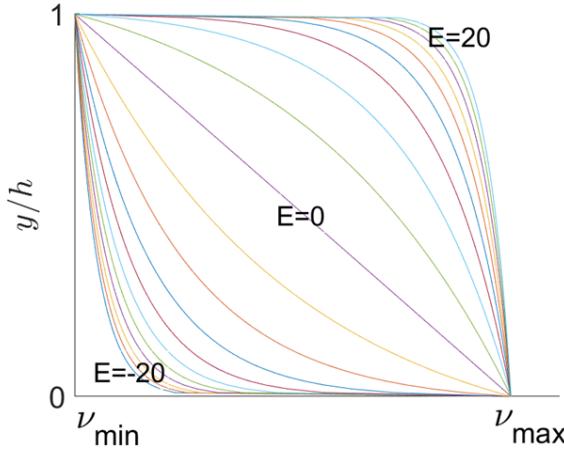


Figure 5.2: Entropic concentration profiles from equation (5.3) for different values of the entropic parameter.

concentration profile is approximately linear.

The minimum and maximum concentrations correspond to the values of the concentration at the top of the sediment layer and at the surface of the erodible bed, respectively. As explained in Pasini and Jenkins [162], a ballistic layer, in which the concentration is so small that the length of the particle trajectory in between collisions is much larger than the mean free path of kinetic theory, must be present on top of the actual collisional layer. In the ballistic layer, the influence of the external forces cannot be ignored, when deriving the constitutive relations for the particle stresses. Here, we assume that the additional contribution to the total sediment transport from the ballistic layer is negligible, and simply take $v_{\min} = 0$. As shown in Berzi, Jenkins, and Richard [25, 26], the interface between the flow and the erodible bed is characterized by a critical value of the particle concentration, v_c , which, for spheres, is solely dependent on the sliding friction coefficient. For cylinders, the critical concentration would depend on the sliding friction and the aspect ratio [20]. The critical concentration is the minimum value of v , at which rate-independent components of the stresses first develop [41]. Then, here, we take $v_{\max} = v_c$. With these, the concentration distribution in the transport layer, parametrized in terms of E , simplifies to

$$v = \frac{v_c}{E} \ln \left[\exp E + (1 - \exp E) \frac{y}{h} \right] \quad (5.4)$$

which gives the following expression for the average concentration in the transport layer:

$$\bar{v} = \frac{1}{h} \int_0^h v dy = -v_c \left(\frac{1}{E} + \frac{\exp E}{1 - \exp E} \right) \quad (5.5)$$

The balance of particle momentum along the direction perpendicular to the flow (y direction) is

$$p' = -v \cos \phi \quad (5.6)$$

where p is the particle pressure. Here, and in what follows, a prime indicates a derivative along y . As mentioned, we have neglected the turbulent lift force associated with the correlation between the fluctuations of particle concentration and liquid velocity. Integrating equation (5.6), with equation (5.4), gives

$$p = p_0 - h \left[\left(\frac{y}{h} + \frac{\exp E}{1 - \exp E} \right) v - \frac{v_c}{E} \left(\frac{y}{h} + \frac{E \exp E}{1 - \exp E} \right) \right] \cos \phi \quad (5.7)$$

where p_0 is the granular pressure at the surface of the bed ($y = 0$),

$$p_0 = \bar{v} h \cos \phi \quad (5.8)$$

Equations (5.7) and (5.8) imply that the particle pressure vanishes at $y = h$. To actually determine p for a given entropic parameter E , we need the depth of the transport layer h . To do this, we first assume that the particle shear stress, s , is at yield at the bed, that is $s(y = 0) = s_0 = k_0 p_0$, where the yielding coefficient k_0 is taken to be as the ratio of the particle shear stress over the particle pressure where the concentration is equal to v_c [27]. Its expression as a function of e_n and e is reported in Table 1. Then, we define the Shields number, Θ , as the dimensionless total shear stress of the mixture at the surface of the bed. The Shields number quantifies the intensity of the shearing flows, and we take it as an input of the problem. At large concentrations, the fluid turbulence is heavily suppressed, but the velocity fluctuations of the particles induce shear stress in the fluid proportional, through a function of the concentration to that of the particles [23]. Hence, $s_0 + S_0 = \Theta$, and, with equation (5.8),

$$h = \frac{\Theta}{k_0 \bar{v} \cos \phi} \left(1 + \frac{2}{5} \frac{1}{2\sigma} \frac{1 + 2v_c}{1 - v_c} \right)^{-1} \quad (5.9)$$

The last term between parentheses in equation (5.9) represents the proportionality factor between the fluid and the particle shear stress at the bed. It differs with respect to the expression of Berzi and Fraccarollo [23] by a factor $2/5$, which permits to better reproduce the dependence of the mass hold-up, $\bar{v}h$, on the Shields number and the angle of inclination measured in the experiments (see Figure 5.3).

When collisions are the dominant source of stresses, the constitutive expression of the particle pressure can be deduced from the kinetic theory of hard, inelastic spheres. However, as suggested by Berzi, Jenkins, and Richard [26], flows over erodible beds imply that the concentration must reach its critical value v_c at the surface of the bed. This is possible only if

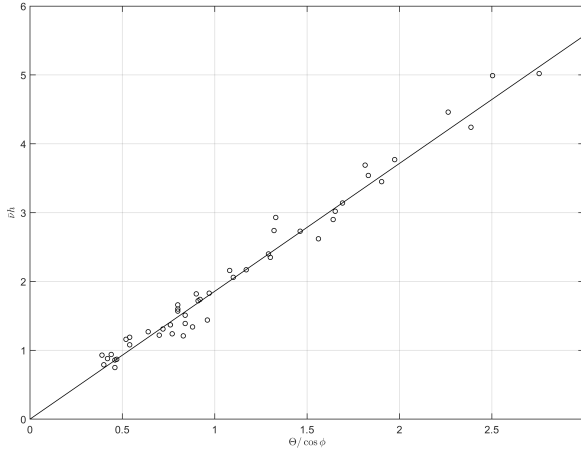


Figure 5.3: Measured (circles, Capart and Fraccarollo [37]) and predicted (line, equation 9, with $k_0 = 0.35, \sigma = 1.51$ and $v_c = 0.61$, as appropriated for plastic cylinders) mass hold-up, $\bar{v}h$, against $\Theta / \cos \phi$.

the actual finite stiffness of the particles and the associated finite contact duration during collisions is accounted for, leading to [24]:

$$p = f_1 T \left(1 + \frac{12}{5} v \chi_0 \frac{T^{1/2}}{k_n^{1/2}} \right)^{-1} \quad (5.10)$$

where f_1 , a coefficient, and χ_0 (Table A.1), the radial distribution function at contact, are both functions of v , which is singular at v_c . Here, T is the granular temperature, one-third of the mean square of the particle velocity fluctuations. The term between parentheses in equation 5.10 is the correction due to the finite contact duration, in which k_n is the dimensionless particle stiffness [24]. With p and v known at every y , equation (5.10) is quadratic in the square root of the granular temperature that gives

$$T = \left[-\frac{6}{5} \frac{pv\chi_0}{f_1 k_n^{1/2}} + \frac{1}{2f_1} \sqrt{\left(\frac{12}{5} \frac{pv\chi_0}{k_n^{1/2}} \right)^2 + 4f_1 p} \right]^2 \quad (5.11)$$

Irrespectively of the entropic parameter E , the Shields number or the angle of inclination, equation (5.11) implies that the granular temperature decreases near the top of the transport layer, where the concentration is small. Experiments and discrete simulations of flows of granular-fluid mixtures and dry granular materials over erodible beds indicate, instead, that the granular temperature monotonically increases with the distance from the bed [8, 23, 26], eventually saturating and becoming independent of y in the

ballistic layer [162]. In the dilute limit, $p = vT$ [73], and, with equation (5.6), we obtain

$$T' = \left(\frac{v' \int v dy}{hv^2} - 1 \right) \cos \phi \quad (5.12)$$

In order to agree with the experimental observation that $T' \geq 0$ near the top, then,

$$v' \frac{1}{h} \int v dy \geq v^2 \quad (5.13)$$

It is easy to show that this condition cannot be satisfied by the logarithmic distribution of the concentration of equation (5.3), implying that the assumptions about the PDF $P(y | v)$ are not satisfied, at least near the top of the transport layer. An exponential distribution of the concentration, such as that typical of saltation [50], the dominant mode of transport for wind-blown sand, is the only profile compatible with a uniform distribution of the granular temperature. However, despite the unphysical consequence of equation (5.3) for the distribution of the granular temperature near the top of the transport layer, we will show that the rest of the hydrodynamic variables can be reasonably well predicted assuming its validity throughout the flow.

Now that we have determined the distribution of the granular temperature in the transport layer, we can employ the fluctuation energy balance, that, for steady and fully developed collisional granular-fluid flows [91], reduces to

$$-Q' + su' - \Gamma + (2.3\sqrt{3T2K} - 3T)C_D v = 0 \quad (5.14)$$

where: Q' is the fluctuation energy diffusion associated with the particle agitation; su' is the fluctuation energy production through the work of the particle shear stress; G is the energy dissipation due to the inelastic nature of collisions [26]; and the last term accounts for the particle agitation produced by the fluid turbulence (where K is the turbulent kinetic energy) and its suppression due to the drag exerted by the fluid on the particles. We take the drag coefficient to be that appropriated for spheres (hence, neglecting the influence of the particle shape) in the case of Stokes flows, $C_D = \frac{18}{(1-v)^{3.1}\sigma R'}$, with the concentration dependence suggested by Richardson and Zaki [170]. A more physically grounded expression for the drag coefficient, such as that suggested in Jenkins and Hanes [96], should include the form as well as the friction drag and incorporate the role of the particle velocity fluctuations. However, we checked that this does not significantly alter the present results while making implicit the system of equations (and the description of its solution less straightforward).

The term associated with the production of fluctuation energy due to the fluid turbulence is taken to be proportional to $\sqrt{3T2K}$, the geometric mean of the intensity of the particle and the fluid fluctuations, rather than simply to $2K$ as in Hsu, Jenkins, and Liu [91], which we deem as more appropriate given that it originates from the average of the product of the velocity fluctuations of the particle and those of the fluid. The numerical factor 2.3 in front of it permits to reproduction of the behaviour of the granular temperature in

the dilute part of the flow described in Berzi and Fraccarollo [23].

In the spirit of a simple treatment of turbulence, we take the turbulent kinetic energy to be $K = l_m^2 U'^2$, with l_m the mixing length. Berzi and Fraccarollo [23] found that the mixing length in collisional suspensions at a concentration larger than 0.2 was only a function of the concentration itself, implying that the size of the turbulent eddies was constrained by the size of the interparticle gap. When the concentration is less than 0.2, however, the size of the turbulent structures should increase and eventually, we should recover the classical result that the mixing length increases linearly with the distance from some reference position (being the von Karman's constant, $\kappa = 0.41$, the coefficient of proportionality). Indeed, as shown in Revil-Baudard et al. [168], the influence of the sediments on the mixing length extends well beyond the transport layer, in a region where the concentration is negligible. Revil-Baudard et al. [168] proposed to change the von Karman's constant to the reduced value of 0.225 to account for this phenomenon. In doing so, however, they cannot recover the classical expression for the mixing length in the absence of sediments. Here, we propose the following expression for the mixing length,

$$l_m = 3 (v_{rcp} - v)^3 + \kappa y \left[1 - \exp \left(-0.3 \frac{y}{h} \right) \right] \quad (5.15)$$

where the first term on the right-hand side of the equation (5.15) is the local mixing length suggested in Berzi and Fraccarollo [23], being v_{rcp} the concentration at random close packing [207]. The second term represents the nonlocal growing of the mixing length, in which we have introduced the damping factor, $1 - \exp \left(-0.3 \frac{y}{h} \right)$, in the spirit of Van Driest's model of turbulence [212], where the thickness of the transport layer is the natural length scale for the damping of the eddies in the presence of sediments. Figure 5.4 shows that equation (5.15) can reproduce the values of the mixing length measured in the experiments [168]. The increase of the mixing length in the proximity of the erodible bed is actually a signature of the component of the fluid viscosity associated with the particle agitation, as shown later.

Although not strictly necessary, here we assume, as in Berzi and Fraccarollo [23], that the energy diffusion in equation (5.14) is negligible (we can always remove this assumption and make use of the constitutive relation of the pseudo-thermal flux of kinetic theory if deemed important). Then, we employ the following constitutive relations for the particle shear stress [24]:

$$s = f_2 T^{1/2} \left(1 + \frac{12}{5} v \chi_0 \frac{T^{1/2}}{k_n^{1/2}} \right)^{-1} u' \quad (5.16)$$

where the dependence of the coefficient f_2 on the concentration and the normal coefficient of restitution is reported in Table A.1; and for the rate of collisional dissipation of the fluctuation energy, Γ , [24]:

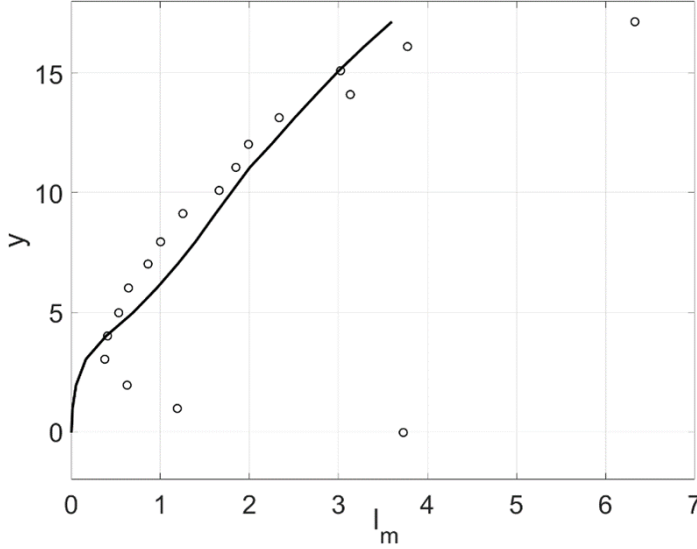


Figure 5.4: Measured (circles, Revil-Baudard et al. [168]) and predicted (line, equation 15, with $v_{rcp} = 0.64$ and $h = 10$) mixing length as a function of the distance from the erodible bed.

$$\Gamma = \frac{f_3}{L} T^{3/2} \left(1 + \frac{12}{5} v \chi_0 \frac{T^{1/2}}{k_n^{1/2}} \right)^{-1} \quad (5.17)$$

where the coefficient f_3 (Table A.1) depends on the concentration and the effective coefficient of restitution ε ; and L is the correlation length [94], which accounts for the fact that, at concentrations larger than the freezing point, 0.49, correlations in the fluctuation velocities of the particles develop [143], thus reducing the energy dissipated in collisions. Here, for the sake of simplicity, we employ the expression for the correlation length that has been determined in numerical simulations of simple shearing flows [27]:

$$L = 1 + \frac{26(1 - \varepsilon)}{15} \frac{\max(v - 0.49, 0)}{v_{rcp} - v} \quad (5.18)$$

Using equations (5.16) and (5.17) into equation (5.14), with l_m and L determined from equation (5.15) and (5.18) once the distribution of the concentration is known, neglecting Q' and assuming for simplicity that $u' \simeq U'$, so that $K \simeq l_m^2 u'^2$, permits to re-write equation (5.14) as a quadratic equation in the particle shear rate, u' , that can then be calculated at every position inside the transport layer. Then, with equation (5.16), we obtain also the distribution of the particle shear stress.

With u' known at any position, we can numerically solve by quadrature

the integral $u = \int_0^y u' dy$, with the boundary conditions $u = 0$ at the surface of the bed, to obtain the particle velocity distribution in the transport layer. The particle velocity at the surface of the bed is actually nonzero because the bed creeps [101]. However, the contribution of the creep motion of the particles inside the bed to the total transport rate can be ignored [26].

The momentum balance of the mixture in the flow direction [21] permits the determination of the distribution of the fluid shear stress in the transport layer and in the clear fluid region above it,

$$S = \frac{H - y}{\sigma - 1} \sin \phi + p \tan \phi - s \quad (5.19)$$

given that p and s are zero for $y > h$. Then, the total flow depth H can be obtained by taking $s + S = \Theta$ at the surface of the bed in equation (5.19), so that, with equation (5.8),

$$H = \frac{\sigma - 1}{\sin \phi} \Theta - (\sigma - 1) \bar{v} h \quad (5.20)$$

As suggested in Berzi and Fraccarollo [23], we take the fluid shear stress to be the sum of two contributions: one associated with turbulence, which we describe using the aforementioned mixing length approach; and one associated with the momentum exchange induced by the particle agitation, with the associated viscosity is proportional to the granular viscosity. Then,

$$S = \frac{1 - v}{\sigma} l_m^2 U'^2 + \frac{2}{5} \frac{1}{\sigma} \frac{1 + 2v}{2(1 - v)} f_2 \left(1 + \frac{12}{5} v \chi_0 \frac{T^{1/2}}{k_n^{1/2}} \right)^{-1} T^{1/2} U' \quad (5.21)$$

The pre-factor in front of the granular viscosity, s/u' , in the second term of the right-hand side of the equation (5.19) is the concentration-dependent coefficient of proportionality that we have already employed in the determination of the depth of the transport layer (equation 5.9).

With the distribution of the fluid shear stress given by equation (5.19), the fluid shear rate, U' , can be determined by solving the quadratic equation (5.21). Then, with U' known at any position, we can numerically solve by quadrature the integral $U = \int_0^y U' dy$, with the boundary conditions, $U = U_0$ (see later), at the surface of the bed, to obtain the fluid velocity distribution in the transport layer.

The momentum balance for the fluid in the flow direction [23] permits to determination of the distribution of the drag, D , exerted by the fluid on the particles as

$$D = + \frac{1 - v}{\sigma - 1} \sin \phi + S' \quad (5.22)$$

where the derivative of the fluid shear stress must be calculated numerically from the distribution of S in the transport layer. We model the drag as [96]

$$D = v C_D (U - u). \quad (5.23)$$

which includes the role of the particle velocity fluctuations and the concentration dependence suggested by Richardson and Zaki [170]. Using equation (5.22) into equation (5.23), and ignoring the derivative of the fluid shear stress at the surface of the erodible bed permits to determine U_0 there as

$$U_0 = \frac{\sigma}{\sigma - 1} \frac{(1 - v_c)^{4.1}}{v_c} \frac{R}{18} \sin \phi \quad (5.24)$$

Equation (5.23) is the equivalent of Darcy's law (Whitaker [218], "Flow in porous media I: A theoretical derivation of Darcy's law". *Transport in Porous Media*. 1: 3-25.) to evaluate the fluid velocity in a porous medium when gravity is the sole driving force.

As pointed out in Pasini and Jenkins [162], the constitutive relations for the particle stresses of the kinetic theory are valid if the mean free path (the mean distance covered by a particle in between two successive collisions) is less than the typical length of a ballistic trajectory (the path followed by a particle under the influence of gravity and, in our case, buoyancy and drag). With the expression of the mean free path of kinetic theory [39], and the length of a ballistic trajectory approximated as twice the maximum height reached by a saltating particle given in Berzi, Buettner, and Curtis [20] in terms of drag coefficient and granular temperature, this criterion translates into

$$2 \frac{C_D \sqrt{2T} - \ln(C_D \sqrt{2T} + 1)}{C_D^2} > \frac{\sqrt{2}}{12v\chi_0} \quad (5.25)$$

Actually, we might expect that, even if the length of a ballistic trajectory is larger than the mean free path, there is a layer in which the two quantities have similar values, thus indicating the existence of some kind of transitional regime between purely collisional and purely ballistic.

Application of the criterion of equation (5.25) to the experimental measurements of Capart and Fraccarollo [37] indicates that a significant portion of the transport layer is actually characterized by a mix of ballistic and collisional behaviour. In the cases of Aeolian transport [162] and gravity-driven dry granular flows [26], the ballistic layer has, instead, a negligible contribution to the total transport.

The above-described full solution of the hydrodynamic variables requires as input the angle of inclination of the bed, ϕ , the Shields number, Θ , and the entropic parameter, E . These three degrees of freedom are at odds with the experimental evidence (e.g., Capart and Fraccarollo [37]) that there are actually only two degrees of freedom: steady, fully-developed inclined flows of particles and liquid over erodible beds are completely determined once the angle of inclination of the bed and the Shields number (or, equivalently, the particle and liquid flow rates) are assigned. To eliminate the additional degree of freedom, we choose E as the optimum value of the entropic parameter that minimizes the mean variance of the residuals between the drag distribution determined by the momentum balance (equation 5.22) and that determined by its constitutive relation (equation 5.23), in the region where

the mean free path is less than 20% of the length of the ballistic trajectory.

5.3 Results and comparisons

Herein, we present a comparison between the results of the present theory and the experiments performed by Capart and Fraccarollo [37] with plastic cylinders (ratio of length-to-diameter equal to 0.8 and diameter of the equivalent sphere equal to 3.35 mm) and water, with $\sigma = 1.51$ and $R = 370$. The experiments were performed in a rectangular channel, covering a range of Shields numbers from 0.4 to 2.8, and angles of inclination of the erodible bed from 0.6° to 4.5° . We take the coefficients of restitution and friction from the measurements of the impact of two Delrin spheres reported in Foerster et al. [65]: $e_n = 0.97$, $e_t = 0.44$ and $\mu = 0.2$.

With these, the calculations suggested in Larcher and Jenkins [109] give an effective coefficient of restitution $\varepsilon = 0.77$. The discrete numerical simulations of steady, simple shearing of true cylinders reported in Berzi, Buettner, and Curtis [20] indicate that the critical volume fraction v_c is equal to 0.61 for cylinders with an aspect ratio of 0.8 and friction equal to 0.2 and that $v_{rcp} = 0.68$. Finally, Young's modulus of plastic translates into a dimensionless stiffness k_n approximately equal to 10^8 . In the experimental measurements, we set the position of the bed and the origin of the y -axis where the velocity of the particles in the x -direction falls below the sensitivity limit of the tools used to determine it. This is in conflict with the criterion $v = v_c$ that we employ to identify the erodible bed in the previously described semi-analytical treatment based on kinetic theory, and must be kept in mind when assessing the agreement between the theory and the experiments.

The behaviour of the optimum entropic parameter with the Shields number and the angle of inclination of the erodible bed in the case of plastic cylinders transported in water is depicted in Figure 5.5. We found that E monotonically increases with ϕ , indicating that more convex concentration profiles are associated with steeper flows. The dependence on the Shields number is, instead, non-monotonic, with a maximum at about $\Theta = 2$. However, a large Shields number causes the concentration profile to become more concave.

Figure 5.6 depicts the theoretical profiles of the particle, liquid and total shear stresses in the transport layer for assigned input values of ϕ and Θ . Here and in what follows, unless differently stated, the results of the theory only refer to the region of the flow for which the criterion given by equation (5.25) is satisfied. The particle shear stress decreases toward the top of the transport layer, where eventually it vanishes, and reaches a maximum slightly above the interface with the erodible bed. This maximum reflects the minimum in the liquid shear stress, due to the different dependence of its two components (equation 5.21) on the presence of the particles: the liquid turbulence decreases when the particle concentration increases, while the momentum exchange induced by particle agitation increases towards the bed.

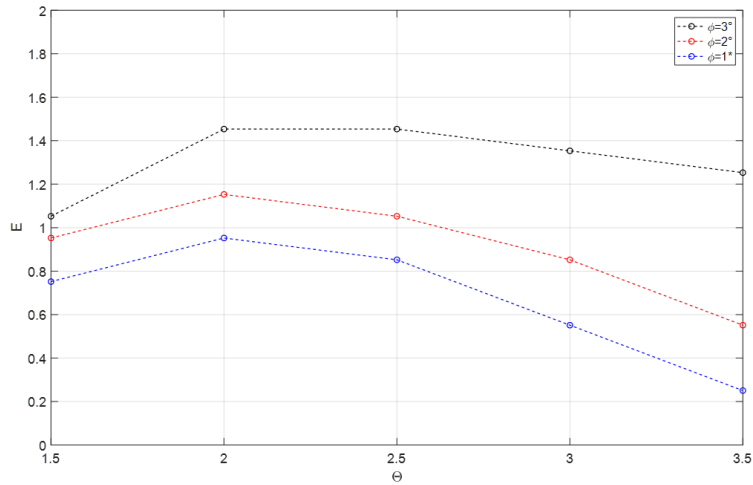


Figure 5.5: Optimum entropic parameter as a function of the Shields number for three different angles of the inclination of the bed in the case of sediment transport of plastic cylinders in water.

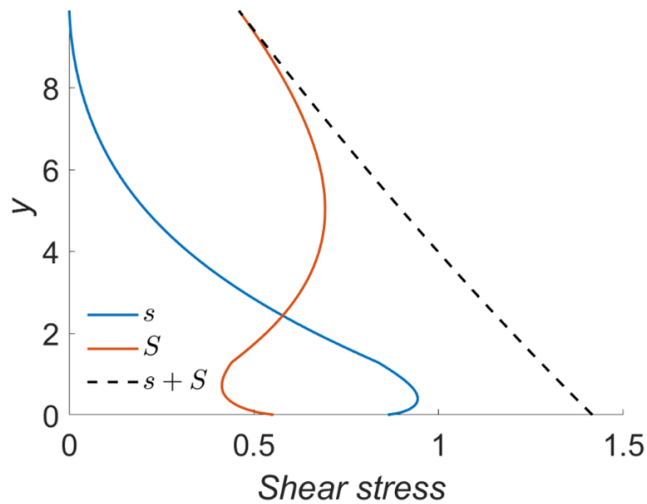


Figure 5.6: Profiles of particle, liquid | and total shear stress in the transport layer for $\phi = 1.9^\circ$ and $\Theta = 1.7$, with the corresponding optimum $E = 0.95$.

Figure 5.7a illustrates the comparisons between the experiments and the theoretical predictions in terms of profiles of concentration, particle velocity and granular temperature for two of the runs performed by Capart and Fraccarollo [37], characterized by large enough values of the Shields number that the region of the transport layer dominated by collisions is a significant portion of the total flow thickness. Similar results, not shown here for brevity, are obtained for the rest of the experimental runs with intense sediment transport. The agreement between the experiments and the theoretical predictions is remarkable, and more so if the region in which collisions dominate (represented by the extension along the y -axis of the lines relative to velocity and granular temperature profiles in Figure 5.7a) covers the majority of the thickness of the transport layer (represented by the extension along the y -axis of the line relative to the concentration profile in Figure 5.7a). One can notice the evident improvement when the collisional region goes from being around 50% of the transport layer (Figure 5.7a) to almost 70% (Figure 5.7b).

A striking feature of sediment transport in water is that the top of the region dominated by particle collisions is characterized by a non-negligible particle concentration, about 0.2 to 0.3. That means that the collisionless region, i.e., where the trajectories of the particles in between collisions are strongly affected by external forces such as gravity, buoyancy and drag, is a significant portion of the transport layer. Once again, this is very different from both inclined granular flows [26] and Aeolian transport [162], where collisions are dominant and, therefore, kinetic theory of granular gases is relevant even at very small values of the particle concentration, say of order 10^{-2} .

Although not measured in the experiments, we also show in Figure 5.7 the theoretical profiles of the liquid velocity in the flow direction. As assumed to simplify part of the analytical treatment, the liquid and particle shear rates are rather similar, with the velocity difference more pronounced near the top of the transport layer.

5.4 Concluding remarks

In this chapter, the steady inclined collisional flow of sediments immersed in a turbulent liquid over an erodible bed has been modelled in the frame of the kinetic theory of granular gases. In doing so we have accounted for particle surface friction, cylindrical shape, finite-duration of contacts, exchange between turbulent kinetic energy and fluctuation kinetic energy of the particles, suppression of turbulence due to the presence of the particles, and fluid momentum exchange induced by particle agitation. The complicated set of differential equations composed of balances of momentum and energy, closed by a series of constitutive relations, has been solved analytically by assuming that the particle concentration followed a one-parameter logarithmic distribution, in order to satisfy the Shannon maximum Entropy principle. The entropic parameter of the distribution was chosen as to minimize the

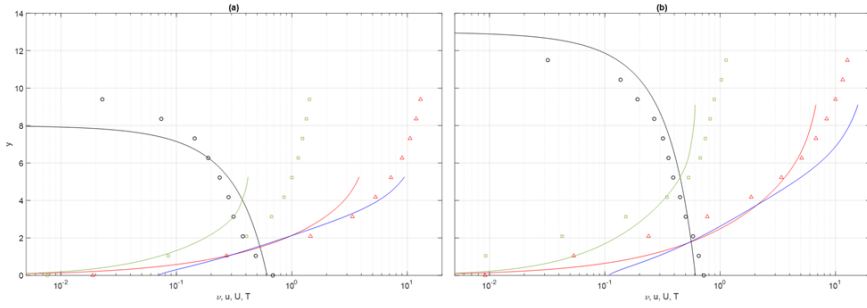


Figure 5.7: Experimental measurements (symbols) and theoretical predictions (lines) of profiles of concentration (black lines and circles), particle (red lines and triangles) and liquid (blue lines) velocity, and granular temperature (green lines and squares) when: (a) $\phi = 1.9^\circ$ and $\Theta = 1.7$, with the corresponding optimum $E = 0.95$; (b) $\phi = 3.0^\circ$ and $\Theta = 2.9$, with the corresponding optimum $E = 1.35$.

mismatch between the distribution of the fluid drag obtained by solving the fluid momentum balance in the flow direction and that obtained by employing a constitutive relation for the drag based upon a linear dependence on the velocity difference between the fluid and the particles. We have shown that the optimum entropic parameter depends on the angle of inclination of the bed and the intensity of the shearing fluid. We have determined the analytical profiles of different hydrodynamic fields - particle and fluid shear stresses, velocities and granular temperature - and made successful comparisons against several experimental measurements on the collisional transport of plastic cylinders in water, in a range of slope and Shields values. We have confirmed that, unlike the case of aeolian transport, in a significant upper part of the transport layer, the length of the particle trajectories influenced by external forces in between successive collisions is shorter or of the same order of magnitude than the mean free path of kinetic theory. Hence, the ballistic regime plays a significant role even in the case of intense sediment transport, supposedly dominated by interparticle collisions.

Chapter 6

Conclusions and future research

According to the major aims of PRIN project "Enterprising", synthesized in monitoring and modelling high-flow conditions in rivers, the key-stone idea the project started from was to check freshwater mussels as potential reliable bioindicators. We investigated, as a first attempt to our knowledge, the effects of hydrodynamic perturbations of the aquatic environment on the biotic community, both in the laboratory and in natural sites. On another side of this work, two different measurement devices for turbidity and streambed scour and deposition have been introduced and successfully tested in a laboratory flume, assessing the potential of being used in the field. Finally, on more theoretical ground, we got some inferences on ordinary and intense sediment transport, made possible by using in a specific way the entropy theory. We validated as much as possible all the theoretical premises we introduced, either through experiments or field observations. The interdisciplinary nature of these pursuits required intense collaborative efforts across diverse fields and approaches, ranging from mechanical devices (electronic boards and sensors) to biotic communities (live organisms, FMs), which enabled us to reach a wider view of the processes and of their representation through measurements. Resuming what represented in this thesis through its chapters, the following ones are those I deem as my key research results:

- free and immobilised freshwater mussels can serve as effective ecosystem warning indicators in aquatic environments, though they need a specific installation depending on the expected stressors, riverbed and flow rate conditions (Chapter 2);
- continuous wavelet transform proves to be a valuable tool for interpreting the FMs signals, in terms of identifying pseudo-frequency features present in the signal over time and using them to describe the response of FMs to external perturbations, providing more informative results than only looking at discontinuities in the opening time series (Chapter 2);
- laboratory and field experiments with immobilised mussels demonstrate their response to hydrodynamic stresses within a frequency of

valve gaping ranging from 10^{-3} Hz to 1 Hz. This frequency range is larger than the background frequency range during normal behaviour (around $10^{-4} - 10^{-3}$ Hz when taking the median across multiple individuals). These frequency values correspond to conditions that indicate the presence of stressful conditions for the FMs, thus underscoring the potential use of FMs as real-time BEWS for identifying potential threats to the aquatic ecosystem (Chapter 2);

- a new BED-sensors string based on LDRs has been employed and successfully tested in the laboratory for different applications such as check dam and pier of bridge dealing with streambed scour and deposition. A promising result indicates that this device can also be used in the field (Chapter 3);
- a new turbidimeter based on low-cost turbidity sensors has been introduced with a new design and waterproof housing. This device was successfully calibrated and then tested in the flume with different turbidity stages (increase and decrease in flow turbidity). A promising result at high turbidity indicates that this device can be used in the laboratory and field and with an improvement in the calibration method, the device also can be reliable in low turbidity (Chapter 3);
- statistical information for ordinary bed-load transport (low Shields values) is inferred through an innovative methodology that also involves surface velocity measurements. A new way to deal with the particle resting-time statistics is achieved within the frame of the general Shannon entropy principle and by adopting the Einstein approach to ordinary bedload processes; both well and poorly sorted bed texture have been faced (Chapter 4);
- concentration profiles obtained by adopting the entropy law as offered in several papers, without connection to the respect of mechanical principles, was the input underpinning a solution involving velocity of both phases and granular temperature in the stratified layer of collisional bed-load layers. These flow conditions take place over a mobile bed when Shields and slope values are in an intermediate range, between ordinary bed load and either turbulent suspension or debris flows. We got solutions by a quasi-analytical integration of differential equations expressing mass, momentum, and energy conservation in the frame of kinetic theory (Chapter 5);

Several future research challenges stem from this PhD work and state-of-art literature on the faced topics. Sediment transport, at different regimes, offers so many aspects to explore that are still obscure and important. Monitoring it with improved and more efficient technology, as we meant to do by exploiting light and turbidity sensors, or understanding how the solid and liquid phases collaborate to merge their momentum and energy fluxes, their production and dissipation mechanisms are quite fundamental scientific tasks. Last but not least, "asking" more intriguing questions to "our"

mussels, that is for instance, how they allow us to distinguish between different stressors inducing a change in their behaviour, would be hectic. Still, we need to find a "communicative language". I am eager to see how the restless research work of our bio-fluid-mechanics community will progress in all these aspects, and further but related ones, that are even difficult to conceive in the present, and I shall remain happy to have worked and, hopefully, have contributed to this joint effort.

Appendix A

Appendix A

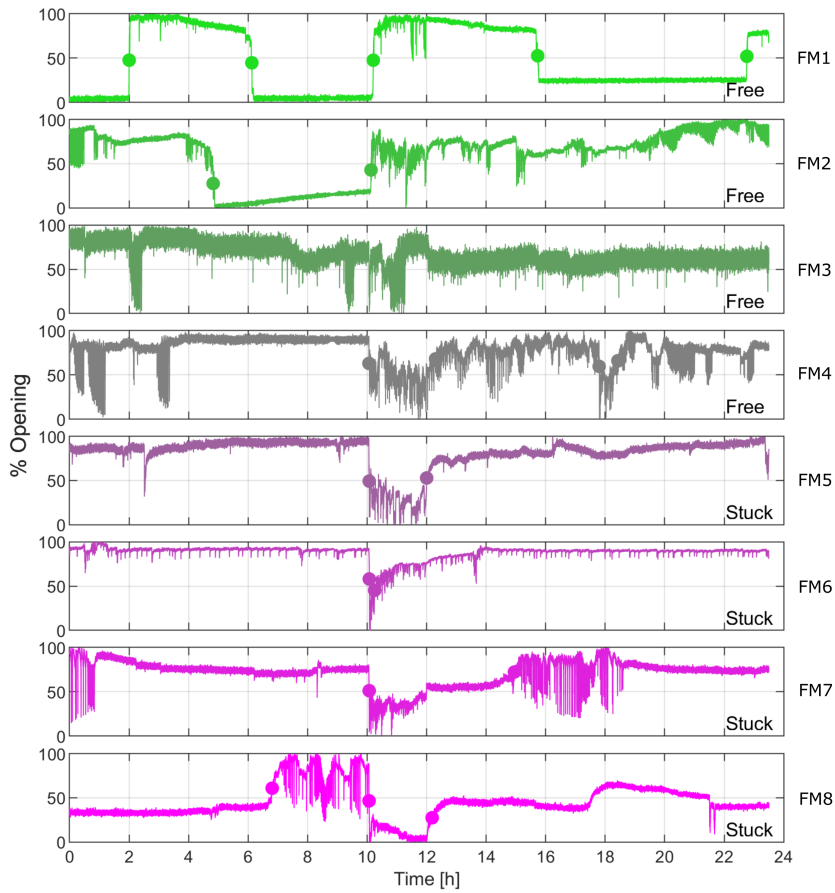


Figure A.1: Valve opening signals for the individual free and immobilised FMs deployed in the laboratory experiment (dots indicate abrupt change points in the mean of the opening signals when the mean opening changes by more than 25%).

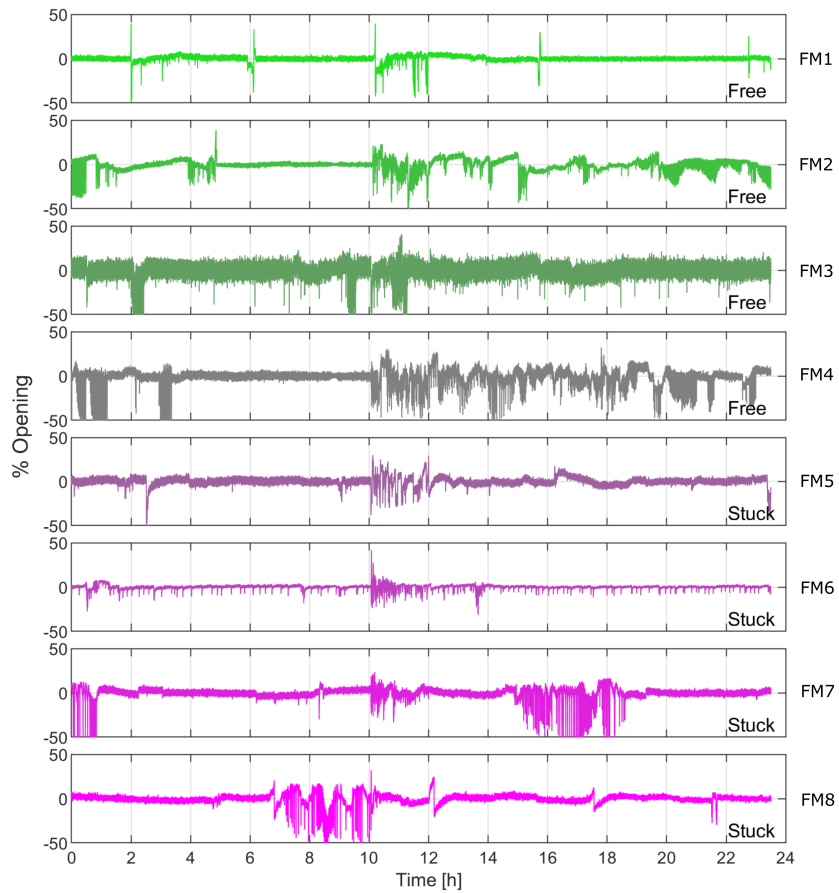


Figure A.2: Valve opening signals for the individual free and immobilised FMs deployed in the laboratory experiment after detrending and removal of step changes in the mean valve opening.

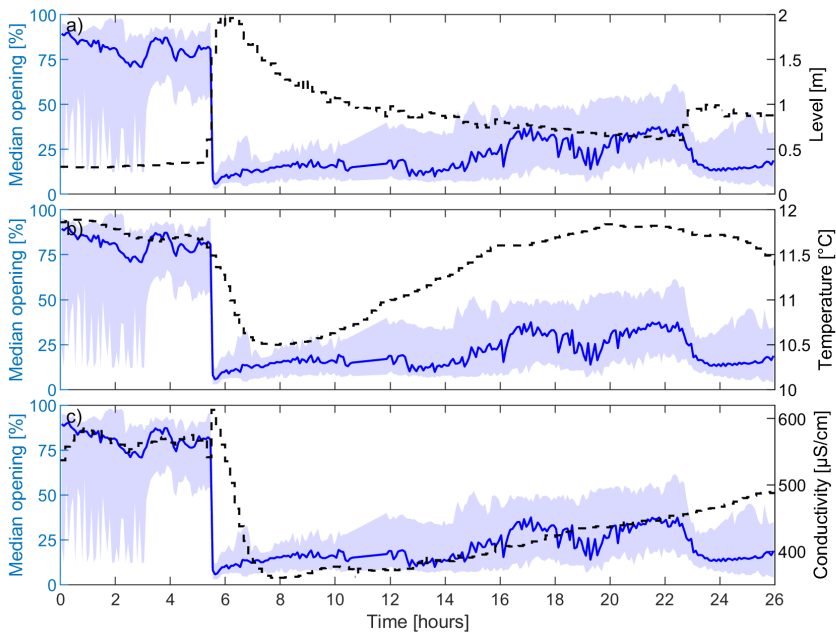


Figure A.3: Data from the multiparametric sensor installed at the field monitoring site; a) left y-axis: median valve opening signal with 25th and 75th percentiles indicated by the shaded area; right y-axis: water level; b) left y-axis: as in a); right y-axis: water temperature; c) left y-axis: as in a); right y-axis: water conductivity.

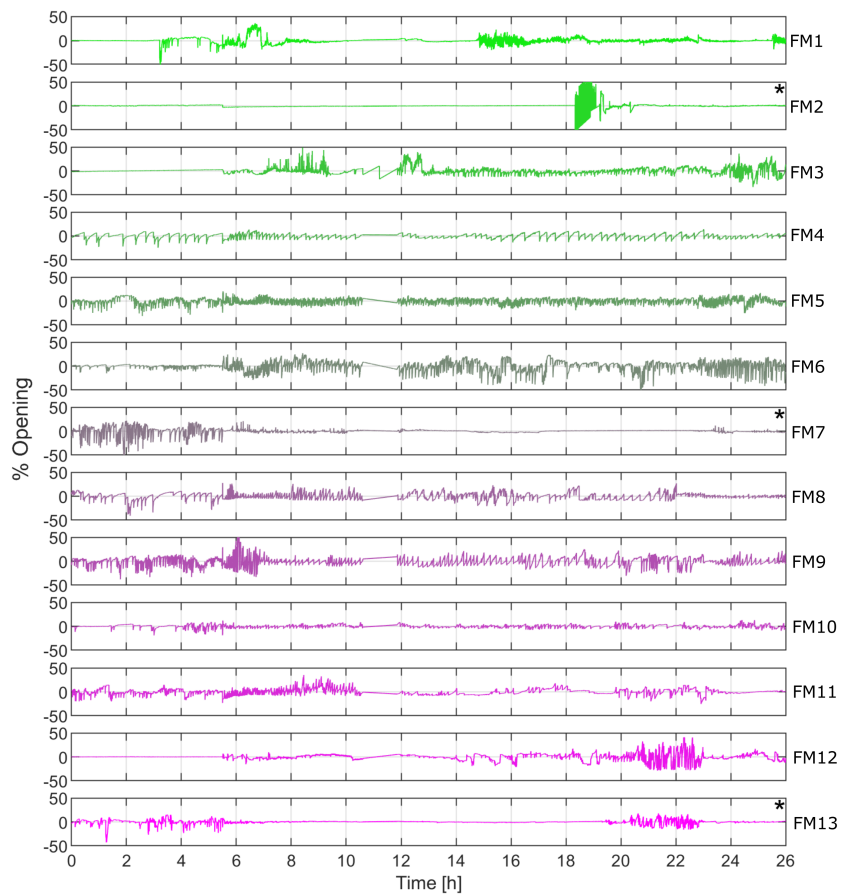


Figure A.4: Valve opening signals for the individual immobilised FMs deployed at the field monitoring site after detrending and removal of step changes in the mean valve opening. The asterisk * depicts FMs that are excluded from the wavelet transform analysis presented in Figure 5 in the main text.

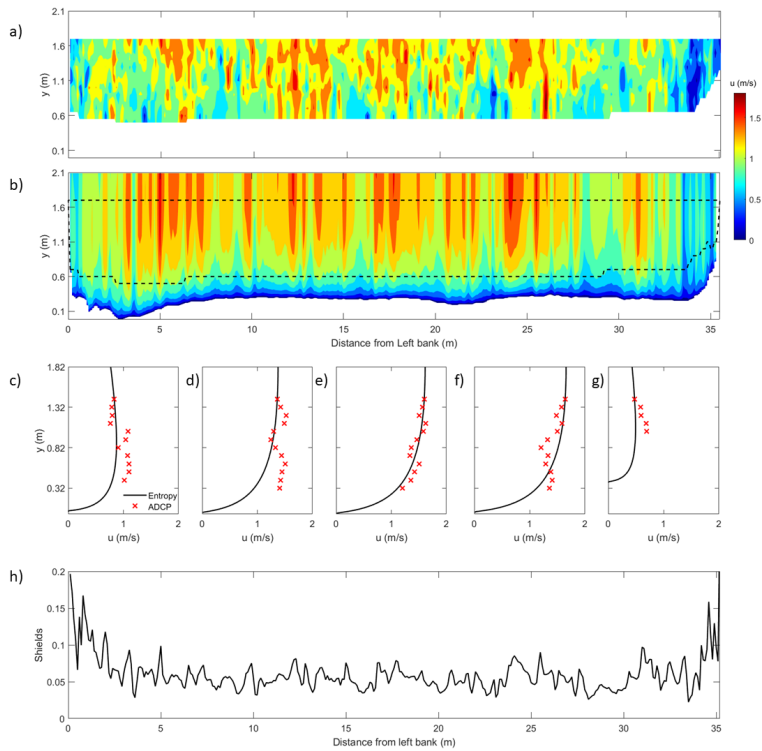


Figure A.5: Colour maps of the Velocity field in the cross-section for the low flow condition: a) based on the ADCP data, b) based on the Entropy theory. Ponte Adige cross section, high flow condition. c to g) random velocity profiles from the left bank to the right bank. h) distribution of Shields stress.

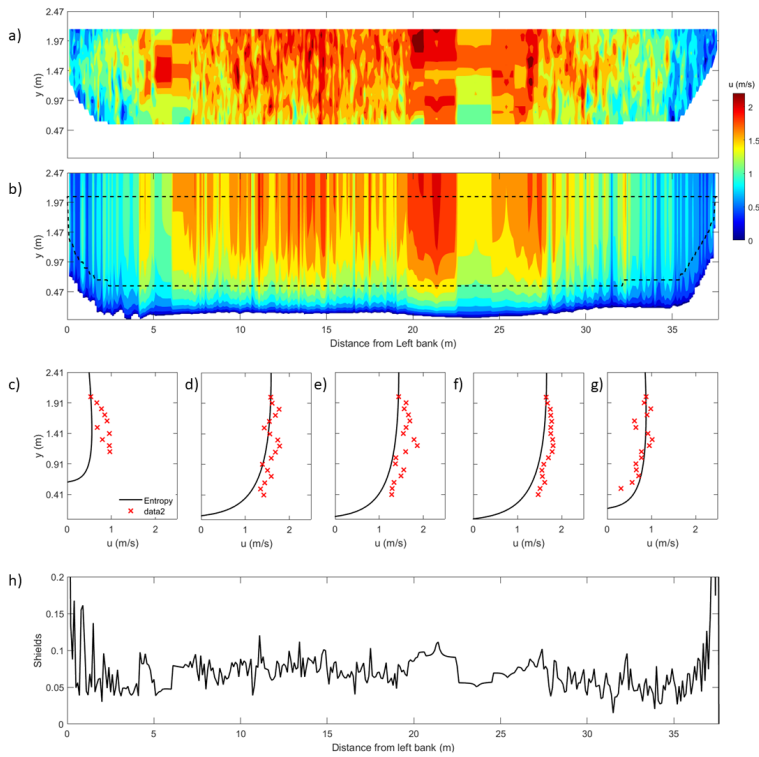


Figure A.6: Colour maps of the Velocity field in the cross-section for the moderate flow condition: a) based on the ADCP data, b) based on the Entropy theory. Ponte Adige cross section, high flow condition. c to g) random velocity profiles from the left bank to the right bank. h) distribution of Shields stress.

Table A.1: Functions of extended kinetic theory in the dense limit.

$$f_1 = 2(1 + e_n) v G$$

$$f_2 = \frac{8J}{5\pi^{1/2}} v G$$

$$f_3 = \frac{12}{\pi^{1/2}} v G (1 - e^2)$$

$$G = v \chi_0$$

$$J = \frac{1+e_n}{2} + \frac{\pi}{4} \frac{(3e_n-1)(1+e_n)^2}{[24-(1-e_n)(11-e_n)]}$$

$$e = e_n - \frac{3}{2} \mu \exp(-3\mu)$$

$$\chi_0 = f \frac{2-v}{2(1-v)^3} + (1-f) \frac{2}{v_c-v}$$

$$f = \begin{cases} 1 & \text{if } v < 0.4, \\ \frac{v^2 - 0.8v + v_c(0.8 - v_c)}{0.8v_c - 0.16 - v_c^2} & \text{otherwise,} \end{cases}$$

Bibliography

- [1] Hossein Afzalimehr and François Anctil. "Velocity distribution and shear velocity behaviour of decelerating flows over a gravel bed". In: *Canadian Journal of Civil Engineering* 26.4 (1999), pp. 468–475. ISSN: 0315-1468.
- [2] Hassan B. Akberali and John Davenport. "The detection of salinity changes by the marine bivalve molluscs *Scrobicularia plana* (da Costa) and *Mytilus edulis* L." In: *Journal of Experimental Marine Biology and Ecology* 58.1 (1982), pp. 59–71. ISSN: 0022-0981.
- [3] Christophe Ancey et al. "Statistical description of sediment transport experiments". In: *Physical Review E* 74.1 (2006), p. 011302.
- [4] Thorbjørn J. Andersen, Morten Pejrup, and Allan Aasbjerg Nielsen. "Long-term and high-resolution measurements of bed level changes in a temperate, microtidal coastal lagoon". In: *Marine Geology* 226.1-2 (2006), pp. 115–125.
- [5] Bruno Andreotti. "A two-species model of aeolian sand transport". In: *Journal of Fluid Mechanics* 510 (2004), pp. 47–70. ISSN: 0022-1120. DOI: [10.1017/S0022112004009073](https://doi.org/10.1017/S0022112004009073).
- [6] E.D. Andrews. "Entrainment of gravel from naturally sorted riverbed material". In: *Geological Society of America Bulletin* 94.10 (1983), pp. 1225–1231.
- [7] Michal Antala et al. "Impact of climate change-induced alterations in peatland vegetation phenology and composition on carbon balance". In: *Science of the total environment* 827 (2022), p. 154294. ISSN: 0048-9697.
- [8] Aronne Armanini, Luigi Fraccarollo, and Michele Larcher. "Debris Flow". In: *Encyclopedia of Hydrological Sciences* (2006).
- [9] Kazuo Ashida and Masanori Michiue. "Studies on bed load transportation for nonuniform sediment and river bed variation". In: *Disaster Prevention Research Institute Annuals* 14 (1972).
- [10] Abimbola Atijosan et al. "Development of a low-cost community-based real-time flood monitoring and early warning system". In: *International Journal of Scientific Research in Science, Engineering and Technology* 3.3 (2017), pp. 189–195.

- [11] Mi-Jung Bae and Young-Seuk Park. "Biological early warning system based on the responses of aquatic organisms to disturbances: a review". In: *Science of the Total Environment* 466 (2014), pp. 635–649. ISSN: 0048-9697.
- [12] R.A. Bagnold. *The Physics of Blown Sand and Desert Dunes*. New York: Methuen, 1941.
- [13] Farhad Bahmanpouri et al. "Bed compaction effect on dam break flow over erodible bed; experimental and numerical modeling". In: *Journal of Hydrology* 594 (2021), p. 125645. ISSN: 0022-1694.
- [14] Farhad Bahmanpouri et al. "Estimating flood discharge at river bridges using the entropy theory. Insights from Computational Fluid Dynamics flow fields". In: *Hydrology and Earth System Sciences Discussions* 2023 (2023), pp. 1–29.
- [15] Farhad Bahmanpouri et al. "Estimating the Average River Cross-Section Velocity by Observing Only One Surface Velocity Value and Calibrating the Entropic Parameter". In: *Water Resources Research* 58.10 (2022), e2021WR031821. ISSN: 0043-1397.
- [16] Farhad Bahmanpouri et al. "Prediction of river discharges at confluences based on entropy theory and surface-velocity measurements". In: *Journal of Hydrology* 606 (2022), p. 127404. ISSN: 0022-1694.
- [17] Olga Barron et al. "Climate change effects on water-dependent ecosystems in south-western Australia". In: *Journal of Hydrology* 434 (2012), pp. 95–109. ISSN: 0022-1694.
- [18] Sebastian Beggel and Juergen Geist. "Acute effects of salinity exposure on glochidia viability and host infection of the freshwater mussel *Anodonta anatina* (Linnaeus, 1758)". In: *Science of the Total Environment* 502 (2015), pp. 659–665. ISSN: 0048-9697.
- [19] Diego Berzi. "Analytical Solution of Collisional Sheet Flows". In: *Journal of Hydraulic Engineering - ASCE* 137.10 (2011), pp. 1200–1207. DOI: [10.1061/\(ASCE\)HY.1943-7900.0000420](https://doi.org/10.1061/(ASCE)HY.1943-7900.0000420)..
- [20] Diego Berzi, Kevin E. Buettner, and Jennifer S. Curtis. "Dense shearing flows of soft, frictional cylinders". In: *Soft Matter* 18.1 (2022), pp. 80–88. ISSN: 17446848. DOI: [10.1039/d1sm01395e](https://doi.org/10.1039/d1sm01395e).
- [21] Diego Berzi and Luigi Fraccarollo. "Inclined, collisional sediment transport". In: *Physics of Fluids* 25.10 (2013). ISSN: 1070-6631.
- [22] Diego Berzi and Luigi Fraccarollo. "Intense sediment transport: Collisional to turbulent suspension". In: *Physics of Fluids* 28.2 (2016). ISSN: 1070-6631.
- [23] Diego Berzi and Luigi Fraccarollo. "Turbulence locality and granular-like fluid shear viscosity in collisional suspensions". In: *Physical review letters* 115.19 (2015), p. 194501.

- [24] Diego Berzi and James T. Jenkins. “Steady shearing flows of deformable, inelastic spheres”. In: *Soft Matter* 11.24 (2015), pp. 4799–4808. ISSN: 10706631. DOI: [10.1039/C5SM00337G](https://doi.org/10.1039/C5SM00337G). URL: <http://dx.doi.org/10.1039/C5SM00337G>.
- [25] Diego Berzi, James T. Jenkins, and Patrick Richard. “Erodible, granular beds are fragile”. In: *Soft Matter* 15 (2019), pp. 7173–7178. ISSN: 1744-683X. DOI: [10.1039/c9sm01372e](https://doi.org/10.1039/c9sm01372e). URL: <http://dx.doi.org/10.1039/C9SM01372E>.
- [26] Diego Berzi, James T. Jenkins, and Patrick Richard. “Extended kinetic theory for granular flow over and within an inclined erodible bed”. In: *J. Fluid Mech* 885 (2020), A27. DOI: [10.1017/jfm.2019.1017](https://doi.org/10.1017/jfm.2019.1017).
- [27] Diego Berzi and Dalila Vescovi. “Different singularities in the functions of extended kinetic theory at the origin of the yield stress in granular flows”. In: *Physics of Fluids (1994–present)* 27.1 (2015), p. 013302. DOI: [10.1063/1.4905461](https://doi.org/10.1063/1.4905461).
- [28] J. Borcharding. “Valve movement of the mussel *Dreissena polymorpha* as a monitoring system for bodies of water”. In: *Schriftenreihe des Vereins für Wasser-, Boden- und Lufthygiene* 89 (1992), pp. 361–373. ISSN: 0300-8665.
- [29] A. Brahms. “Elements of darn and hydraulic engineering”. In: *Aurich, Germany* 1 (1757), p. 105.
- [30] James Brasington, BT Rumsby, and RA McVey. “Monitoring and modelling morphological change in a braided gravel-bed river using high resolution GPS-based survey”. In: *Earth surface processes and landforms: the journal of the British Geomorphological Research Group* 25.9 (2000), pp. 973–990.
- [31] Frank M. Butterworth, Rafael Villalobos-Pietrini, and María E. Gonsé-batt. “Introduction: Biomonitoring and Biomarkers as Indicators of Environmental Change, Volume 2”. In: *Biomonitoring and Biomarkers as Indicators of Environmental Change 2: A Handbook*. Springer, 2001, pp. 1–8.
- [32] Donald R. Cahoon et al. “High-precision measurements of wetland sediment elevation: I. Recent improvements to the sedimentation-erosion table”. In: *Journal of Sedimentary Research* 72.5 (2002), pp. 730–733.
- [33] John Cairns, G.P. Patil, and W.E. Waters. *Biological monitoring—concept and scope*. 1979.
- [34] Jenny Campagnol, Alessio Radice, and Francesco Ballio. “Scale-based statistical analysis of sediment fluxes”. In: *Acta Geophysica* 60.6 (2012), pp. 1744–1777.
- [35] Jenny Campagnol et al. “Lagrangian analysis of bed-load sediment motion: database contribution”. In: *Journal of Hydraulic Research* 51.5 (2013), pp. 589–596. ISSN: 0022-1686.

- [36] Qi Cao et al. "Monitoring water quality of the Haihe River based on ground-based hyperspectral remote sensing". In: *Water* 14.1 (2021), p. 22. ISSN: 2073-4441.
- [37] Hervé Capart and Luigi Fraccarollo. "Transport layer structure in intense bed-load". In: *Geophysical Research Letters* 38 (Oct. 2011), p. L20402. ISSN: 0094-8276. DOI: [10.1029/2011GL049408](https://doi.org/10.1029/2011GL049408).
- [38] Anthony J. Capraro, Ronald T. Verrillo, and Jozef J. Zwislocki. "Psychophysical evidence for a triplex system of cutaneous mechanoreception." In: *Sensory Processes* (1979). ISSN: 0363-3799.
- [39] S. Chapman and T.G. Cowling. *The mathematical theory of non-uniform gases*. Vol. 27. 1970. ISBN: 0252725484. DOI: [10.2307/3611062](https://doi.org/10.2307/3611062).
- [40] Rémi Chassagne, Cyrille Bonamy, and Julien Chauchat. "A frictional-collisional model for bedload transport based on kinetic theory of granular flows: Discrete and continuum approaches". In: *Journal of Fluid Mechanics* 964 (2023), pp. 1–39. ISSN: 14697645. DOI: [10.1017/jfm.2023.335](https://doi.org/10.1017/jfm.2023.335).
- [41] Sebastian Chialvo, Jin Sun, and Sankaran Sundaresan. "Bridging the rheology of granular flows in three regimes". In: *Physical Review E* 85.2 (Feb. 2012), p. 021305. ISSN: 1539-3755. DOI: [10.1103/PhysRevE.85.021305](https://doi.org/10.1103/PhysRevE.85.021305).
- [42] Chao-Lin Chiu. "Entropy and 2-D velocity distribution in open channels". In: *Journal of Hydraulic Engineering* 114.7 (1988), pp. 738–756. ISSN: 0733-9429.
- [43] Chao-Lin Chiu. "Velocity distribution in open channel flow". In: *Journal of Hydraulic Engineering* 115.5 (1989), pp. 576–594. ISSN: 0733-9429.
- [44] Chao-Lin Chiu, Weixia Jin, and Yen-Chang Chen. "Mathematical models of distribution of sediment concentration". In: *Journal of Hydraulic Engineering* 126.1 (2000), pp. 16–23. ISSN: 0733-9429.
- [45] Chao-Lin Chiu and Chairil A. Abidin Said. "Maximum and mean velocities and entropy in open-channel flow". In: *Journal of Hydraulic Engineering* 121.1 (1995), pp. 26–35. ISSN: 0733-9429.
- [46] Chao-Lin Chiu, Shih-Meng Hsu, and Ning-Chien Tung. "Efficient methods of discharge measurements in rivers and streams based on the probability concept". In: *Hydrological Processes: An International Journal* 19.20 (2005), pp. 3935–3946. ISSN: 0885-6087.
- [47] Mohammad Salah Uddin Chowdury et al. "IoT based real-time river water quality monitoring system". In: *Procedia computer science* 155 (2019), pp. 161–168. ISSN: 1877-0509.
- [48] Michael Clare et al. "Lessons learned from the monitoring of turbidity currents and guidance for future platform designs". In: *Geological Society, London, Special Publications* 500.1 (2020), pp. 605–634.
- [49] David Coker. *Automated biomonitoring: Living sensors as environmental monitors*: Edited by David S. Gruber and Jerome M. Diamond. Ellis Horwood, Chichester. Pp. 208. 1988. £ 29.50. 1989.

- [50] M. Creyssels et al. "Saltating particles in a turbulent boundary layer: experiment and theory". In: *Journal of Fluid Mechanics* 625 (Apr. 2009), p. 47. ISSN: 0022-1120. DOI: [10.1017/S0022112008005491](https://doi.org/10.1017/S0022112008005491).
- [51] John Davenport. "The isolation response of mussels (*Mytilus edulis* L.) exposed to falling sea-water concentrations". In: *Journal of the Marine Biological Association of the United Kingdom* 59.1 (1979), pp. 123–132. ISSN: 1469-7769.
- [52] John Davenport. "The opening response of mussels (*Mytilus edulis*) exposed to rising sea-water concentrations". In: *Journal of the Marine Biological Association of the United Kingdom* 61.3 (1981), pp. 667–678. ISSN: 1469-7769.
- [53] Andrea Dell'Agnese et al. "A bedload tracer experiment in a high-elevation mountain basin (Strimm basin, Eastern Italian Alps)". In: *EGU General Assembly Conference Abstracts*. 2014, p. 6634.
- [54] Timothy DeWeese, Daniele Tonina, and Charles Luce. "Monitoring streambed scour/deposition under nonideal temperature signal and flood conditions". In: *Water Resources Research* 53.12 (2017), pp. 10257–10273.
- [55] Jessica Droujko and Peter Molnar. "Open-source, low-cost, in-situ turbidity sensor for river network monitoring". In: *Scientific Reports* 12.1 (2022), p. 10341.
- [56] Alexander G Dvoretzky and Vladimir G Dvoretzky. "Shellfish as biosensors in online monitoring of aquatic ecosystems: A review of Russian studies". In: *Fishes* 8.2 (2023), p. 102. ISSN: 2410-3888.
- [57] Isa Ebtahaj et al. "An integrated framework of extreme learning machines for predicting scour at pile groups in clear water condition". In: *Coastal Engineering* 135 (2018), pp. 1–15. ISSN: 0378-3839.
- [58] I.V. Egiazaroff. "Calculation of nonuniform sediment concentrations". In: *Journal of the Hydraulics Division* 91.4 (1965), pp. 225–247.
- [59] Hans Albert Einstein. *The bed-load function for sediment transportation in open channel flows*. 1026. US Department of Agriculture, 1950.
- [60] Frank Engelund and Jørgen Fredsøe. "A sediment transport model for straight alluvial channels". In: *Hydrology Research* 7.5 (1976), pp. 293–306.
- [61] Siobhan L. Fathel, David Jon Furbish, and Mark W. Schmeckle. "Experimental evidence of statistical ensemble behavior in bed load sediment transport". In: *Journal of Geophysical Research: Earth Surface* 120.11 (2015), pp. 2298–2317.
- [62] R. Fernandez Luque and R. Van Beek. "Erosion and transport of bed-load sediment". In: *Journal of hydraulic research* 14.2 (1976), pp. 127–144.
- [63] Harindra Joseph Fernando. "Handbook of environmental fluid dynamics, volume one: overview and fundamentals". In: (2012).

- [64] Murray Fisher. "Analysis and evaluation of existing and novel turbulent dynamic pressure based methods for measuring bridge pier and abutment scour". PhD thesis. Clemson University, 2012.
- [65] Samuel F. Foerster et al. "Measurements of the collision properties of small spheres". In: *Physics of Fluids* 6.3 (1994), pp. 1108–1115. ISSN: 10706631. DOI: [10.1063/1.868282](https://doi.org/10.1063/1.868282).
- [66] Silvia Folegot et al. "The effects of a sediment flushing on Alpine macroinvertebrate communities". In: *Hydrobiologia* 848.17 (2021), pp. 3921–3941. ISSN: 0018-8158.
- [67] Mark A. Fonstad et al. "Topographic structure from motion: a new development in photogrammetric measurement". In: *Earth surface processes and Landforms* 38.4 (2013), pp. 421–430.
- [68] Luigi Fraccarollo and Marwan A. Hassan. "Einstein conjecture and resting-time statistics in the bed-load transport of monodispersed particles". In: *Journal of Fluid Mechanics* 876 (2019), pp. 1077–1089. ISSN: 0022-1120.
- [69] David Jon Furbish et al. "Probability distributions of bed load particle velocities, accelerations, hop distances, and travel times informed by Jaynes's principle of maximum entropy". In: *Journal of Geophysical Research: Earth Surface* 121.7 (2016), pp. 1373–1390. ISSN: 2169-9003.
- [70] Emmanuel J. Gabet. "Lateral migration and bank erosion in a salt-marsh tidal channel in San Francisco Bay, California". In: *Estuaries* 21 (1998), pp. 745–753.
- [71] Florian Ganthy, Aldo Sottolichio, and Romaric Verney. "Seasonal modification of tidal flat sediment dynamics by seagrass meadows of *Zostera noltii* (Bassin d'Arcachon, France)". In: *Journal of Marine Systems* 109 (2013), S233–S240.
- [72] Peng Gao. "Transition between Two Bed-Load Transport Regimes : Saltation and Sheet Flow". In: *Journal of Hydraulic Engineering* 134.March (2008), pp. 340–349. ISSN: 0733-9429. DOI: [10.1061/\(ASCE\)0733-9429\(2008\)134:3\(340\)](https://doi.org/10.1061/(ASCE)0733-9429(2008)134:3(340)).
- [73] V. Garzó and J.W. Dufty. "Dense fluid transport for inelastic hard spheres". In: *Physical Review E* 59.5 (May 1999), pp. 5895–5911. ISSN: 1063-651X. URL: <http://www.ncbi.nlm.nih.gov/pubmed/11969571>.
- [74] Almut Gerhardt et al. "In situ on-line toxicity biomonitoring in water: Recent developments". In: *Environmental Toxicology and Chemistry: An International Journal* 25.9 (2006), pp. 2263–2271. ISSN: 0730-7268.
- [75] Anatoly Gitelson et al. "Quantitative remote sensing methods for real-time monitoring of inland waters quality". In: *International Journal of Remote Sensing* 14.7 (1993), pp. 1269–1295. ISSN: 0143-1161.
- [76] Edward D. Goldberg. "The mussel watch-a first step in global marine monitoring." In: (1975).

- [77] Alena Sonia Gsell et al. "Evaluating early-warning indicators of critical transitions in natural aquatic ecosystems". In: *Proceedings of the National Academy of Sciences* 113.50 (2016), E8089–E8095. ISSN: 0027-8424.
- [78] Bruna V. Guterres et al. "Intelligent classifiers on the construction of pollution biosensors based on bivalves behavior". In: *Brazilian Conference on Intelligent Systems*. Springer, 2020, pp. 588–603.
- [79] A. Gyr. "Towards a better definition of the three types of sediment transport". In: *Journal of Hydraulic Research* 21.1 (1983), pp. 1–15.
- [80] H.M. Habersack. "Radio-tracking gravel particles in a large braided river in New Zealand: A field test of the stochastic theory of bed load transport proposed by Einstein". In: *Hydrological Processes* 15.3 (2001), pp. 377–391.
- [81] Jason T. Hartmann et al. "Establishing mussel behavior as a biomarker in ecotoxicology". In: *Aquatic Toxicology* 170 (2016), pp. 279–288. ISSN: 0166-445X.
- [82] Marwan A. Hassan et al. "Displacement characteristics of coarse fluvial bed sediment". In: *Journal of Geophysical Research: Earth Surface* 118.1 (2013), pp. 155–165.
- [83] Christine E. Hatch et al. "Quantifying surface water–groundwater interactions using time series analysis of streambed thermal records: Method development". In: *Water Resources Research* 42.10 (2006).
- [84] George L Heritage and Andrew RG Large. "Laser Scanning for the Environmental Sciences". In: (2009).
- [85] A.G. Hernandez-Ramirez et al. "Detection, provenance and associated environmental risks of water quality pollutants during anomaly events in River Atoyac, Central Mexico: A real-time monitoring approach". In: *Science of the Total Environment* 669 (2019), pp. 1019–1032. ISSN: 0048-9697.
- [86] Paul J. Higgins. "Effects of food availability on the valve movements and feeding behavior of juvenile *Crassostrea virginica* (Gmelin). I. Valve movements and periodic activity". In: *Journal of Experimental Marine Biology and Ecology* 45.2 (1980), pp. 229–244. ISSN: 0022-0981.
- [87] Mark Hollins et al. "Time course and action spectrum of vibrotactile adaptation". In: *Somatosensory & motor research* 7.2 (1990), pp. 205–221. ISSN: 0899-0220.
- [88] E.A. Holt and S.W. Miller. "Bioindicators: Using organisms to measure". In: *Nature* 3 (2011), pp. 8–13.
- [89] Janet Hooke. "Coarse sediment connectivity in river channel systems: a conceptual framework and methodology". In: *Geomorphology* 56.1-2 (2003), pp. 79–94.
- [90] Tony Howes, Charles Lemckert, and Andrew Moss. "Long term monitoring of estuarine water quality: Brisbane River turbidity". In: *Water* 29.6 (2002), pp. 37–39.

- [91] Tian-Jian Hsu, James T. Jenkins, and Philip L.-F. Liu. "On two-phase sediment transport: sheet flow of massive particles". In: *Proceedings of the Royal Society A: Mathematical, Physical and Engineering Sciences* 460 (Aug. 2004), pp. 2223–2250. ISSN: 1364-5021. DOI: [10.1098/rspa.2003.1273](https://doi.org/10.1098/rspa.2003.1273).
- [92] Zhan Hu et al. "Continuous monitoring bed-level dynamics on an intertidal flat: Introducing novel, stand-alone high-resolution SED-sensors". In: *Geomorphology* 245 (2015), pp. 223–230.
- [93] Razieh Jalalabadi and Thorsten Stoesser. "Reynolds and dispersive shear stress in free-surface turbulent channel flow over square bars". In: *Physical Review E* 105.3 (2022), p. 35102.
- [94] James T. Jenkins. "Dense inclined flows of inelastic spheres". In: *Granular Matter* 10.1 (Aug. 2007), pp. 47–52. ISSN: 1434-5021. DOI: [10.1007/s10035-007-0057-z](https://doi.org/10.1007/s10035-007-0057-z). URL: <http://www.springerlink.com/index/10.1007/s10035-007-0057-z>.
- [95] James T. Jenkins and Diego Berzi. "Steady, inclined flow of a mixture of grains and fluid over a rigid base". In: *AIP Conference Proceedings*. Vol. 1227. 2010. ISBN: 9780735407725. DOI: [10.1063/1.3435402](https://doi.org/10.1063/1.3435402).
- [96] James T. Jenkins and Daniel M. Hanes. "Collisional sheet flows of sediment driven by a turbulent fluid". In: *Journal of Fluid Mechanics* 370 (1998), pp. 29–52.
- [97] James T. Jenkins and S.B. Savage. "A theory for the rapid flow of identical, smooth, nearly elastic, spherical particles". In: *Journal of Fluid Mechanics* 130 (1983), pp. 187–202. URL: http://journals.cambridge.org/abstract_S0022112083001044.
- [98] James T. Jenkins and Chao Zhang. "Kinetic theory for identical, frictional, nearly elastic spheres". In: *Physics of Fluids* 14.3 (2002), pp. 1228–1235. ISSN: 10706631. DOI: [10.1063/1.1449466](https://doi.org/10.1063/1.1449466). URL: <http://link.aip.org/link/PHFLE6/v14/i3/p1228/s1&Agg=doi>.
- [99] Xiaobo Jia, Xianyou Mou, and Honglan Ji. "Experimental study on local scour protection and contact pressure of the facing water surface at the pier based on the guide pillar". In: *Ocean Engineering* 302 (2024), p. 117670.
- [100] Peter C. Klingeman. "Hydrologic evaluations in bridge pier scour design". In: *Journal of the Hydraulics Division* 99.12 (1973), pp. 2175–2184.
- [101] Teruhisa Komatsu et al. "Creep Motion in a Granular Pile Exhibiting Steady Surface Flow". In: *Physical Review Letters* 86.9 (Feb. 2001), pp. 1757–1760. ISSN: 0031-9007. DOI: [10.1103/PhysRevLett.86.1757](https://doi.org/10.1103/PhysRevLett.86.1757).
- [102] Kees J M Kramer and Edwin M Foekema. "The "Musselmonitor®" as Biological Early Warning System: The First Decade". In: *Biomonitoring and biomarkers as indicators of environmental change 2: a handbook* (2001), pp. 59–87. ISSN: 1461354889.

- [103] Kees J. M. Kramer, Henk A. Jenner, and Dick de Zwart. "The valve movement response of mussels: a tool in biological monitoring". In: *Hydrobiologia* 188 (1989), pp. 433–443. ISSN: 0018-8158.
- [104] Snehasis Kundu and Koeli Ghoshal. "Effects of secondary current and stratification on suspension concentration in an open channel flow". In: *Environmental Fluid Mechanics* 14 (2014), pp. 1357–1380. ISSN: 1567-7419.
- [105] Eric Lajeunesse, Luce Malverti, and François Charru. "Bed load transport in turbulent flow at the grain scale: Experiments and modeling". In: *Journal of Geophysical Research: Earth Surface* 115.F4 (2010).
- [106] Jean-Baptiste Pierre Antoine de Monet Lamarck. *Histoire naturelle des animaux sans vertèbres*. Vol. t.6(1). Paris: published by the author, 1819, p. 343.
- [107] Theofanis P. Lambrou et al. "A low-cost sensor network for real-time monitoring and contamination detection in drinking water distribution systems". In: *IEEE sensors journal* 14.8 (2014), pp. 2765–2772.
- [108] Michael J. Langland and Thomas M. Cronin. *A summary report of sediment processes in Chesapeake Bay and watershed*. US Department of the Interior, US Geological Survey, 2003.
- [109] Michele Larcher and James T. Jenkins. "Segregation and mixture profiles in dense, inclined flows of two types of spheres". In: *Physics of Fluids* 25.11 (2013), p. 113301. ISSN: 10706631. DOI: [10.1063/1.4830115](https://doi.org/10.1063/1.4830115).
- [110] Laura K. Lutz. "Impacts of nonideal field conditions on vertical water velocity estimates from streambed temperature time series". In: *Water Resources Research* 46.1 (2010).
- [111] DM Lawler. "A new technique for the automatic monitoring of erosion and deposition rates". In: *Water resources research* 27.8 (1991), pp. 2125–2128.
- [112] Caroline Le Bouteiller and J G Venditti. "Sediment transport and shear stress partitioning in a vegetated flow". In: *Water Resources Research* 51.4 (2015), pp. 2901–2922. ISSN: 0043-1397.
- [113] Hong-Yuan Lee et al. "On three-dimensional continuous saltating process of sediment particles near the channel bed". In: *Journal of Hydraulic Research* 44.3 (2006), pp. 374–389. ISSN: 0022-1686.
- [114] Clement Lewsey, Gonzalo Cid, and Edward Kruse. "Assessing climate change impacts on coastal infrastructure in the Eastern Caribbean". In: *Marine Policy* 28.5 (2004), pp. 393–409. ISSN: 0308-597X.
- [115] Li Li, Binghui Zheng, and Lusan Liu. "Biomonitoring and bioindicators used for river ecosystems: definitions, approaches and trends". In: *Procedia environmental sciences* 2 (2010), pp. 1510–1524. ISSN: 1878-0296.

- [116] Frédéric Liébault et al. "Bedload tracing in a high-sediment-load mountain stream". In: *Earth Surface Processes and Landforms* 37.4 (2012), pp. 385–399.
- [117] Hui-Pang Lien and Fang-Wu Tsai. "Sediment Concentration Distribution of Debris Flow". In: *Journal of Hydraulic Engineering* 129.12 (2003), pp. 995–1000. ISSN: 0733-9429. DOI: [10.1061/\(asce\)0733-9429\(2003\)129:12\(995\)](https://doi.org/10.1061/(asce)0733-9429(2003)129:12(995)).
- [118] Hui-Pang Lien and Fang-Wu Tsai. "Sediment concentration distribution of debris flow". In: *Journal of Hydraulic Engineering* 129.12 (2003), pp. 995–1000.
- [119] Yung Bin Lin et al. "Flood scour monitoring system using fiber Bragg grating sensors". In: *Smart materials and Structures* 15.6 (2006), p. 1950.
- [120] Charles H. Luce et al. "Solutions for the diurnally forced advection-diffusion equation to estimate bulk fluid velocity and diffusivity in streambeds from temperature time series". In: *Water Resources Research* 49.1 (2013), pp. 488–506.
- [121] Darren Lumbroso, David Ramsbottom, and M. Spaliviero. "Sustainable flood risk management strategies to reduce rural communities' vulnerability to flooding in Mozambique". In: *Journal of Flood Risk Management* 1.1 (2008), pp. 34–42.
- [122] Christopher S. Magirl et al. "Large-scale dam removal on the Elwha River, Washington, USA: Fluvial sediment load". In: *Geomorphology* 246 (2015), pp. 669–686.
- [123] Koleka Makanda, Stanley Nzama, and Thokozani Kanyerere. "Assessing the role of water resources protection practice for sustainable water resources management: a review". In: *Water* 14.19 (2022), p. 3153. ISSN: 2073-4441.
- [124] Francesco Mancini et al. "Using unmanned aerial vehicles (UAV) for high-resolution reconstruction of topography: The structure from motion approach on coastal environments". In: *Remote sensing* 5.12 (2013), pp. 6880–6898.
- [125] Luca Mao et al. "Controls over particle motion and resting times of coarse bed load transport in a glacier-fed mountain stream". In: *Journal of Geophysical Research: Earth Surface* 125.4 (2020), e2019JF005253. ISSN: 2169-9003.
- [126] Luca Mao et al. "Sediment transport in proglacial rivers". In: *Geomorphology of proglacial systems: Landform and sediment dynamics in recently deglaciated alpine landscapes* (2019), pp. 199–217.
- [127] Fr Marceau. *Recherches sur la morphologie, l'histologie et la physiologie comparées de muscles adducteurs des mollusques acéphales*. Librairie Albert Schulz, 1909.

- [128] Pierre Martel et al. "Evaluation of caged freshwater mussels as an alternative method for environmental effects monitoring (EEM) studies". In: *Environmental pollution* 124.3 (2003), pp. 471–483. ISSN: 0269-7491.
- [129] Raleigh L Martin, Douglas J Jerolmack, and Rina Schumer. "The physical basis for anomalous diffusion in bed load transport". In: *Journal of Geophysical Research: Earth Surface* 117.F1 (2012). ISSN: 0148-0227.
- [130] Patricia Diniz Martins and Cristiano Poletto. "Entropy for determination of suspended sediment concentration: Parameter related to granulometry". In: *Journal of Environmental Engineering* 144.3 (2018), p. 4017111. ISSN: 0733-9372.
- [131] Patrícia Diniz Martins and Cristiano Poletto. "Principle of maximum entropy in the estimation of suspended sediment concentration". In: *RBRH* 22 (2017). ISSN: 1414-381X.
- [132] Tiago Matos et al. "Design of a multipoint cost-effective optical instrument for continuous in-situ monitoring of turbidity and sediment". In: *Sensors* 20.11 (2020), p. 3194.
- [133] Tiago Matos et al. "Development of a cost-effective optical sensor for continuous monitoring of turbidity and suspended particulate matter in marine environment". In: *Sensors* 19.20 (2019), p. 4439.
- [134] A.M. McCallum et al. "A 1-D analytical method for estimating surface water-groundwater interactions and effective thermal diffusivity using temperature time series". In: *Water Resources Research* 48.11 (2012).
- [135] Antonio Menacho et al. "Arduino-based water analysis pocket lab". In: *2021 World Engineering Education Forum/Global Engineering Deans Council (WEEF/GEDC)*. IEEE. 2021, pp. 205–210.
- [136] Fanlin Meng, Guangtao Fu, and David Butler. "Cost-effective river water quality management using integrated real-time control technology". In: *Environmental science & technology* 51.17 (2017), pp. 9876–9886. ISSN: 0013-936X.
- [137] Robert A. Metcalfe et al. "Aquatic ecosystem assessments for rivers". In: *Ministry of Natural Resources: Peterborough, ON, Canada* (2013).
- [138] Eugen Meyer-Peter and Robert Müller. "Formulas for bed-load transport". In: *IAHSR 2nd meeting, Stockholm, appendix 2*. IAHR. 1948.
- [139] Steven D. Meyers, Brian G. Kelly, and James J. O'Brien. "An introduction to wavelet analysis in oceanography and meteorology: With application to the dispersion of Yanai waves". In: *Monthly weather review* 121.10 (1993), pp. 2858–2866. ISSN: 1520-0493.
- [140] Panagiotis Michalis et al. "Wireless monitoring of scour and re-deposited sediment evolution at bridge foundations based on soil electromagnetic properties". In: *Smart Materials and Structures* 24.12 (2015), p. 125029.
- [141] Koreen Millard et al. "Use of GIS and high resolution LiDAR in salt marsh restoration site suitability assessments in the upper Bay of Fundy, Canada". In: *Wetlands Ecology and Management* 21 (2013), pp. 243–262.

- [142] Domenica Mirauda, Marilena Pannone, and Annamaria De Vincenzo. "An entropic model for the assessment of streamwise velocity dip in wide open channels". In: *Entropy* 20.1 (2018), p. 69. ISSN: 1099-4300.
- [143] Namiko Mitarai and Hiizu Nakanishi. "Velocity correlations in dense granular shear flows: Effects on energy dissipation and normal stress". In: *Physical Review E* 75.3 (Mar. 2007), p. 031305. ISSN: 1539-3755. DOI: [10.1103/PhysRevE.75.031305](https://doi.org/10.1103/PhysRevE.75.031305).
- [144] Vanessa Modesto et al. "Mussel behaviour as a tool to measure the impact of hydrodynamic stressors". In: *Hydrobiologia* 850.4 (2023), pp. 807–820. ISSN: 1573-5117.
- [145] Nahashon Mokuu, Wa Maina Ciira, and Henry Kiragu. "A Raw Water Quality Monitoring System using Wireless Sensor Networks". In: (2021).
- [146] Tommaso Moramarco, Carla Saltalippi, and Vijay P Singh. "Estimation of mean velocity in natural channels based on Chiu's velocity distribution equation". In: *Journal of Hydrologic Engineering* 9.1 (2004), pp. 42–50. ISSN: 1084-0699.
- [147] Tommaso Moramarco, Carla Saltalippi, and Vijay P Singh. "Velocity profiles assessment in natural channels during high floods". In: *Hydrology Research* 42.2-3 (2011), pp. 162–170. ISSN: 0029-1277.
- [148] Tommaso Moramarco and Vijay P Singh. "Formulation of the entropy parameter based on hydraulic and geometric characteristics of river cross sections". In: *Journal of Hydrologic Engineering* 15.10 (2010), pp. 852–858. ISSN: 1084-0699.
- [149] Tommaso Moramarco et al. "An entropy-based method for determining the flow depth distribution in natural channels". In: *Journal of hydrology* 497 (2013), pp. 176–188. ISSN: 0022-1694.
- [150] David S. Mueller and Mark N. Landers. "Development of bridge-scour instrumentation for inspection and maintenance personnel". In: *Proceedings of the National Conference on Hydraulic Engineering*. pt 2. 1993, pp. 2045–2050.
- [151] M. Muste et al. "On the capabilities of emerging nonintrusive methods to estimate bedform characteristics and bedload rates". In: *Water resources research* 59.6 (2023), e2022WR034266. ISSN: 0043-1397.
- [152] M. Muste et al. "On the capabilities of emerging nonintrusive methods to estimate bedform characteristics and bedload rates". In: *Water resources research* 59.6 (2023), e2022WR034266.
- [153] M. Muste et al. "Practical aspects of ADCP data use for quantification of mean river flow characteristics; Part II: fixed-vessel measurements". In: *Flow measurement and instrumentation* 15.1 (2004), pp. 17–28. ISSN: 0955-5986.

- [154] Kiyohito Nagai et al. "Detecting the shellfish killer *Heterocapsa circularisquama* (Dinophyceae) by measuring bivalve valve activity with a Hall element sensor". In: *Aquaculture* 255.1-4 (2006), pp. 395–401. ISSN: 0044-8486.
- [155] Ali K. Nawar and Manaf K. Altaleb. "A low-cost real-time monitoring system for the river level in wasit province". In: *2021 International Conference on Advance of Sustainable Engineering and its Application (ICASEA)*. IEEE, 2021, pp. 54–58. ISBN: 166549736X.
- [156] Vladimir Nikora et al. "On bed particle diffusion in gravel bed flows under weak bed load transport". In: *Water Resources Research* 38.6 (2002), pp. 17–1.
- [157] Thomas Pätz and Orencio Durán. "The cessation threshold of non-suspended sediment transport across aeolian and fluvial environments". In: *Journal of Geophysical Research: Earth Surface* 123.8 (2018), pp. 1638–1666. ISSN: 2169-9003.
- [158] A.S. Paintal. "A stochastic model of bed load transport". In: *Journal of Hydraulic Research* 9.4 (1971), pp. 527–554.
- [159] Gary Parker. "Surface-based bedload transport relation for gravel rivers". In: *Journal of hydraulic research* 28.4 (1990), pp. 417–436.
- [160] Gary Parker, Sundararajan Dhamotharan, and Heinz Stefan. "Model experiments on mobile, paved gravel bed streams". In: *Water Resources Research* 18.5 (1982), pp. 1395–1408.
- [161] Sathish Pasika and Sai Teja Gandla. "Smart water quality monitoring system with cost-effective using IoT". In: *Heliyon* 6.7 (2020). ISSN: 2405-8440.
- [162] José Miguel Pasini and James T. Jenkins. "Aeolian transport with collisional suspension." In: *Philosophical transactions. Series A, Mathematical, physical, and engineering sciences* 363.1832 (July 2005), pp. 1625–46. ISSN: 1364-503X. DOI: [10.1098/rsta.2005.1598](https://doi.org/10.1098/rsta.2005.1598).
- [163] Sebastiano Piccolroaz et al. "Exploring and quantifying river thermal response to heatwaves". In: *Water* 10.8 (2018), p. 1098. ISSN: 2073-4441.
- [164] Ashkan Pilbala et al. "Real-Time Biological Early Warning System based on Freshwater Mussels' Valvometry Data". In: *EGUsphere* 2023 (2023), pp. 1–21.
- [165] Francois J. Pugh and Kenneth C. Wilson. "Velocity and concentration distributions in sheet flow above plane beds". In: *Journal of Hydraulic Engineering* 125.2 (1999), pp. 117–125.
- [166] Sai Qu et al. "Distinguishing the impacts of climate change and anthropogenic factors on vegetation dynamics in the Yangtze River Basin, China". In: *Ecological Indicators* 108 (2020), p. 105724. ISSN: 1470-160X.
- [167] J.L. Ralaiarisoa et al. "Transition from Saltation to Collisional Regime in Windblown Sand". In: *Physical Review Letters* 124.19 (2020), p. 198501. ISSN: 10797114. DOI: [10.1103/PhysRevLett.124.198501](https://doi.org/10.1103/PhysRevLett.124.198501).

- [168] Thibaud Revil-Baudard et al. "Investigation of sheet-flow processes based on novel acoustic high-resolution velocity and concentration measurements". In: *Journal of Fluid Mechanics* 767 (2015), pp. 1–30. ISSN: 0022-1120. DOI: [10.1017/jfm.2015.23](https://doi.org/10.1017/jfm.2015.23).
- [169] Manel Rhif et al. "Wavelet transform application for/in non-stationary time-series analysis: A review". In: *Applied Sciences* 9.7 (2019), p. 1345. ISSN: 2076-3417.
- [170] J.F. Richardson and W.N. Zaki. "The sedimentation of a suspension of uniform spheres under conditions of viscous flow". In: *Chemical Engineering Science* 3.2 (1954), pp. 65–73.
- [171] Peter V. Ridd. "A sediment level sensor for erosion and siltation detection". In: *Estuarine, Coastal and Shelf Science* 35.4 (1992), pp. 353–362.
- [172] Leo C van Rijn. "Sediment transport, part II: suspended load transport". In: *Journal of hydraulic engineering* 110.11 (1984), pp. 1613–1641.
- [173] Leo C. van Rijn. "Sediment transport, part I: bed load transport". In: *Journal of hydraulic engineering* 110.10 (1984), pp. 1431–1456. DOI: [10.1061/\(ASCE\)0733-9429\(1984\)110:10\(1431\)](https://doi.org/10.1061/(ASCE)0733-9429(1984)110:10(1431)).
- [174] A.A. Robson et al. "Valve gape and exhalant pumping in bivalves: optimization of measurement". In: *Aquatic Biology* 6 (2009), pp. 191–200. ISSN: 1864-7782.
- [175] Giorgio Rosatti and Luigi Fraccarollo. "A well-balanced approach for flows over mobile-bed with high sediment-transport". In: *Journal of Computational Physics* 220.1 (2006), pp. 312–338. ISSN: 0021-9991.
- [176] Hunter Rouse. "Experiments on the Mechanics of Sediment Suspension". In: *Fifth International Congress for Applied Mechanics*. New York: John Wiley and Sons, 1939, pp. 550–554.
- [177] J. Salanki. "Mussel test for biological control of water pollution". In: *Hidrol. Kozl.:(Hungary)* 56.6 (1976).
- [178] Gerd Sauermann, Klaus Kroy, and Hans J. Herrmann. "Continuum saltation model for sand dunes". In: *Physical Review E* 64.3 (2001), p. 10. ISSN: 1063651X. DOI: [10.1103/PhysRevE.64.031305](https://doi.org/10.1103/PhysRevE.64.031305). arXiv: [0101377 \[cond-mat\]](https://arxiv.org/abs/0101377).
- [179] Bridget R Scanlon et al. "Global water resources and the role of groundwater in a resilient water future". In: *Nature Reviews Earth & Environment* 4.2 (2023), pp. 87–101. ISSN: 2662-138X.
- [180] Bernd R Schöne and Richard A Krause Jr. "Retrospective environmental biomonitoring–Mussel Watch expanded". In: *Global and Planetary Change* 144 (2016), pp. 228–251. ISSN: 0921-8181.
- [181] B J Schuring and M J Geense. "Een elektronische schakeling voor het registreren van openingshoek van de mossel *Mytilus edulis* L". In: *TNO-Rapport CL 72.8* (1972).

- [182] Vittoria Scorpio et al. "Channelization of a large Alpine river: what is left of its original morphodynamics?" In: *Earth Surface Processes and Landforms* 43.5 (2018), pp. 1044–1062. ISSN: 0197-9337.
- [183] Eva Sebok, Peter Engesgaard, and Carlos Duque. "Long-term monitoring of streambed sedimentation and scour in a dynamic stream based on streambed temperature time series". In: *Environmental Monitoring and Assessment* 189 (2017), pp. 1–15.
- [184] Philippe Séchet and Benoit Le Guennec. "Bursting phenomenon and incipient motion of solid particles in bed-load transport". In: *Journal of Hydraulic Research* 37.5 (1999), pp. 683–696. ISSN: 0022-1686.
- [185] Claude Elwood Shannon. "A mathematical theory of communication". In: *The Bell system technical journal* 27.3 (1948), pp. 379–423.
- [186] Albert Shields. "Application of similarity principles and turbulence research to bed-load movement". In: (1936).
- [187] Ahmed A.H. Siddig et al. "How do ecologists select and use indicator species to monitor ecological change? Insights from 14 years of publication in *Ecological Indicators*". In: *Ecological Indicators* 60 (2016), pp. 223–230. ISSN: 1470-160X.
- [188] Tiago André Silva et al. "Geomorphological response of the salt-marshes in the Tagus estuary to sea level rise". In: *journal of coastal research* 65 (2013), pp. 582–587.
- [189] Louise C Sime, Robert I Ferguson, and Michael Church. "Estimating shear stress from moving boat acoustic Doppler velocity measurements in a large gravel bed river". In: *Water Resources Research* 43.3 (2007). ISSN: 0043-1397.
- [190] Raj Mohan Singh. "Wavelet-ANN model for flood events". In: *Proceedings of the international conference on soft computing for problem solving (SocProS 2011) December 20-22, 2011: volume 2*. Springer, 2012, pp. 165–175. ISBN: 8132204905.
- [191] Vijay P Singh and Huijuan Cui. "Modeling sediment concentration in debris flow by Tsallis entropy". In: *Physica A: Statistical Mechanics and its Applications* 420 (2015), pp. 49–58.
- [192] Vijay P Singh, Bellie Sivakumar, and Huijuan Cui. "Tsallis entropy theory for modeling in water engineering: A review". In: *Entropy* 19.12 (2017), p. 641. ISSN: 1099-4300.
- [193] Eva Skarbøvik and Roger Roseth. "Use of sensor data for turbidity, pH and conductivity as an alternative to conventional water quality monitoring in four Norwegian case studies". In: *Acta Agriculturae Scandinavica, Section B—Soil & Plant Science* 65.1 (2015), pp. 63–73.
- [194] Mohamedou Sow et al. "Water quality assessment by means of HFNI valvometry and high-frequency data modeling". In: *Environmental monitoring and assessment* 182 (2011), pp. 155–170. ISSN: 0167-6369.

- [195] R.W. Stallman. "Steady one-dimensional fluid flow in a semi-infinite porous medium with sinusoidal surface temperature". In: *Journal of geophysical Research* 70.12 (1965), pp. 2821–2827.
- [196] Mark Sterling and Donald Knight. "An attempt at using the entropy approach to predict the transverse distribution of boundary shear stress in open channel flow". In: *Stochastic Environmental Research and Risk Assessment* 16 (2002), pp. 127–142. ISSN: 1436-3240.
- [197] Debra J Stokes, Terry R Healy, and Penelope J Cooke. "Expansion dynamics of monospecific, temperate mangroves and sedimentation in two embayments of a barrier-enclosed lagoon, Tauranga Harbour, New Zealand". In: *Journal of Coastal Research* 26.1 (2010), pp. 113–122.
- [198] S Sukanya and Sabu Joseph. "Climate change impacts on water resources: An overview". In: *Visualization Techniques for Climate Change with Machine Learning and Artificial Intelligence* (2023), pp. 55–76.
- [199] Nicola Surian and Massimo Rinaldi. "Morphological response to river engineering and management in alluvial channels in Italy". In: *Geomorphology* 50.4 (2003), pp. 307–326.
- [200] James Sutherland, Alan Brampton, and RJS Whitehouse. "Toe scour at seawalls: monitoring, prediction and mitigation". In: (2006).
- [201] Mudrakola Swapna et al. "Bio-signals in medical applications and challenges using artificial intelligence". In: *Journal of Sensor and Actuator Networks* 11.1 (2022), p. 17. ISSN: 2224-2708.
- [202] Donatella Termini and Tommaso Moramarco. "Application of entropic approach to estimate the mean flow velocity and Manning roughness coefficient in a high-curvature flume". In: *Hydrology Research* 48.3 (2017), pp. 634–645. ISSN: 0029-1277.
- [203] Donatella Termini et al. "Identification of hydrodynamic changes in rivers by means of freshwater mussels' behavioural response: an experimental investigation". In: *Ecohydrology* (2023), e2544. ISSN: 1936-0584.
- [204] Charlotte E. L. Thompson et al. "The manifestation of fluid-transmitted bed shear stress in a smooth annular flume—a comparison of methods". In: *Journal of Coastal Research* (2003), pp. 1094–1103. ISSN: 0749-0208.
- [205] Daniele Tonina, Charles Luce, and Frank Gariglio. "Quantifying streambed deposition and scour from stream and hyporheic water temperature time series". In: *Water Resources Research* 50.1 (2014), pp. 287–292.
- [206] Łukasz Topczewski et al. "Monitoring of scour around bridge piers and abutments". In: *Transportation Research Procedia* 14 (2016), pp. 3963–3971.
- [207] S Torquato. "Nearest-neighbor statistics for packings of hard spheres and disks". In: *Physical Review E* 51.4 (1995), pp. 3170–3182.

- [208] Damien Tran et al. "Estimation of potential and limits of bivalve closure response to detect contaminants: application to cadmium". In: *Environmental Toxicology and Chemistry: An International Journal* 22.4 (2003), pp. 914–920. ISSN: 0730-7268.
- [209] Damien Tran et al. "Inorganic mercury detection by valve closure response in the freshwater clam *Corbicula fluminea*: integration of time and water metal concentration changes". In: *Environmental Toxicology and Chemistry: An International Journal* 26.7 (2007), pp. 1545–1551. ISSN: 0730-7268.
- [210] Jarrod Trevathan, Wayne Read, and Simon Schmidtke. "Towards the development of an affordable and practical light attenuation turbidity sensor for remote near real-time aquatic monitoring". In: *Sensors* 20.7 (2020), p. 1993.
- [211] Alexandre Valance et al. "The physics of Aeolian sand transport". In: *Comptes Rendus Physique* 16.1 (2015), pp. 105–117. DOI: [10.1016/j.crhy.2015.01.006](https://doi.org/10.1016/j.crhy.2015.01.006).
- [212] E. R. Van Driest. "On Turbulent Flow Near a Wall". In: *Journal of the Aeronautical Sciences* 23.11 (1956), pp. 1007–1011. DOI: [10.2514/8.3713](https://doi.org/10.2514/8.3713).
- [213] P.A. Van Rijn et al. "Epitope mapping of envelope glycoprotein E1 of hog cholera virus strain Brescia". In: *Journal of general virology* 74.10 (1993), pp. 2053–2060.
- [214] HJ Van Wijnen and JP Bakker. "Long-term surface elevation change in salt marshes: a prediction of marsh response to future sea-level rise". In: *Estuarine, Coastal and Shelf Science* 52.3 (2001), pp. 381–390.
- [215] James E Vereycken and David C Aldridge. "Bivalve molluscs as biosensors of water quality: state of the art and future directions". In: *Hydrobiologia* 850.2 (2023), pp. 231–256. ISSN: 0018-8158.
- [216] Sarah R Weiskopf et al. "Climate change effects on biodiversity, ecosystems, ecosystem services, and natural resource management in the United States". In: *Science of the Total Environment* 733 (2020), p. 137782. ISSN: 0048-9697.
- [217] Matilde Welber et al. "Field assessment of noncontact stream gauging using portable surface velocity radars (SVR)". In: *Water Resources Research* 52.2 (2016), pp. 1108–1126. ISSN: 0043-1397.
- [218] Stephen Whitaker. "Flow in porous media I: A theoretical derivation of Darcy's law". In: *Transport in Porous Media* 1.1 (1986), pp. 3–25. ISSN: 01693913. DOI: [10.1007/BF01036523](https://doi.org/10.1007/BF01036523).
- [219] Peter R Wilcock. "Estimating local bed shear stress from velocity observations". In: *Water Resources Research* 32.11 (1996), pp. 3361–3366.
- [220] R Wilson et al. "Lip-reading in remote subjects: an attempt to quantify and separate ingestion, breathing and vocalisation in free-living animals using penguins as a model". In: *Marine Biology* 140 (2002), pp. 17–27. ISSN: 0025-3162.

- [221] Shu-Qing Yang and Joong-Woo Lee. "Reynolds shear stress distributions in a gradually varied flow in a roughened channel". In: *Journal of hydraulic research* 45.4 (2007), pp. 462–471. ISSN: 0022-1686.
- [222] Qin Zhu, Shilun Yang, and Yanxia Ma. "Intra-tidal sedimentary processes associated with combined wave–current action on an exposed, erosional mudflat, southeastern Yangtze River Delta, China". In: *Marine Geology* 347 (2014), pp. 95–106.
- [223] Alexandra Zieritz et al. "A global synthesis of ecosystem services provided and disrupted by freshwater bivalve molluscs". In: *Biological Reviews* 97.5 (2022), pp. 1967–1998. ISSN: 1464-7931.
- [224] Qingping Zou, Anthony J Bowen, and Alex E Hay. "Vertical distribution of wave shear stress in variable water depth: Theory and field observations". In: *Journal of geophysical research: Oceans* 111.C9 (2006). ISSN: 0148-0227.

This study has been carried out as a part of the PRIN project “Enterprising”, a project with the aim of monitoring and modelling river flow processes during floods. In this context, in my work, I dealt with the impact of hydrodynamic processes on river biotic communities, miniaturized gauges, and theoretical methods. The aims of the present PhD work, therefore, followed different paths which share a common phenomenology and contribute from different points of view to form a robust and consistent understanding of it. The work can be described through the following list of separate activities: 1) evaluating the impact of external stressors on aquatic ecosystems directly by using biotic communities as real-time indicators; 2) developing low-cost systems for monitoring bedload and suspended sediment transport; and 3) developing sediment transport theories based on Entropic theory.

In this study, freshwater mussels (FM) as reliable bioindicators for detecting environmental disturbances in aquatic ecosystems were utilized. We performed experiments in a laboratory flume and field to evaluate the suitability of using FM for developing a tailored real-time biological early warning system (BEWS) for detecting disturbances to the aquatic ecosystem due to external stressors. Besides FM investigation, two low-cost systems for continuous monitoring of turbidity and streambed scour/deposition were tested. Different experiments have been done in the laboratory, specifically testing a vertical string of photoresistors. The results obtained from both systems were convincing. Finally, two different types of sediment transport theories, ordinary and intense bedload, were developed based on Entropy theory. This theory developed with the aim of having sediment discharge using surface velocity for the ordinary bedload, further enabling us to find its relation to particle resting time. For the intense sediment transport, the extended Kinetic theory has been applied to unidirectional steady-uniform flow through a statistic-mechanical model endowed with entropic information on the concentration profile.